AERODYNAMIC OPTIMISATION OF SMALL SCALE HORIZONTAL AXIS WIND TURBINE BLADES

A thesis submitted in fulfilment of the requirements for the degree Master of Engineering.

Abdulkadir Mohamed Ali

BSc in Aerospace Engineering

School of Aerospace, Mechanical and Manufacturing Engineering

RMIT University, Melbourne, Australia

October, 2014

DECLARATION OF ORIGINALITY

I, Abdulkadir Ali, certify that except where due acknowledgement has been made, the work is that of the author alone; the work has not been submitted previously, in whole or in part, to qualify for any other academic award; the content of the thesis is the result of work which has been carried out since the official commencement date of the approved research program; any editorial work, paid or unpaid, carried out by a third party is acknowledged; and, ethics procedures and guidelines have been followed.

……...

Abdulkadir Ali

Date: 09/10/2014

Acknowledgements

First and foremost, I want to express my whole hearted thanks and gratitude to my senior supervisor, my mentor, Associate Professor Firoz Alam, for his guidance, encouragement, advice, constructive criticism and assistance. I am also indebted to Dr Harun Chowdhury for his inspiration, support and providing me with innovative ideas to assist in my project.

I owe heartfelt thanks to my post graduate colleagues whom their mental and moral supports were invaluable during my research. I thank Mr Iftekhar Uddin Khan, Mr Fayez Aldawi, Mr Christopher Pevitt, Mr Victor Djamovski and Mr Inam Ullah. I would also like to express my sincere thanks to Mr Bavin Loganathan for assisting me in my experimental work at RMIT Industrial Wind Tunnel.

I would like to acknowledge the assistance and advice of the technical staff especially Mr Patrick Wilkins and Mr Gil Atkins, School of Aerospace, Mechanical and Manufacturing Engineering. I also acknowledge Mr Thierry Perret-Ellena for his assistance and expertise in modelling of the wind turbine blades.

Last but not least, I would like to express my sincerest appreciation to my mother, Mrs Jamila Issa and my father, Mr Mohamed Ali for their encouragement, patience and tolerance during the time it took to complete this work. I would also like to express my sincere appreciation to my brothers and sisters for their encouragement and support.

Table of Contents

List of Figures

List of Figures (APPENDIX)

List of Tables

Nomenclature

P_D	Dynamic Pressure (Pa)
Re	Reynolds Number
V	Air Speed (m/s)
μ	Dynamic Viscosity (N.s/m²)
v	Kinematic Viscosity (m²/s)
ρ	Air Density (kg/m^3)
q_{ref}	Reference Pressure (Pa)
D	Drag Force (N)
C_D	Drag Coefficient
L	Lift Force (N)
C_L	Lift Coefficient
L/D	Lift/Drag ratio
F_T	Tip Loss Correction Factor
F_R	Root Loss Correction Factor
F_S	Side Force (N)
$\dot{m}$	Mass Flow Rate (kg/s)
P	Pressure (Pa)
P_T	Total Pressure (Pa)
P_S	Static Pressure (Pa)
T	Thrust (N)
A	Cross Sectional Area (m²)
a	Axial Induction Factor
a'	Tangential Induction Factor
C_P	Coefficient of Power

C_T	Coefficient of Thrust
Q	Torque (N.m)
λ	Tip Speed Ratio
U_T	Tangential Velocity (m/s)
U_A	Axial Velocity (m/s)
W	Relative Wind Velocity (m/s)
α	Angle of Attack (0°)
σ	Blade Solidity
θ	Yaw Angle (0°)
ϕ	Angle of Relative Wind Velocity (0°)

LIST OF ABBREVIATIONS AND ACRONYMS

AJVG	Air Jet Vortex Generators
BEM	Blade Element Momentum
BET	Blade Element Theory
CFD	Computational Fluid Dynamics
CSIRO	Commonwealth Scientific and Industrial Research Organisation
HAWT	Horizontal Axis Wind Turbine
IEC	International Electrotechnical Commission
MRF	Multiple Reference Frame
OPEC	Organization of the Petroleum Exporting Countries
RET	Renewable Energy Target
RMIT	Royal Melbourne Institute of Technology
TSR	Tip Speed Ratio
VAWT	Vertical Axis Wind Turbine

ABSTRACT

The use of conventional energy resources of the past four decades has had a significant impact on the developed and developing countries economic and technological advancement. The economic prosperity and security of industrialised nations are largely driven by the extraction and consumption of conventional energy resources. It is no secret that these conventional energy sources are adversely affecting the health and condition of the environment. The burning of fossil fuels which emit carbon dioxide into the atmosphere has resulted in global warming. Additionally, the finite amount of fossil fuel is likely to deplete by 2050 at the current consumption rate. To reduce the impact of global warming and conserve fossil fuel, the utilisation of wind energy to generate power is a viable alternative among all renewable sources. The power generation by a Horizontal Axis Wind Turbine (HAWT) is considered to be at the forefront of technology due to its reliability and cost effectiveness. However the efficiency of wind turbines is not at the desired level due to inefficient extraction of power from the wind by the turbine blades. The turbine blades experience an undesirable phenomenon at the tip of the blade known as vortex due to the pressure difference on the surface of the blade. The presence of the vortex impairs the performance of the turbine blades as it reduces the lift to drag ratio. Hence, the primary objective of this study is to understand and augment the aerodynamic performance of small scale HAWT for the application in built-up areas.

The research was undertaken using both experimental investigation in wind tunnel and computational fluid dynamics (CFD) modelling. Three sets of blade configuration were used in this study. Each set of wind turbine blade is distinguished by its unique blade tip design. A straight tapered blade with no winglet attached, backward facing winglet blade and a forward facing winglet blade were designed and manufactured. A series of tests were conducted at RMIT Industrial Wind Tunnel where the aerodynamic characteristics of the wind turbine blades (lift, drag and side force) and the power generation capabilities (C_P) were investigated. Additionally, the influence of the interference drag caused by the presence of the nacelle was also examined. The aerodynamic behaviour of the turbine was undertaken at a range of wind speeds and yaw angles. CFD modelling also employed to determine and understand the power output potential and flow behaviour of the wind turbine.

The aerodynamic behaviour of each wind turbine blade tip configuration significantly differed. The forward facing winglet blade produced a greater lift coefficient C_L at 0° yaw angle in comparison to the straight blade (with no winglets) and the backward facing winglet blade. The findings show that the forward facing winglet increases the lift to drag ratio (L/D) of 26% compared to the straight blade. However, the backward facing winglet blade decreases the L/D ratio of 27%. The turbine power coefficient has increased notably for the forward facing winglet compared the baseline blade (straight blade). A significant reduction in power coefficient was noted for the backward facing winglet.

Positioning the winglet at the suction side of the blade effectively reduces the spanwise airflow at the tip thereby improves the aerodynamic performance. It was also found that extending the gap between the wind turbine hub and the nacelle increases the power output.

As the power output obtained in this study is based on the mechanical power, it would be useful to evaluate the performance of the blades using an electrical generator. The effects of sweep and twist angles of the winglet was not accounted in this study but it would be worthy of further investigation as they influence the aerodynamic behaviour of the winglet.

CHAPTER 1

INTRODUCTION

The utilisation of energy resources has played a key role in the advancement of human civilization. Conventional energy sources such as fossil fuel and coal have significantly helped developed and industrialised nations grow and prosper economically. However, in recent years there has been growing concern about the environmental impact in which the utilisation of fossil fuel and coal is having on the world. The consensus among the scientific community is that the emission of carbon dioxide into the atmosphere produced as a result of burning fossil fuel and coal, is the number one culprit for the contribution of climate change. Climate change has the undesirable effect on the environment such as increased flooding, drought and rise in sea levels and high temperature (Hughes, 2003). Studies conducted by the Commonwealth Scientific and Industrial Research Organisation (CSIRO) have alarmingly indicated that an increase in temperature of 2 degree Celsius will significantly put the survival of the great barrier reef at great risk. The rise in ocean temperature and the acidity levels cause major changes to the coral reefs affecting the natural ecosystems.

In addition to the growing concern imposed on our environment, the demand for energy has meant that more energy will need to be harvested from fossil fuel intensive energy sources. As we continue to witness the exponential growth in population, the consumption of energy will inevitably rise and therefore the emission of carbon dioxide will continue. In order to minimise the environmental impact of fossil fuel based energy, many of the world's

developed nations, under the Kyoto Treaty, have agreed to cut back on its emission of carbon dioxide, in an attempt to lessen the impact of global warming, by setting a renewable energy target (RET). Like many developed countries, Australia, has set a renewable energy target of 20 per cent by the year 2020 (Valentine, 2010). It is highly anticipated that by the year 2020, 20 per cent of Australia's overall energy generation will come from renewable energy sources. In Australia alone, carbon pollution is projected to increase to 679 million tonnes without any intervention undertaken. This represents an increase of 22 per cent over the last two decades from 2000 to 2020. In a bid to curb the effects of global warming, the Australian government has recently introduced the carbon tax law (Gillard et al., 2011). The carbon tax is designed to create a powerful incentive for carbon intensive businesses to reduce their carbon emission levels by embracing cleaner renewable energy technology. Renewable energy sources such as solar and wind, have shown to be a viable alternative sources energy to fossil fuel and coal based energy. Wind energy is at the forefront of technology in comparison to other renewable energy sources and as a result many countries are continually utilising wind energy for power generation (Charlier & Justus, 1993).

1.1 Wind Energy

The utilisation of wind energy is one of the oldest technologies known to mankind. The power of the wind was initially harvested for applications such as grinding grain and pumping water (Hansen, 2013). It also served as a means of providing propulsive power for sailing boats. One of the earliest wind turbines used for power generation, a 12 kW (Kilowatts) DC generator, was developed and constructed by Brush in the USA in late nineteenth century (Burton et al. 2001). The advancement of wind energy technology progressed very slowly as the world continued to be engaged in the rapid industrialisation of the some of the leading economic countries today. The utilisation of energy from the wind became more attractive as the energy prices of fossil fuel (liquid fuel and coal) rises by a substantial amount. The use of wind energy as a source of power generation gained interest during the oil crisis of the 1970's when fossil fuel driven energy sources became expensive due to the Middle East War and OPEC oil embargo (Yergin, 1988). Although the wind energy industry is relatively new, it has become one of the fastest growing energy sources in the world. This is largely due to the advancement of the technology and low operating cost compared to other renewable energy sources. Commercial wind turbines have increased significantly in size, which has resulted in more energy being extracted from the wind.

Although Australia continues to be far behind the rest of the developed nations in regards to harnessing wind energy, with an installed capacity of 1,880MW as of 2013. It has the potential to become a world leader in wind energy due to the enormous untapped wind resources in the south and south eastern coastal belts. Over the last two decades, the wind energy sector in Australia had an average growth of 30 per cent annually (GWEC, 2012). On a global scale, China continues to dominate the rest of the world with a total installed capacity of more than 60,000MW (Megawatts) and closely followed by the USA with an installed capacity of 48,000MW as shown in Figure 1.2.

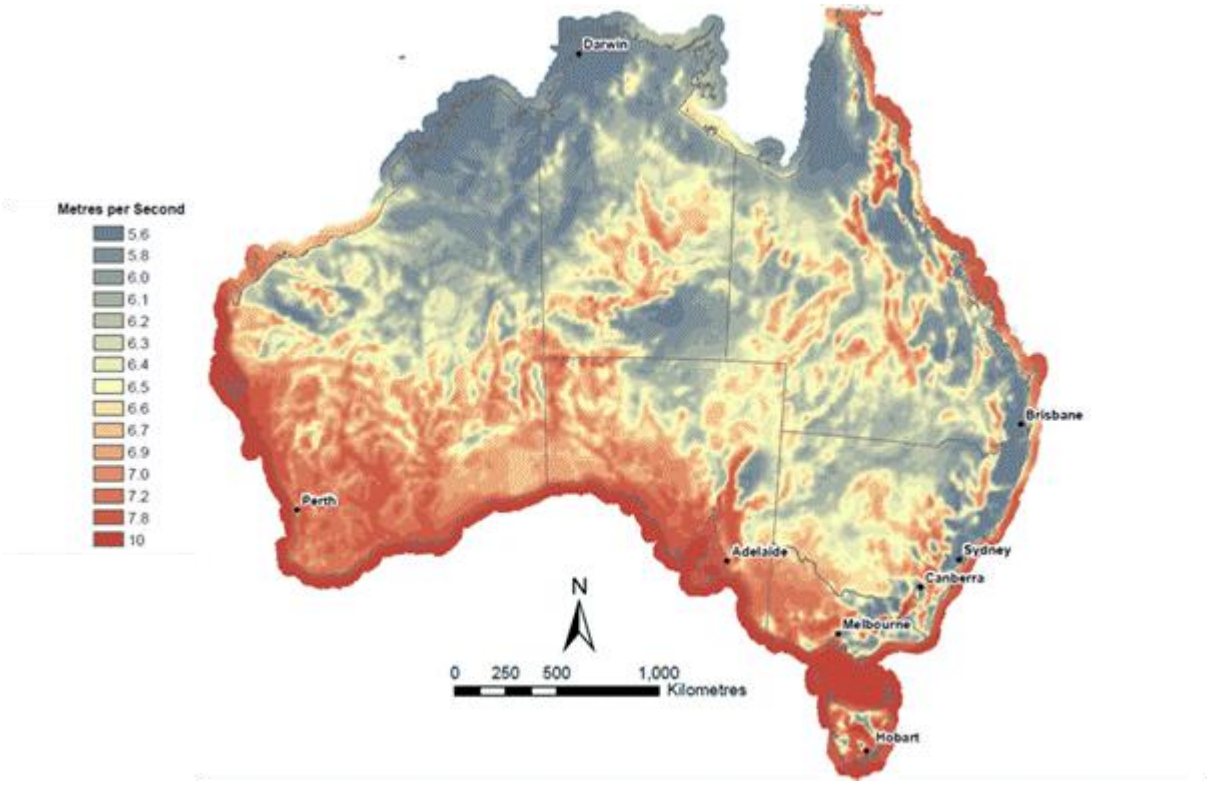

Figure 1.1: Untapped wind resource of Australia (Dopita, 2009)

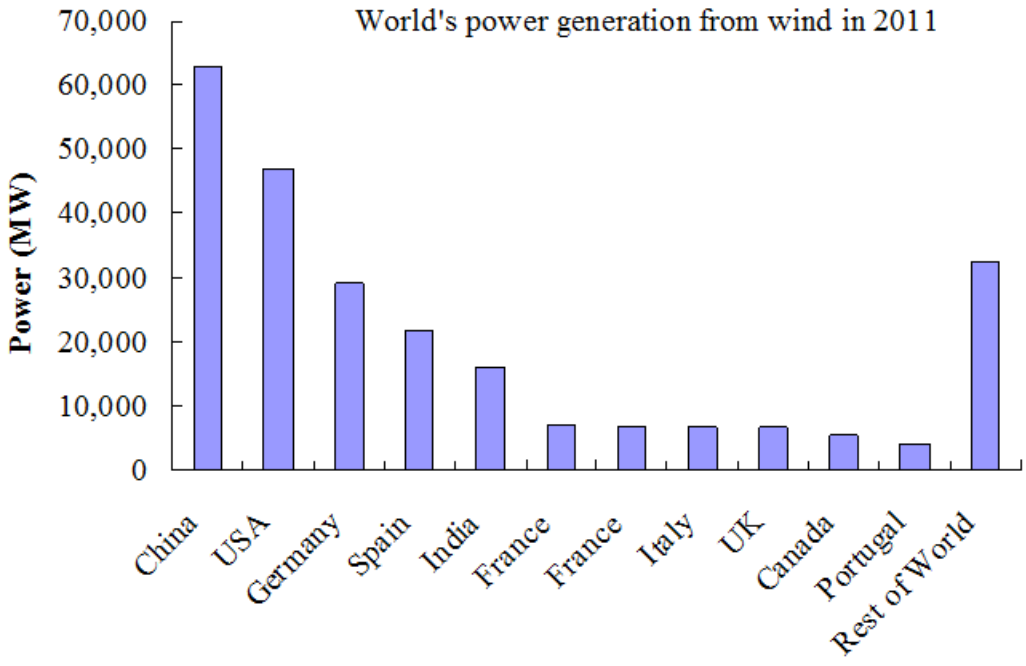

Figure 1.2: Top ten wind power generating countries (GWEC, 2012)

The success of wind energy as an alternative source of renewable energy is largely due to the use of commercial wind turbines which come in different sizes and configurations. The technological improvement of wind turbines has primarily focused on the commercial use of wind turbines and not so much for the utilisation in urban residential environment. However, in recent years the use of small scale wind turbines in urban residential areas has drawn interest and as a result the small scale wind turbine market is expanding although the technology is not at the same level maturity as commercial wind turbines.

1.2 Wind Turbine

The main concept of a wind turbine system is to convert the kinetic energy of the moving air particles into mechanical energy and ultimately into an electrical energy via an electrical generator. Wind turbines come in many shapes and sizes depending on the environmental location in which it was intended to operate. There are two main categories of wind turbines utilised to extract energy from the wind: Horizontal Axis Wind Turbine (HAWT) and Vertical Axis Wind Turbine (VAWT). It is important to understand the differences between the two as the power output of the turbine can be selected based on the energy available on site which dictates the overall size of the turbine.

1.2.1 Horizontal Axis Wind Turbine (HAWT)

Horizontal axis wind turbines are the most common type of wind turbine employed commercially and domestically. The turbines axis of rotation is parallel to the direction of free stream flow, hence it is called a horizontal axis wind turbine. Horizontal axis wind turbines work on the fundamental principle of lift. The torque generated to rotate the turbine is produced as a result of the pressure difference on top and bottom surface of the wind turbine blade. The widely accepted design configuration that is is the three bladed wind turbine design as shown Figure 1.2. The advantages of using a horizontal axis wind turbine are as follows:

- Highly efficient in terms of energy extraction from the wind
- Proven reliability as it has been used extensively in the commercial applications
- Cost effective

The underlying factor which continues to over shadow horizontal axis wind turbines is the level of noise it produces. The sound generated from a wind turbine can be divided in mechanical noise and aerodynamic noise. The mechanical noise is generated by different components within a wind turbine system such as the gearbox and the electrical generator housed inside the nacelle. The aerodynamic noise however, is generally the dominant noise source in comparison to the former and it is also very difficult to treat. Lee et al. (2013) investigated both experimentally and numerically the aerodynamic noise generated from small horizontal axis wind turbine. The study employed a 10 kW wind turbine and found that the noise levels become dominant for a blunt trailing edge turbine when compared to a sharp trailing edge wind turbine which reduces the aerodynamic noise generated. Various techniques and methods to minimise the aerodynamic noise of wind turbines have been investigated. This will be discussed further in this chapter.

(a) (b)

Figure 1.3: Horizontal axis wind turbine (a) Commercial wind turbine (b) Small domestic scale wind turbine (Wood,2011)

1.2.2 Vertical Axis Wind Turbine (VAWT)

One notable difference of the vertical axis wind turbine (VAWT) is that the axis of rotation is perpendicular to the direction of the free stream flow. VAWT are categorised as into two distinct categories; Savonius and Darrieus according to the principle used to capture energy from the wind. Savonius type wind turbines operate using the principles of drag whereas Darrieus type wind turbines operate primarily on the principle of lift. Although VAWT's are not as efficient as HAWT, they are increasingly popular in urban residential areas. This is largely due to the fact that a VAWT possesses fewer moving parts and operates at a low tip speed ratio which makes it significantly quieter and thus well suited for urban residential areas (Eriksson, Bernhoff, & Leijon, 2008). HAWTs require a yaw mechanism to redirect itself in the direction of the wind, whereas VAWTs are less sensitive to the changing wind direction and turbulence. Another advantage associated with VAWTs is the simplicity in design. Unlike HAWTs, the gearbox and generator is located at ground level which significantly reduces the complexity of the design and is also relatively easy to maintain and thus lowering the maintenance cost. Figure 1.3 (b) shows the innovative concept of a Darrieus VAWT named Turby which was designed by the University TU Delft. The Turby

concept eliminates some of the undesirable characteristics such as the inability to extract the same level of energy from the wind.

(a) (b)

Figure 1.4: Vertical axis wind turbine (a) Savonius type wind turbine. (b) Darrieus type wind turbine (Van Bussel, 2004)

1.3 Small Scale Wind Turbine

According to the international standardisation body, the IEC defines Small scale wind turbines as those having a swept area less than 200 m². The viability of small wind turbines for use in urban areas has generated a growing interest. Small scale wind turbines have the potential to be integrated on the rooves of houses and building and contribute significantly in the reduction of the average house hold electricity costs. The technological improvements of small wind turbine, although not quite as advanced as commercial wind turbines, have contributed to the increase in the overall power output.

1.3.1 Growth of Small Scale Wind Turbine Market

In recent years, small scale wind turbine market has had an average growth of 27 per cent annually (WWEA, 2013). The global installed capacity for small wind turbines has reached

more than 576 MW. China has become the largest manufacturer of both commercial and domestic wind turbines and has continued to dominate the wind energy market. Of the total global installed capacity of 576 MW, China accounts for 40 per cent which is closely followed by the USA of 35 per cent as shown in Figure 1.5.

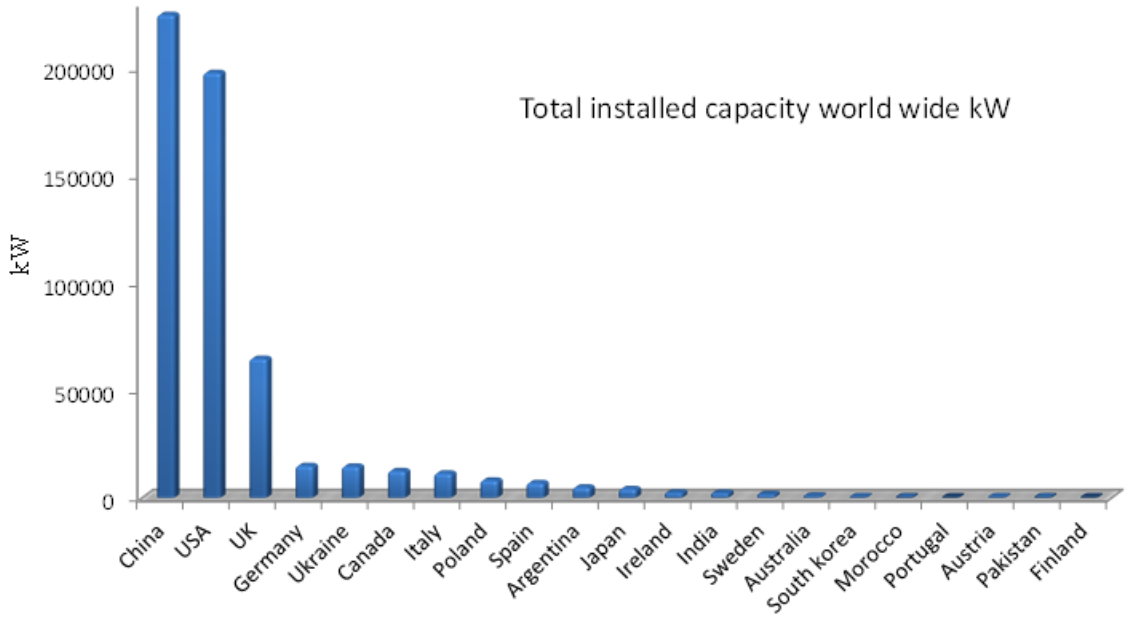

Figure 1.5: Total installed capacity worldwide (kW) (WWEA, 2013)

The significant growth of small scale wind turbines is largely driven by the policies introduced such as tax credits. The overall cost of small wind turbines continues to be one of the main challenges yet be overcome. As the small wind industry is still under developed compared to the commercial industry, the growth of small wind market is essential in order to reduce the costs. Enhancement in aerodynamic efficiency of small wind turbines is essential in order to generate more power.

1.3.2 Building Integrated Wind Turbine

Small scale wind turbines have the potential to be utilised on the roof of buildings without the need of a long length tower. The integration of wind turbines on the rooves of buildings could potentially decrease the overall cost of the wind turbine system without compromising the power output of the turbine. The influence of obstacles such as buildings in urban environment has been investigated by Capeluto et al. (2003) and Ricciardelli & Polimeno (2006). The consensus reached by both studies is that the wind speed within built up

environments such as in urban residential areas, heavily depends on the geometrical shape of the buildings.

The speed and direction of wind are significantly influenced by the surface roughness of the earth. The atmospheric boundary layer generally refers to the velocity gradient which extends from the earth's surface up to an altitude where the wind is no longer influenced by the surface roughness of the ground. The mean wind speed increases with height up to a certain height above the ground surface in which the surface friction has no effect on the wind speed. As shown in Figure 1.6, it is clear that in areas which have high building density, the flow of air is obstructed by the buildings and as a result it causes the turbulence intensity to increase and has the undesirable of effect of decreasing the mean speed. However, in low terrain roughness such as in the dessert or in wind farms, the wind flow is less undisturbed and this yields a greater mean wind speed at a relatively low height. Studies conducted by Kubota & Ahmad, (2005); Lim et al., (2009); Lien et al., (2004); Sun & Huang, (2001); Tutar & Oguz, (2002). Blocken & Carmeliet (2004), on the possibility of increasing the wind speed around the sharp edges of a building, found that the wind speed increases at the sharp edges of buildings and as a result the kinetic energy is significantly increased.

Although it is undesirable to place a wind turbine in densely built up areas, the speeding effect generated as a result of the airflow hitting the edges of the building can be greatly utilised to increase the power output of a turbine. Figure 1.7 illustrates the flow behaviour around a typical building, using computational fluid dynamics, in which the flow gains momentum at the edge of the building. A wind turbine is strategically placed on the roof of the building to capture the added momentum in the wind, immediately after the airflow comes into contact with the roof edge of the building. It is also important to avoid placing the wind turbine at close proximity to the base of the roof where turbulence is dominant.

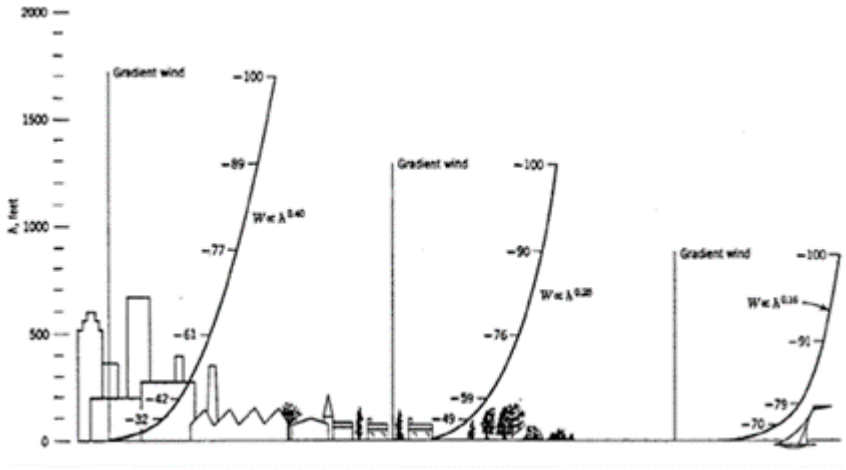

Figure 1.6: Profile of mean wind velocity influenced by variety of terrain roughness (Etkin, 2012)

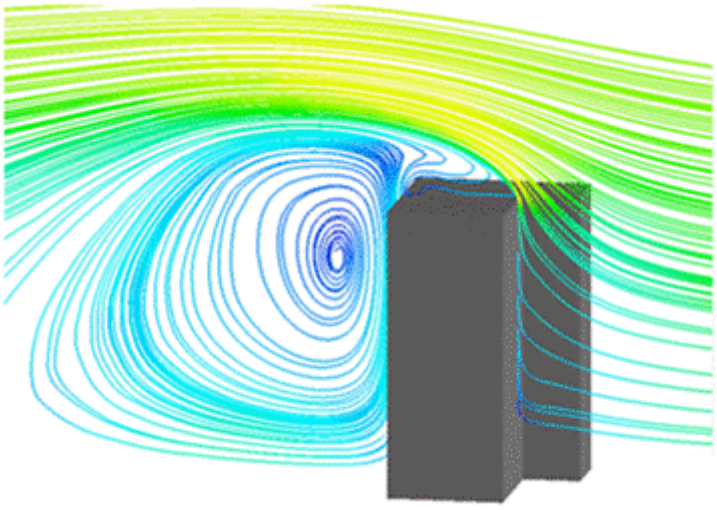

Figure 1.7: CFD flow visualisation around a building

1.4 Aerodynamic Losses of Wind Turbine

As small scale wind turbines do not have a bigger swept area, it is not capable of extracting more energy from the wind. The limitation in swept area causes a significant reduction in the overall power production. The aim of this research is to improve the aerodynamic performance of a small scale horizontal axis wind turbine, it is important to understand the flow behaviour at the tip of a blade. Horizontal axis wind turbines in general operate using the principle of aerodynamic lift which is generated on the entire length of the blade as the result of the pressure differences between the upper surface and lower surface of the wind turbine blade. As the blade is finite, the high pressure air region of the blade is attracted to the

low pressure air due to the pressure gradient force as illustrated in Figure 1.8. At the tip of the blade, a vortex is generated. A vortex is the rotational motion of fluid which comprises of a strong region of low pressure in its core (Mattos, 2003).

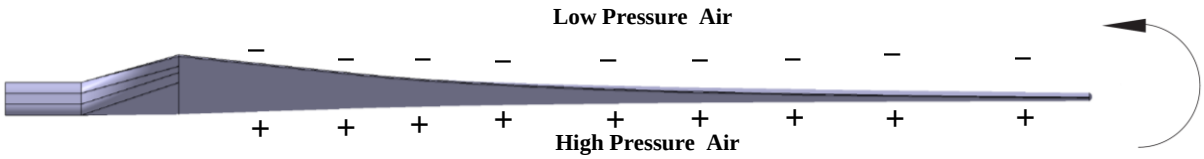

Figure 1.8: Inflow air distribution around the blade tip

The presence of the vortex at the tip of the blade significantly adds to the overall drag of the blade by adding an additional drag component called induced drag and as a result the lift generated on the blades is reduced. This causes a reduction in the aerodynamic performance characteristics of the blade and therefore reduces the power output of the turbine. The vortices at the tip of the blade also have the undesirable effect of significantly contributing to the noise generated by the blades. Several techniques or methods have been investigated which have the potential of enhancing the aerodynamic performance as well as minimising the noise levels of wind turbines. These methods include:

- Tip Vanes (Winglets)
- Micro Tabs
- Boundary Layer Suction

1.5 Potential Performance Enhancing Devices

Various devices can potentially be used to enhance the performance of wind turbines. Although the technology readiness level for most of these devices is low, they continue to demonstrate potential for augmenting the performance of wind turbines. Some of these devices are discussed further in the following sub sections.

1.5.1 Tip Vanes (Winglets)

Winglets are streamlined vertical surfaces that are generally attached to the tip of a wing of an aircraft. The use of winglets have been extensively investigated and utilised in the aeronautical industry to minimise the overall drag on the wing and ultimately reduce the fuel consumption of the aircraft. The sole purpose of a winglet is to minimise the tip vortices

generated at the tip of a finite wing thus reduce the induced drag and increase the lift to drag ratio of the wing profile as illustrated in Figure 1.8. In order for the winglets to be effective, Whitcomb (1976) discovered that the winglet must produce side forces to minimise the inflow above the wing tip and the outflow below the wing tip.

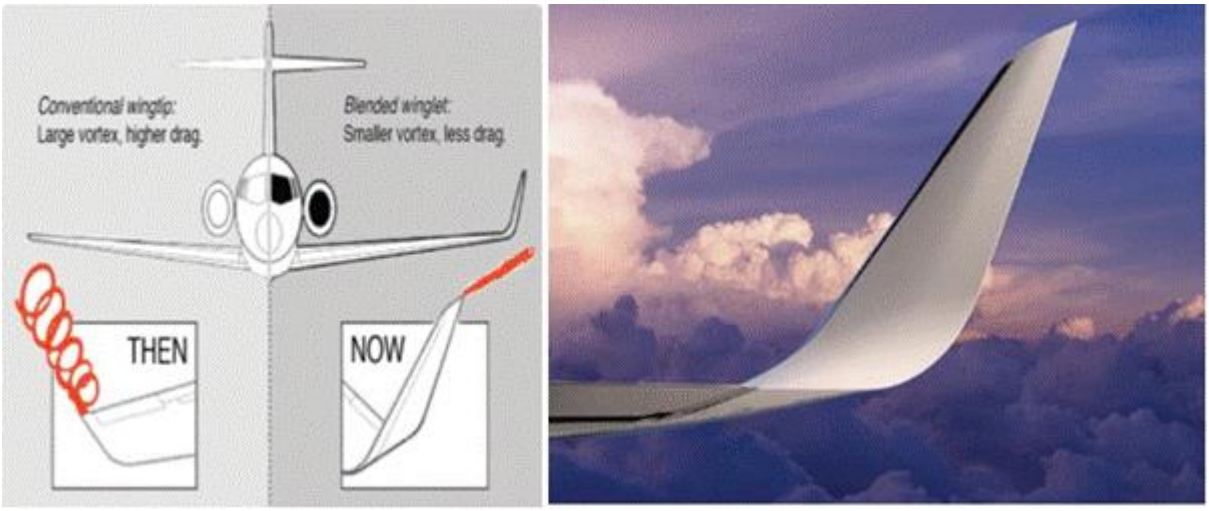

Figure 1.9: Diffusion of vortices around wing tip using winglets (AviationPartners, 2012)

Johansen et al. (2006) numerically investigated the aerodynamics performance of a wind turbine blade with winglet type device at 90° angle using Computational Fluid Dynamics (CFD). The winglets were optimised to minimise the induced drag from the blade by changing the downwash distribution. The investigation revealed that adding a winglet to wind turbine blades can increase the force distribution of the blade. However, Johansen et al. did not look at the aerodynamic effects of other angles. Additionally they did not take into account the effects of sweep angles which could potentially improve the performance of the winglets. No experimental validation of their computational findings was reported in the study.

Peng & Jinglong (2012) conducted a computational study of flutter characteristics of an aircraft wing with wing tip devices. Both a conventional winglet and a C-type winglet were used in this study. The computational simulation conducted is based on an unsteady aerodynamic flow. The study revealed that the addition of a conventional winglet in subsonic flow resulted in a decrease in flutter speed by more than 10%. The C-type wing tip however, generated a reduction in wing flutter speed of approximately 19%. However, it is not clear if this type of winglets can be applied in wind turbine blades.

Liang et al. (2013) analytically studied the effects of winglets for hydrofoil applications. A theoretical lifting surface model was established in order to evaluate the hydrodynamic loads exerted on the three dimensional hydrofoil winglets. Three types of winglet configuration was studied and analysed. The study revealed that attaching winglets to the hydrofoil substantially increases the lift force while reducing the induced drag. The effects of winglet angles, sweep angles and twist were not considered by Liang et al. in their study.

Savage & Larose (2003) undertook an experimental aerodynamic study of winglets on bluff body such as flat plate. Several benefits of the winglet were observed in the experiment. Positioning the winglets above the leading edge and trailing edges of the rectangular prism enhanced the aeroelastic characteristics. Although the findings by Savage & Larose are encouraging, further study is required for complex geometry.

Lee et al. (2012) used two computational procedures (blade element momentum theory and CFD) to understand the hydrodynamic performance of horizontal axis stream turbine using winglet type device (raked tip). They reported that the raked tip increased cavitation inception performance. However, the study did not include the effects of sweep angles and twist.

Chattot (2009) studied different blade tip modifications using Goldstein vortex model. The study indicated that the power efficiency can be enhanced with blade tip modification. Further investigation is required to evaluate his findings with experimental validation.

Gertz (2011) experimentally investigated the performance of a wind turbine with an exchangeable blade tip configuration. It was reported that the blade tip modification with winglet type device can augment the turbine power output. The investigation was based on 90° cant angle only. No twist effect was considered in Gertz's study.

Shimizu et al. (1992) investigated the augmentation of power of horizontal axis wind turbines using small vanes (Mie Vanes) attached at the tip of the rotor blade. The findings revealed that the Mie vanes influence the performance of wind turbines by increasing the power output.

Døssing (2007) studied the effects of winglet type device on aerodynamic forces of a wind turbine blade. The study was based on free wake vortex lattice method. The study revealed that winglet type device has the potential to increase the performance of a wind turbine. However, due to the uncertainties associated with employing the vortex lattice method in

turbine blade, this method less viable due to the requirement of huge computational resources.

Breitsamter (2011) compiled a review report on various passive devices such as spoilers, flaps, winglets as well as active devices such as oscillating flaps on aerofoils. The review revealed that the vortex shedding can be reduced using passive and active devices on aerofoils thereby enhancing aerodynamic efficiency of the aerofoil. Further study is needed to adapt such devices to wind turbine blades.

1.5.2 Micro Tabs

The use of micro tabs is a new aerodynamic concept inspired by the earlier concept of Gurney flaps. These devises are relatively very small and are positioned near the trailing edges of an aerofoil as illustrated in Figure 1.10. The tabs are deployed normal to the surface of the aerofoil so that the effective camber is increased which results in an increase in lift. The increase in lift can only be achieved when the micro tabs are positioned in the pressure side of the aerofoil. Kuo & Klijn (2012) attempted a numerical study to better understand noise reduction in airframe using micro-tabs. The study revealed that micro-tabs reduce noise when attached at the pressure side of the flap surface near the trailing edge. Kuo & Klijn emphasised the need for further investigation on this device.

This method is relative a new concept that could potentially enhance the performance of wind turbines however, there is still a big gap in knowledge of utilising such devices in wind turbines.

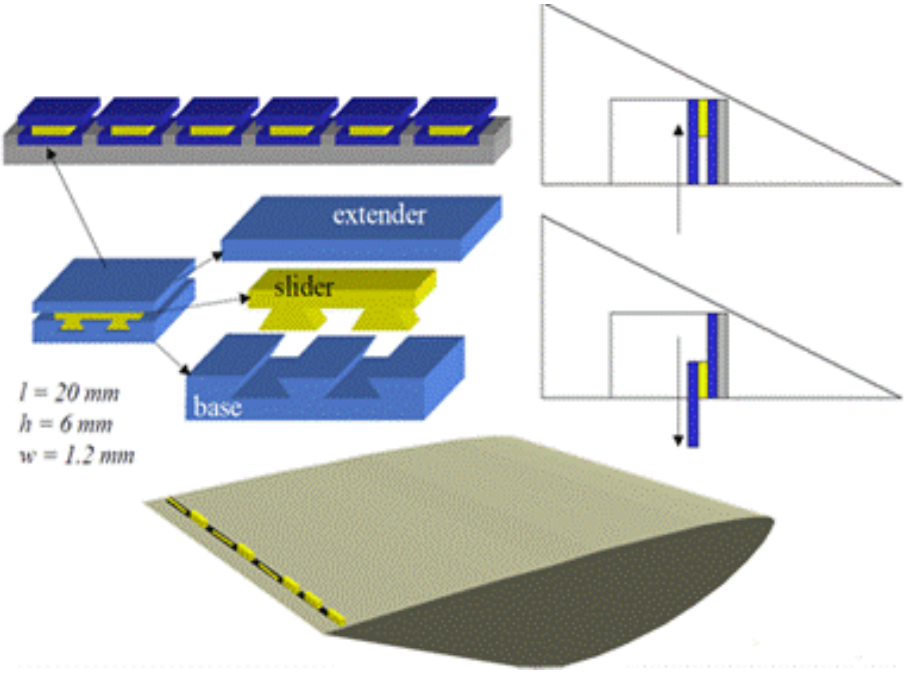

Figure 1.10: Micro tab concept (Yen et al. 2001)

1.5.3 Boundary layer suction

The boundary layer suction is generally utilised to prevent the laminar and turbulent flow from separating over the aerofoil of a wing. This method comprises of an operating powered system that is placed in a spaced vertical slots. The concept of this method is to remove the low momentum flow in the region of high pressure areas where the flow is most likely to separate. A number studies have been conducted which investigated the potential of this method being utilised as drag reducing device and enhancing the performance of wind turbines. Shun & Ahmed (2012), experimentally investigated the potential enhancement of wind turbine performance using Air Jet Vortex Generators (AJVG). The study revealed that AJVG can increase the performance of wind turbines. The study further revealed that AJVG can help reduce the fluctuating aerodynamic loads associated with dynamic stall. Although a handful of studies have indicated that it is possible to enhance the turbine blade performance, using active control methods, there are still many complicated issues that need to be addressed in terms of the integration of the suction in to aircraft wings and wind turbine blades and the overall impact it would have on the structural integrity of the wing.

1.6 Methods of Evaluation for Wind Turbine Performance

Two distinct methods are commonly used in the design and evaluation of wind turbine aerodynamic performance. Depending on the area of interest, each of these methods varies significantly in terms of their capabilities. Each of this method is briefly explained in the following subsections.

1.6.1 Experimental Method

The understanding of the aerodynamic forces exerted on various objects immersed in a fluid was limited until the late 19th century. The first officially recorded test conducted in a wind tunnel was a train model that was experimented on in 1896 according to (Gross, 1898). The majority of wind tunnels are used to simulate the effect of relative airflow over objects such as cars, aircraft and structural building by generating a stream of airflow around the aforementioned objects. Wind tunnels have become an integral part of engineering design and analysis and have significantly contributed to the advancement of many technologies of modern world. There are three main types of wind tunnels widely used: a closed wall section open jet test section and a slotted wall test section (Barlow, 1999). The majority of modern wind tunnels used are closed loop tunnels as the advantages far outweigh the disadvantages. As most wind turbines cannot accommodate the full scale objects, model scale objects generally being tested. However, the accuracy of the simulations of model scale testing significantly depends on the Reynolds number similarity, i.e:

$$\left(\left(\frac{\rho VL}{\mu}\right)_{Full\,scale} = \left(\frac{\rho VL}{\mu}\right)_{Model\,scale}\right) \tag{1.1}$$

In order to obtain an identical magnitude of the aerodynamic force coefficients for both scaled and full scale model, it is important to match the Reynolds number which is dependent on the flow velocity, length of the test object and viscosity of the fluid. Other parameters such as, the level turbulence and blockage ratio, can influence the behaviour of the flow around the test object and therefore it is important to consider these parameters.

1.6.2 Computational Method

Computational Fluid Dynamics (CFD) has made considerable progress recently in the evaluation of aerodynamic forces and moments, and other aeronautical applications especially in aircraft and spacecraft design, as many of these are time independent. Over the last two decades, the application computational fluid dynamics has continuously expanded into various fields including wind energy. Increasing computer processing power is largely responsible for the expansion of CFD as an engineering design tool. Rajendran et al. (2011) investigated the potential of an incompressible Navier Stokes CFD method for the analysis of horizontal axis wind turbines. This study employed a Multiple Reference Frame (MRF) which very few studies have applied this technique in the analysis of wind turbines. The MRF technique allows the modelling of a full scale assembly wind turbine with all the features such as nacelle and tower by dividing the fluid zone into a rotational fluid domain (rotating turbine) and a stationary domain (nacelle and tower). In comparison with experimental results, the results obtained through the MRF technique employed in CFD had very good agreement. Although there are several methods of modelling rotating machinery such as a wind turbine, the MRF method has the advantage of accurately approximating the flow field at a relatively low computational cost. The research undertaken in this will utilise the MRF method in an attempt to verify the experimental results and aid in the objectives of this research. The MRF method is further explained in Chapter 5.

1.7 Conclusions from Prior Work

In conclusion, from the literature review, it is evident that there is further scope for the enhancement of wind turbine power output through developing a smart and efficient blade design. In aeronautical applications, the add-on devices such as winglets seem to be effective in enhancing the lift to drag ratio which in turn can increase the aerodynamic efficiency. However, the application of such devices in wind turbine blades is rather limited due to the limited availability of in-depth scientific research data. Scant information on the aerodynamic effect of winglet physical configurations is available in the open literature especially for small scale horizontal axis wind turbines.

The use of 90° cant angle on a winglet in aeronautical application seems enhancing the aerodynamic performance. However, the effect of other cant angles has not been reported in the public domain.

Most published studies predominantly focused on computational modelling. A small number of studies included experimental validation of their computational modelling findings. The impact of winglets on noise generation especially in small scale wind turbine application is not well studied. Hence, there is a need for comprehensive aerodynamic studies using experimental investigations as well as computational modelling.

The airflow that immediately passes through the turbine is obstructed by the nacelle causing interference drag. The effects of the nacelle on the aerodynamic performance of wind turbines are completely absent in the literature.

Therefore, this research aims to investigate the effects of blade tip configurations by employing winglets at the tip of wind turbine blades, and the effects of the nacelle on aerodynamic efficiency of the turbine.

A summary of reviewed published research work is shown in Table 1.1

Table 1.1: Summary of prior published research work.

	Johansen et al. (2006)	Peng & Jinglong (2010)	Dossing (2007)	Lee et al. (2012)	Gertz (2011)	Chattot (2008)
Methodology	Numeric	Numerical	Numeric	Numeric	Wind tunnel	Numeric
Winglet positioning	Suction & Pressure side	Suction side	Suction side	Suction Side	Suction Side	Suction Side
Aerodynamic forces	Yes	No	No	No	No	No
Winglet cant angle	90°	90°	90°	90°	90	90°
Effects of nacelle	No	No	No	No	No	No
Open field test	No	No	No	No	No	No

As shown most researchers have predominantly focused on the geometrical configuration winglet cant angle of 90°. The aerodynamic forces subjected on wind turbine blades have not been investigated in detail. It is also evident that scant studies have been reported has been published in the public domain about the effects of the nacelle on the overall performance of the wind turbine.

Although small scale wind turbines have great economic potential for utilisation in built up areas, limited research in small scale wind turbines have been undertaken and reported to the public domain.

1.8 Rationale and Scope

The harvesting of conventional energy sources has no doubt contributed to the development of many industrialised nations. The economic growth and prosperity of many nations are largely dependent on the utilisation of conventional energy sources. As the population increases, the demand for energy also significantly increases. Energy demand will translate to more energy being produced and consumed at a substantial rate. It has been revealed recently that the burning of fossil fuel which releases carbon dioxide, methane and nitrous oxide into the atmosphere is having an adverse effect on the biodiversity of the planet. Together with solar energy, wind energy is considered to be at the forefront compared to other renewable energy sources. The utilisation of wind energy is key to achieving the Renewable Energy Target (RET) of most nations including Australia.

As evident from the current literature search, small Horizontal Axis Wind Turbines (HAWT) has the potential to produce useful power for built up areas and reduce energy cost and CO_2 emissions. However, one of the major limitations of small scale wind turbines is the aerodynamic losses at the tip of the blade due to the vortex generated resulting in an induced drag which adversely impacts on the aerodynamic performance of the turbine. Hence, there is sufficient scope for undertaking a detailed research to enhance the aerodynamic efficiency of horizontal axis wind turbine for the use in built up areas. The research aims to utilise alternative blade tip configurations in the form of winglets. The study the nacelle's effect on the overall performance of wind turbines will enhance our understanding as well.

1.9 Research Objectives

From an examination of the prior work undertaken in this area, one may conclude that there are significant gaps in understanding of winglet geometry and cant angles on aerodynamic efficiency of small scale wind turbine blades. Furthermore, the effect of nacelle on such wind turbines is not well understood. Therefore, the main objectives of this study are to:

1. Understand the effect of winglet geometric configuration on aerodynamic efficiency (lift to drag ratio) of small scale HAWT.

2. Investigate the impact of cant angles on aerodynamic performance.
3. Explore the influence of nacelle on power generation capability
4. Develop power curve for small scale wind turbine using winglets

In order to achieve the aforementioned objectives, a comprehensive work would be undertaken using experimental investigation and computationally modelling.

1.10 Overview of Thesis

Chapter 1 (Current chapter), reviews the general background of this research and the relevant literature. It also presents the research aim and objectives and scope of this research.

Chapter 2 describes the fundamental theory of wind turbines. A description of the actuator disc theory and Blade Element Momentum (BEM) theory is also given.

Chapter 3 presents the design of wind turbines from an aerodynamic perspective. It describes the aerodynamic design parameters used; and outlines the process involved in designing the wind turbine. It also presents the methodology used to design the winglets as well as the material of choice for the manufacturing of the turbine blades.

Chapter 4 describes the experimental facilities utilised in this research. It also presents a detailed description of the instrumentation, test equipment, data processing and experimental test setup.

Chapter 5 describes the numerical modelling process through CFD simulation of the wind turbine blades.

Chapter 6 presents and discusses the results obtained from both experimental investigation and computational modelling.

Chapter 7 discusses the general and specific conclusions of the research and outlines the recommendations for further study.

CHAPTER 2

WIND TURBINE THEORY

The primary function of a wind turbine is to extract the kinetic energy from the wind. From the laws of physics, any object in motion possesses a kinetic energy. As the air passes through the wind turbine, the kinetic energy of the air moving particles is absorbed. It is apparent that not all of the kinetic energy of the air can be extracted as this would indicate that there is no flow downstream of the wind turbine. If we were to separate the mass flow of air passing through the turbine from the mass flow which is not affected by the presence of the turbine, a boundary surface can be drawn containing the affected mass. This boundary is extended both upstream and downstream which forms a long stream tube.

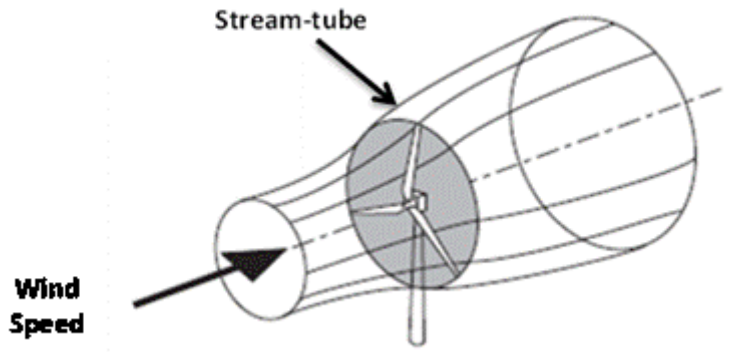

Figure 2.1: Wind energy extraction stream tube (Burton et al., 2001)

Between 1922 and 1925 German Physicist Albert Bertz, formulated a theory which predicted the maximum output that can be achieved by an ideal wind turbine. This theory has its limitation in terms of predicting the maximum power output. A number of assumptions is made to simplify the theory such as: 1) The flow is considered inviscid, incompressible and steady flow 2) Velocity changes in the direction of rotor axis and is considered uniform flow in one dimensional. 3) There is no rotational flow or swirl in the wake. Like Albert Betz, Glauert introduced the Blade Element Momentum (BEM) theory which combines the momentum theory and the blade element theory. This theory allows the user to predict the performance characteristics of an annular section of the rotor.

2.1 Actuator Disc Theory

The actuator disc model (theory) is the simplest form of analytical tool to determine the aerodynamic behaviour of a wind turbine. It is based on the linear momentum theory and widely used to predict the performance of ship propellers. The control volume under this one dimensional model shown in Figure 2.2 comprises of a surface stream tube and two cross section of the stream tube. The airflow is assumed to move across the ends of the stream tube. The turbine in this model is represented as a circular disc stationed in the middle of the stream tube. This model is purely used to assess the overall efficiency of wind turbines. However, this model cannot be utilized to refine the turbine blade for maximising the performance.

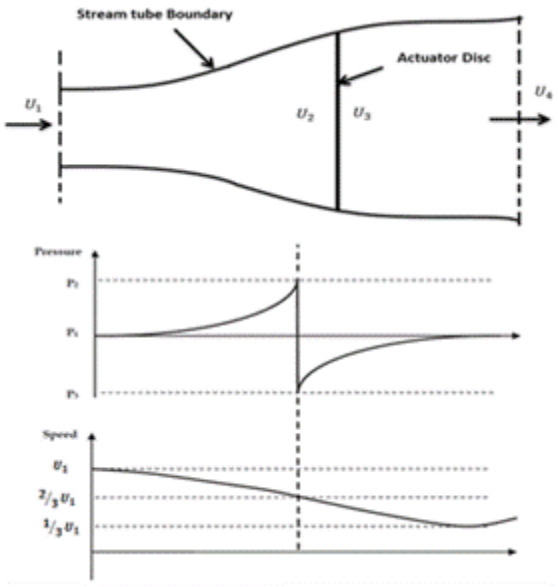

Figure 2.2: Actuator Disc Stream-tube (Burton et al., 2001)

The upstream stream tube has a cross sectional area that is smaller than the downstream, this is because the mass flow rate across the stream tube must be the same everywhere. Mass can neither be destroyed nor created, therefore the mass that enters the stream tube must be equal to the mass that leaves the stream tube. The mass of air which passes through a given cross section of the stream tube in a unit length of time is equal to $\rho U_1 A_1$, where ρ is the density of air, U_1 is the free stream flow velocity and A_1 is the cross sectional area. Since the mass flow rate is the same everywhere, this can be written us:

$$\dot{m}_1 = \dot{m}_2 = \dot{m}_3 = \dot{m}_4 \qquad \text{(Conservation of Mass)} \qquad (2.1)$$

$$\rho U_1 A_1 = \rho U_2 A_2 = \rho U_3 A_3 = \rho U_4 A_4 \qquad (2.2)$$

As the total energy is different for both upstream and downstream, the Bernoulli's equation is applied to derive the equations. Bernoulli's equation states that the total energy in the flow which is made up of, kinetic energy, static pressure energy and gravitational potential energy, remains constant given that there is no work done by the fluid.

Applying Bernoulli's theory at the upstream section of the stream tube ignoring the losses, we have:

$$P_1 + \rho \frac{1}{2} U_1^2 = P_2 + \rho \frac{1}{2} U_2^2 \qquad (2.3)$$

The downstream section of the stream tube is given as:

$$P_3 + \rho \frac{1}{2} U_3^2 = P_4 + \rho \frac{1}{2} U_4^2 \qquad (2.4)$$

By applying the conservation of linear momentum to the control volume, we can determine the net force on the turbine. This force is equal and opposite to the thrust, *T*. Thrust is equivalent to the rate of change of momentum of the air stream. This can be written as:

$$T = U_1(\rho AU)_1 - U_4(\rho AU)_4 \qquad (2.5)$$

Assuming that $P_1 = P_4 = U_2 = U_3$, Thrust can be expressed as the net sum of forces on each side of the actuator disc:

$$T = A_2(P_2 - P_3) \qquad (2.6)$$

To obtain the pressure difference at both ends of actuator disc we have:

$$P_2 = P_1 + \rho\frac{1}{2}U_1^2 - \rho\frac{1}{2}U_2^2 \tag{2.7}$$

$$P_3 = P_4 + \rho\frac{1}{2}U_1^2 - \rho\frac{1}{2}U_2^2 \tag{2.8}$$

The pressure difference from the front and back of the turbine can be obtained and is given as:

$$P_2 - P_3 = \frac{1}{2}\rho(U_1^2 + U_4^2) \tag{2.9}$$

If we substitute equation (2.8) into (2.4) we obtain:

$$T = \frac{1}{2}\rho A_2(U_1^2 - U_4^2) \tag{2.10}$$

If we equate equation (2.8) to (2.4), we have:

$$T = \dot{m}(U_1 - U_4) = \frac{1}{2}\rho A_2(U_1^2 - U_4^2) \tag{2.11}$$

$$\rho A_2 U_2(U_1 - U_4) = \frac{1}{2}\rho A_2(U_1 - U_4)(U_1 + U_4) \tag{2.12}$$

$$U_2 = \frac{1}{2}(U_1 + U_4) \tag{2.13}$$

The actuator disc induces a velocity in the stream tube which is represented by the axial induction factor (a) and is defined as the fractional decrease in wind velocity between the free stream and the turbine plane. This is expressed as:

$$a = \frac{(U_1 - U_2)}{U_1} \tag{2.14}$$

$$U_2 = U_1(1 - a) \tag{2.15}$$

From equation (2.13) and (2.15),

$$\frac{1}{2}(U_1 + U_4) = U_1(1 - a) \tag{2.16}$$

$$U_4 = U_1(1 - 2a) \tag{2.17}$$

The term $U_1 a$ is referred to as the induced velocity at the turbine. The velocity of the wind comprises two velocities, the freestream velocity and the induced velocity of the wind. An increase in the induction factor will result in the speed at the wake to slow down significantly. As the induction approaches a maximum value of 0.5, the wind speed at

downstream of the disc is zero. Therefore in order for the actuator disc theory to work, the speed of at the wake must be greater than zero.

The power output produced by the turbine is equivalent to the thrust times the velocity at the disc.

$$P = \frac{1}{2}\rho A_2(U_1^2 - U_4^2)U_2 = \frac{1}{2}\rho A_2 U_2(U_1 + U_4)(U_1 - U_4) \tag{2.18}$$

By substituting equation (2.13) and (2.15) into (2.16):

$$P = \frac{1}{2}\rho A U^3 4a(1-a)^2 \tag{2.19}$$

Where *A* is the turbine swept area and *U* is the free stream velocity. The coefficient of power is non-dimensional value which is used to measure the efficiency of any particular turbine. It is obtained from dividing the power available in the wind by the power extracted by the turbine. The turbine power coefficient can be defined as:

$$C_p = \frac{P}{\frac{1}{2}\rho A U^3} = \frac{Turbine\ Power\ Output}{Power\ in\ the\ wind} \tag{2.20}$$

Since C_p represents the ratio of the turbine power output and the available power in the wind, we can express the power coefficient as:

$$C_p = 4a(1-a)^2 \tag{2.21}$$

The maximum power coefficient can be determined when:

$$C_p = \frac{16}{27} = 0.5926 \tag{2.22}$$

From equation (2.22), the maximum power coefficient that can be achieved by an ideal turbine is known as Betz limit, named after the German aerodynamicist, Albert Betz. To achieve a power coefficient of 59%, the axial induction factor (a) must be equal to 1/3. This means that the downstream wind velocity must be reduced to a third of the upstream wind velocity. The coefficient of thrust is also expressed as non-dimensional value.

$$C_T = \frac{T}{\frac{1}{2}\rho U^2 A} = \frac{Thrust\ Force}{Dynamic\ Force} \tag{2.23}$$

Figure 2.3 represents both the power coefficient of an ideal turbine and the non-dimensional downstream wind speed. The graph illustrates that the maximum efficiency of an ideal turbine is nearly 59%. This emphasises that maximum efficiency can only be achieved if the axial induction factor is less than 0.4. However in real life, the maximum efficiency of a well-designed turbine is quite lower than Betz limit. As for the thrust created, in practice, the thrust coefficient can exceed the ideal maximum. There are a number of effects which contribute to the decrease in efficiency of a wind turbine that is not taken into account. This includes the fact that there is some drag which is present and is induced by the blades and losses at the tip.

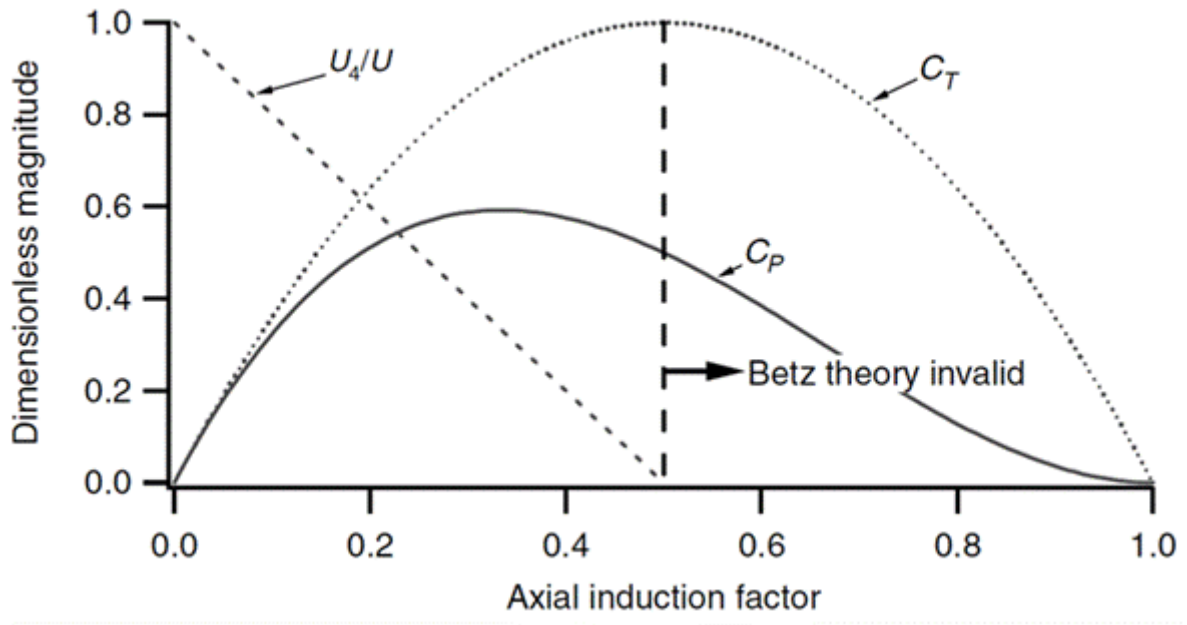

Figure 2.3: The variation in CP and CT with axial induction factor (Manwell et al., 2009)

2.2 Wake Rotation

The linear momentum theory assumes that there is no rotation of flow at the wake of the turbine. However, in reality flow exiting from the turbine has constant rotation and gradually moves downstream. The torque applied on the turbine by the air moving through it requires an equal and opposite torque imposed upon the air. This causes the air to rotate in the opposite direction of the turbine. As the air flow gains momentum, the air particles moving at downstream of the turbine consists of a velocity component not only in the axial direction but also in the tangential direction relative to the rotation of the turbine.

The existence of a rotational flow in the wake results in less energy being extracted by the turbine and as a result losses in kinetic energy occur. The most vulnerable wind turbines with large kinetic energy losses that cannot be recovered are those operating at low rotational speed and high torque (Eggleston & Stoddard, 1987). There are minimal losses however, for wind turbines which have a higher rotational speed and lower torque.

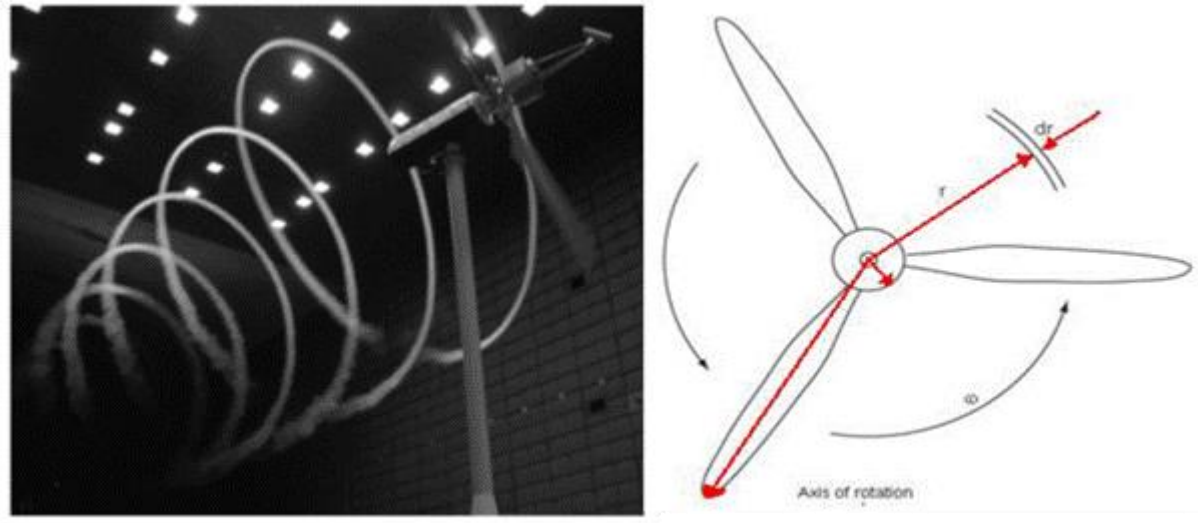

(a) (b)

Figure 2.4: (a) Wind Turbine Wake Rotation (b) Blade Element Length dr at a Radius r (Vermeer, Sørensen, & Crespo, 2003)

Since the tangential velocity is not the same for all radial positions, the axial induced velocity varies. In order for changes to occur for both the tangential and axial induced velocity components, we must consider an annular ring of rotor disc with a radius (r) and of a radial

width of(δr) is considered. It is also important to know that the angular velocity of the air relative to the blades increases from Ω to $\Omega + \omega$. Where Ω is the angular velocity of the turbine blade and ω is the angular velocity of the air flow in the wake.

The torque on the ring is equal to the rate of angular momentum of the air passing through the ring. Therefore:

$$torque = rate\ of\ change\ of\ angular\ momentum$$

$$torque = mass\ flow\ rate\ \times chnage\ of\ tangential\ velocity\ \times radius$$

$$\delta Q = p\delta A_d U_\infty (1-a) 2\Omega a' r^2 \tag{2.24}$$

The angular induction factor is defined as:

$$a' = \frac{\omega}{2\Omega} \tag{2.25}$$

The induced velocity at the rotor comprises of the axial component Ua and$r\Omega a'$. Therefore thrust can be expressed as:

$$dT = 4a'(1+a)\frac{1}{2}\rho\Omega^2 r^2 2\pi r dr \tag{2.26}$$

From linear momentum, the thrust of the rotor as a function of the axial induction factor is:

$$dT = 4a(1-a)\frac{1}{2}\rho U^2 2\pi r dr \tag{2.27}$$

Equating equation (2.26) and (2.27) yields:

$$\frac{a(1-a)}{a'(1+a')} = \frac{\Omega^2 r^2}{U^2} = {\lambda_r}^2 \tag{2.28}$$

The tip speed ratio is defined as the ratio of the blade tips speed to the free stream wind speed and is expressed as:

$$\lambda = \frac{\Omega R}{V_\infty} \tag{2.29}$$

2.3 Blade Element Theory (BET)

The Blade Element Theory is used to predict the forces acting on a blade through lift and drag forces generated at spanwise of the blade sections. In this theory the blade is divided into a number of sections in the spanwise direction. Each section of the blade is independent of the other and operates aerodynamically as a 2D aerofoil. Using the local flow condition, the aerodynamic forces are calculated on each aerofoil at every section of the blade. The sum of all forces at each section are then accumulated to calculate the forces and moments that are been exerted on the turbine blade. There are a number of assumptions taken into account for the blade element theory. It is important to consider that there is no aerodynamic interaction between each element of the blade allowing no radial flow. It is also assumed that the forces on the blades are only determined by the lift and drag characteristics of the aerofoil shape of the blade.

Figure 2.5 shows the sequence of the wind turbine blade divided into a series number of sections. For this particular wind turbine the blade is divided into 9 sections from the root to the tip of the blade at a radius of 0.5 metre.

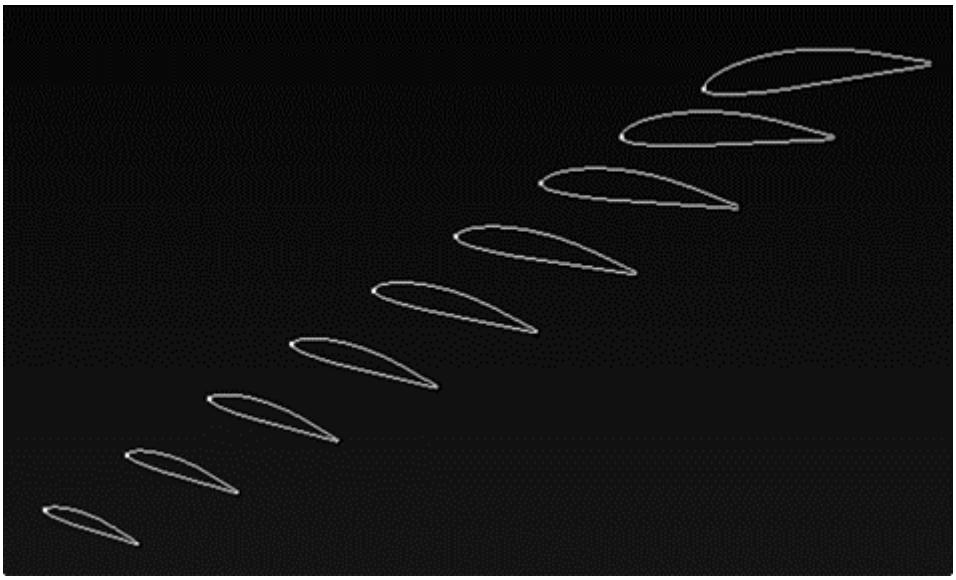

Figure 2.5: Aerofoil segments along blade radius

In order to calculate the relative wind velocity at a section of the blade, both the axial and tangential velocity are combined. The resultant velocity is then used to calculate the lift and drag forces of each blade section. From Figure 2.6, a section of the wind turbine with (N)

number of blades with a tip radius (R) and chord (c) is considered. Assuming that the blades are rotating at an angular velocity of Ω, Let U_∞ be wind the speed and angle ϕ is the angle between the relative wind speed and the plane of rotation.

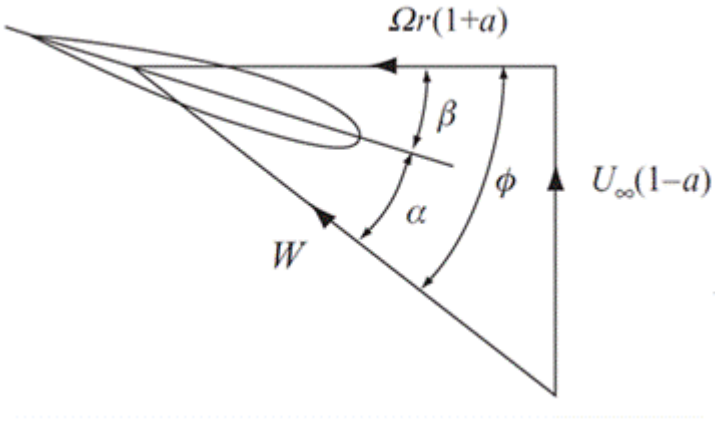

Figure 2.6: Velocities on blade element (Hansen, 2013)

From the diagram shown in Figure 2.6 the velocity vector is represented as:

$$U_A = U_\infty(1-a) \tag{2.30}$$

$$U_T = \Omega r(1+a') \tag{2.31}$$

Where:

$U_A = Axial\ \ velocity\ of\ the\ wind$

$U_T = Tangential\ velocity\ of\ the\ wind$

The relative wind velocity can then be given as:

$$W = \sqrt{(U_\infty(1-a))^2 + (\Omega r(1+a'))^2} \tag{2.32}$$

The angle at which the relative wind velocity coincides with the plane of rotation is given by:

$$\phi = tan^{-1}\left(\frac{U_\infty(1-a)}{\Omega r(1+a')}\right) = \frac{1-a}{(1+a')\lambda_r} \tag{2.33}$$

The angle of attack, which is defined as the angle between the chord line and the relative wind velocity and is given by:

$$\alpha = \phi - \beta \tag{2.34}$$

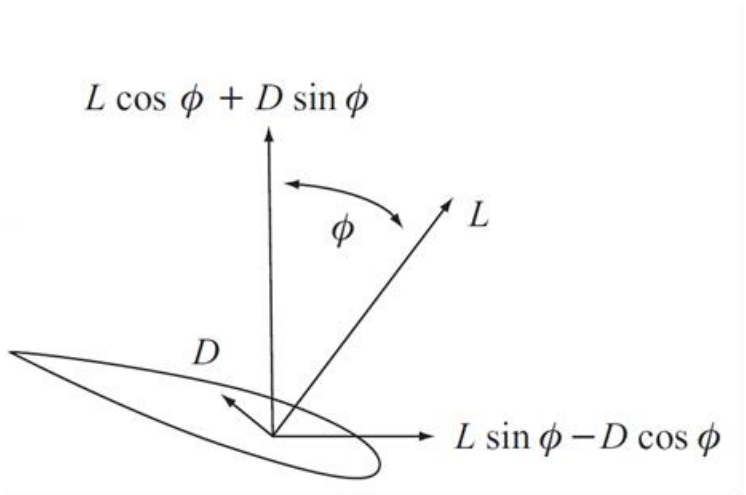

Figure 2.7: Forces on blade element (Hansen, 2013)

As lift is the force produced that is perpendicular to the relative wind velocity and drag is the force parallel to the relative wind velocity. The relative wind velocity is utilised to calculate each of this forces acting on the aerofoil.

The lift and drag forces are given as:

$$\delta L = \frac{1}{2} C_L \rho A W^2 c \delta r \tag{2.35}$$

$$\delta D = \frac{1}{2} C_D \rho A W^2 c \delta r \tag{2.36}$$

The lift and drag forces acting on the aerofoil as depicted in Figure 2.7 is broken down into two components. The first component is the force in the plane of rotation and the other being the force perpendicular to the plane of rotation. The forces in the plane of rotation yields the torque on the turbine and the forces perpendicular to the plane of rotation will result in thrust.

The forces in both the plane of rotation and perpendicular to the plane of rotation are given us:

$$\delta F_A = \delta L cos\phi + \delta D sin\phi \tag{2.37}$$

$$\delta F_T = \delta L sin\phi - \delta D cos\phi \tag{2.38}$$

2.4 Blade Element Momentum (BEM) Theory

Blade element momentum theory is a combination of the blade element theory and momentum theory. This theory lays the foundation for an iterative process that calculates the induced velocities and aerodynamic forces of a wind turbine. Although the BEM theory is used in many applications, there are limitations which are made in order to make the theory simpler. It is assumed that the airflow around an aerofoil will always be in equilibrium and that the flow will accelerate to adjust to the changes in vorticity at the wake region. The combination of equations (2.35) and (2.36) into equation (2.37) will result in total thrust of the turbine and is given as:

$$\delta T = \frac{1}{2}\rho U_{rel}^2 Bc(C_L cos\phi + C_D sin\phi)dr \tag{2.39}$$

Like thrust, the total torque can be found by also combining equation (2.35) and (2.36) into (2.38) and this is given as:

$$\delta Q = \frac{1}{2}\rho U_{rel}^2 Bc(C_L sin\phi - C_D cos\phi)rdr \tag{2.40}$$

If we consider thrust to be the rate of change of linear momentum of the flow passing through an annulus at radius r of width dr and a tip loss factor of F, thrust is expressed as:

$$dT = 4\pi\rho r U^2 a(1-a)Fdr \tag{2.41}$$

As mentioned previously, torque is equal to the rate of change of angular momentum, with tip loss correction factor is given as:

$$dQ = 4\pi\rho r^3 U a'\omega(1-a)Fdr \tag{2.42}$$

In order to obtain the values of both the induction factors a and a', an iterative process using equation (2.41) and (2.42) must be solved. The right hand side of the equation below is evaluated using existing values of the flow induction factors. To solve for both the axial (a) and tangential (a') velocities we utilise equation (2.33) into both the torque and thrust equations. This will gives us:

$$\frac{a}{1-a} = \frac{\sigma(C_L + C_D tan\phi)}{4Ftan\phi sin\phi} \tag{2.43}$$

$$\frac{a'}{1+a'} = \frac{\sigma(C_L + C_D tan\phi)}{4Ftan\phi sin\phi} \tag{2.44}$$

The blade solidity (σ) is defined as the total blade area divided by the rotor disc area and is equal to:

$$\sigma = \frac{Bc}{2\pi r} \tag{2.45}$$

It is important to note that the BEM theory can only be applied if the blades have uniform circulation, that is if a is uniform. For a non-uniform circulation there is a radial interaction and exchange of momentum between flows through adjacent elemental annular rings.

2.4.1 Power and Torque

The extrapolation of both the power and torque depends on the flow induction factors. This can be obtained from the above equation of (2.43) and (2.44). The process of determining the induction factors is usually carried out through an iterative process. This iterative process is initiated by assuming both the induction factors (a) and (a') to be zero. The first iterative process results in determining(ϕ), (C_P) and (C_D). This process is repeated many times until convergence is reached. Figure 2.8 shows a typical performance curve for a modern high tip speed ratio wind turbine. The graph illustrates that the maximum power coefficient occurs at a tip speed ratio of about 7. This corresponds to an axial induction factor that is closer to a value of $\frac{1}{3}$.

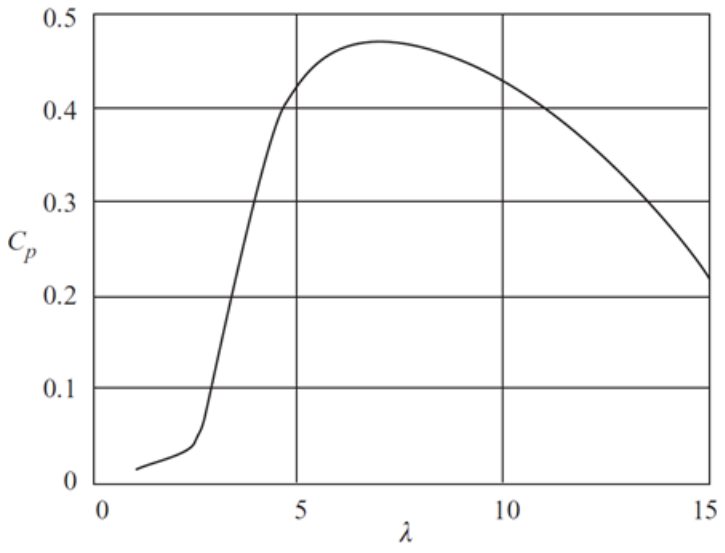

Figure 2.8: Performance curve of wind turbine blade (Jamieson, 2011)

2.4.2 Blade Geometry

An important design feature of a wind turbine is the blade geometry as it is responsible for the extraction of kinetic energy from the wind. Optimising wind turbine blades is to maximise power output and efficiency. An optimal blade design is influenced by many factors such as its mode of operation. It is essential to determine whether the turbines would be operating as a fixed rotational speed or variable rotational speed, depending on the terrain.

For a high tip speed ratio wind turbine, the geometry of the blade would require a long, slender blade. However, a low tip speed ratio wind turbine would be the opposite. It requires a short, thicker blade. Wind turbines cannot always operate at optimum tip speed ratio all the time but for a range of wind speeds, the turbines operate at different tip speed ratios. If the wind turbine were to operate at a tip speed ratio other than the optimum tip speed ratio, then the performance of the turbine would significantly be less than the optimum performance for which the turbine is designed for.

To determine the distribution of the cross-sectional shape on the blade, a number of design parameters are required to satisfy the requirements of the BEM theory equation. Design parameters such as: tip speed ratio, the desired number of blades, the radius of the blade and an aerofoil for which the lift and drag characteristics are known as a function of angle of attack. Once these parameters are selected, it will result in the extrapolation of chord distribution and twist distribution of a blade which closely resembles the Betz limit power production ideal blade. If we assume that the axial and angular induction factors are a function of the radius(r), from equation (2.27), applying the conservation of linear momentum, we can further express thrust as:

$$dT = \rho U^2 4a(1-a)\pi r dr \tag{2.46}$$

The design goal of any wind turbine blade, even though it is impossible, is to try and replicate the Betz limit power production. To achieve Betz limit, the axial induction factor (a) must be equal to $\frac{1}{3}$. Therefore it is assumed that the axial induction is factor (a) is equal to $\frac{1}{3}$. By substituting the value of the axial induction factor (a) into equation (2.46), the result becomes:

$$dT = \rho U^2 4\left(\frac{1}{3}\right)\left(1-\frac{1}{3}\right)\pi r d = \rho U^2\left(\frac{8}{9}\right)\pi r dr \tag{2.47}$$

From equation (2.39), If we assume that (C_D) is equal to zero, the equation becomes:

$$dQ = \frac{1}{2}\rho U_{rel}^2 Bc(C_L sin\phi) r dr \tag{2.48}$$

The relative velocity can be expressed in terms of other variables and is given us:

$$U_{rel} = \frac{U(1-a)}{sin\ \phi} = \frac{2U}{3sin\phi} \tag{2.49}$$

Determining the performance of wind turbine blades requires the combination of momentum theory and blade element theory equations. By equating equation (2.47) and (2.48) and utilising equation (2.49), this yields:

$$\frac{C_L Bc}{4\pi r} = tan\phi sin\phi \tag{2.50}$$

To solve for the geometrical shape of the blade, we must first consider that equation (2.33) which relates to both axial induction and tangential factor. If we assume $(a = \frac{1}{3}\ and\ a' = 0)$ then equation (2.33) becomes:

$$tan\phi = \frac{2}{3\lambda_r} \tag{2.51}$$

Where $\lambda_r$is the tip speed ratio at fraction of rotor radius $(^r/_R)$.

Substituting equation (2.51) into (2.50) yields:

$$\frac{C_L Bc}{4\pi r} = \left(\frac{2}{3\lambda_r}\right) sin\phi \tag{2.52}$$

Rearranging equation (2.51) and (2.50), we solve now for both the angle relative to the wind and the chord distribution along the radius of the blade.

$$\phi = tan^{-1}\left(\frac{2}{3\lambda_r}\right) \tag{2.53}$$

$$c = \frac{8\pi r sin\phi}{3BC_L\lambda_r} \tag{2.54}$$

B= Number of blades

C_L= Lift coefficient

Both equations of (2.53) and (2.54) can be utilised to solve for the twist distribution and chord distribution for a given angle of attack which corresponds to the highest lift to drag

ratio. Figure 2.9 and Figure 2.10 illustrate the optimum chord and twist distribution for a particular wind turbine in a non-dimensional form respectively. It is worth noting that the chord at the root is significantly higher than at the tip. This enables the turbine to generate more talk at the root thus provide more power. Due to many factors, such as increase cost and fabrication difficulty, the optimum chord values at the root cannot be achieved and therefore an alternative method is employed counter this problem. This will be further explained in Chapter 3. The twist distribution in Figure 2.10 shows that the twist at the root is significantly high. This would represent a great deal of complexity in the manufacturing process. Therefore the twist at the root would need to be decreased to a more reasonable value that would not complicate the manufacturing of the blade.

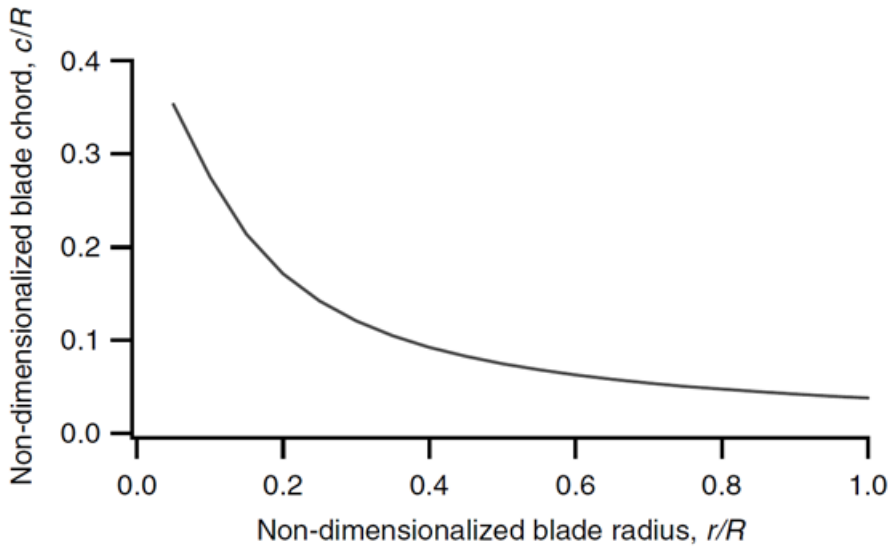

Figure 2.9: Optimum chord distribution of wind turbine blade (Manwell et al., 2009)

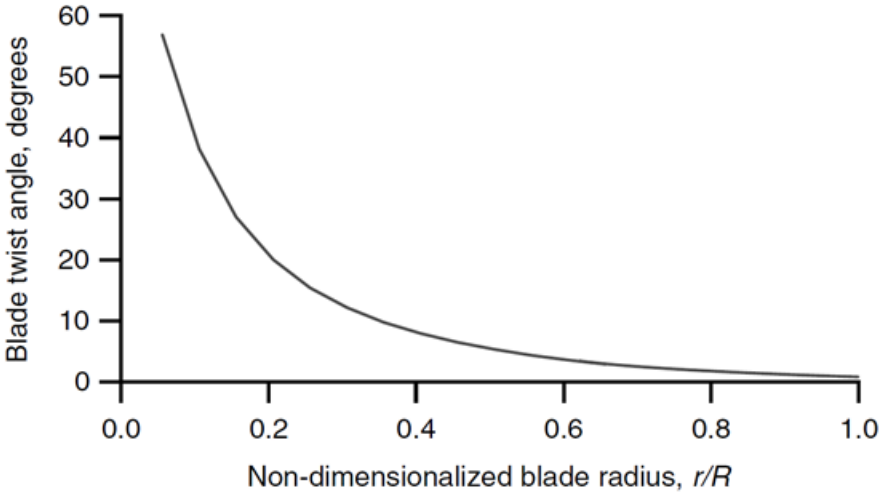

Figure 2.10: Optimum twist distribution wind turbine blade (Manwell et al., 2009)

2.5 Tip Loss Correction

The losses which occur at the tip of the blade cannot be ignored. The losses at the tip occur as a result of the pressure difference that is present between the lower surface of the aerofoil and the upper surface of the aerofoil. The air particles generally have a tendency to move from the high pressure region to the lower region. At the tip of the blade this phenomenon takes effect and generally creates a vortex which dissipates into the wake. As a result of this vortex created at the tip there are losses in the overall power output of the blade.

In BEM theory, there are a number of methods which are applied to account for the losses. The most widely used method is the Prandt method which introduces a tip loss correction factor. The correction factor is a function of the angle relative to the wind, number of blades and also the position of the blade. As the circulation of flow varies from root to tip, the tip loss correction factor allows us to understand the reduction in forces along the blade. Figure 2.11 shows the tip loss factor of the radial blade from root to tip.

The tip loss correction factor varies from 0 to 1. From the root of the blade to about 85 per cent of the blade radius, a constant factor of 1 is maintained. However, at the tip the tip loss factor sharply decreases as it approaches the tip. This corresponds to the fact that the induction factor increases dramatically near the tip. As a result the relative wind speed for a given blade section decreases as well as the angle of attack. This means the lift and drag forces generated at the tip must also decrease as they are a function of relative wind speed and angle of attack.

The tip loss correction factor developed by Ludwig Prandt is given as:

$$F_T = \left(\frac{2}{\pi}\right) cos\left[exp^{((\frac{N}{2})(1-u)/(u))\sqrt{1+(\lambda u)^2/(1-a)^2}}\right] \tag{2.55}$$

Tip losses is not the only losses which a wind turbine experiences. Like the tip of the blade, losses at the root of the blade also take place in a similar manner as that described for the tip. The root loss correction is given as:

$$F_R = \left(\frac{2}{\pi}\right) cos\left[exp^{((\frac{-N}{2})(u-u_R)/(u))\sqrt{1+(\lambda u)^2/(1-a)^2}}\right] \tag{2.56}$$

Where u_R is the normalised root radius.

If equation is (2.54) termed $f_T(r)$ then the complete tip/root loss factor is given as:

$$f(u) = f_T(u) f_R(u) \tag{2.57}$$

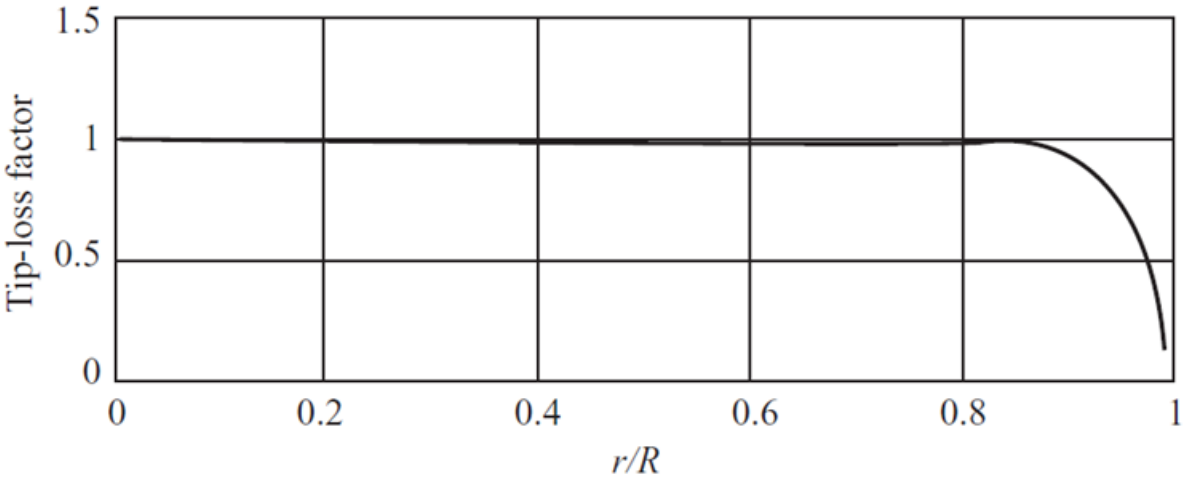

Figure 2.11: Span variation of the tip loss factor of a wind turbine blade (Manwell et al., 2009)

2.6 BEM Algorithm Flow Chart

Figure 2.12 shows the iterative process involved in the BEM theory. Initially, both the axial and tangential induction factors are assumed zero. The flow angle is then calculated. This is the angle at which the relative wind velocity coincides with the plane of rotation. Using the flow angle local angle of attack can be determined. In the BEM theory, the blade is divided into number segments and these segments are independent of each other and analysed individual. Based on the 2D aerofoil type selected, both the lift coefficient and drag coefficient can be determined. The forces on each segment of the blade along the span are summed up to calculate the forces and moments subjected on the turbine.

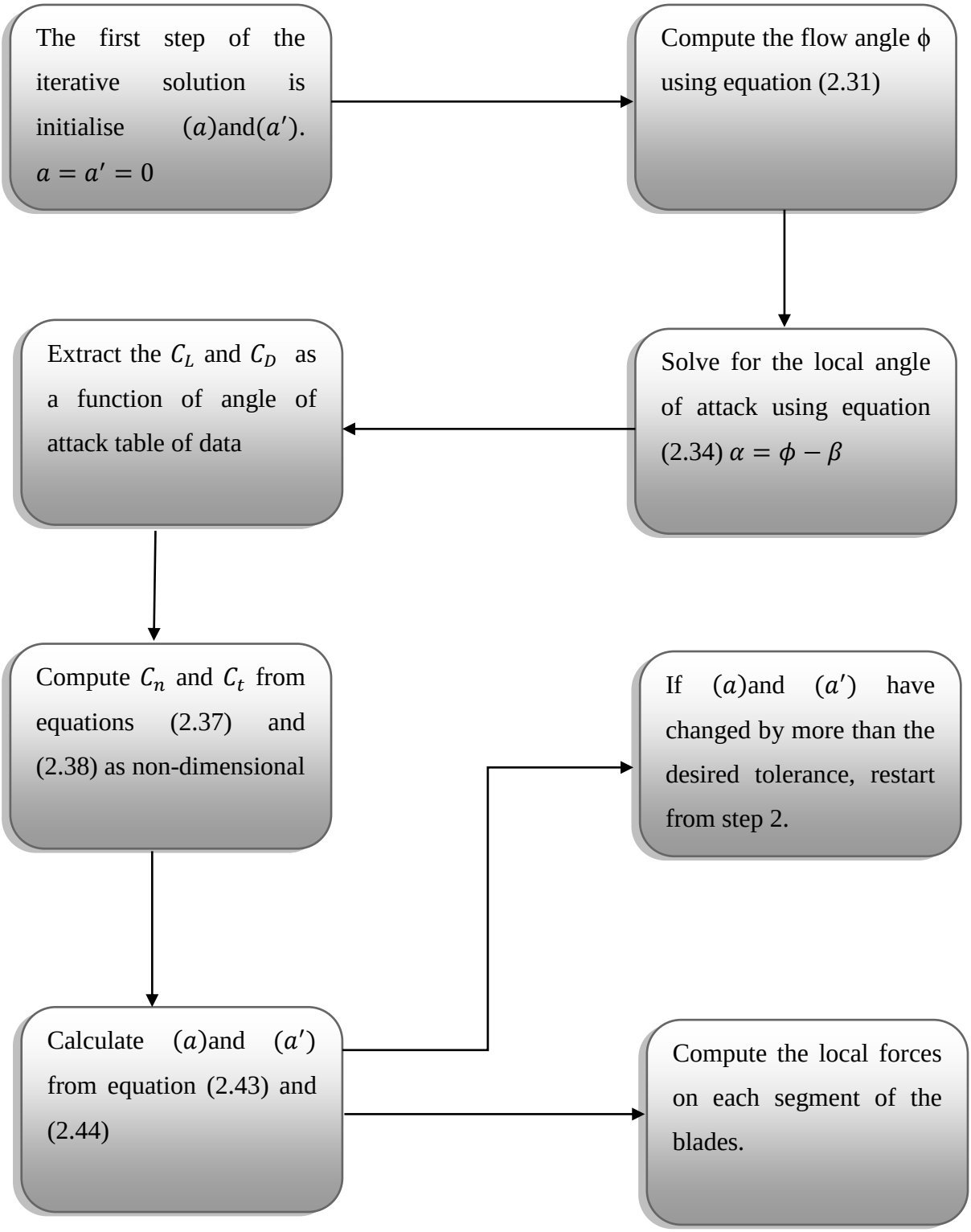

Figure 2.12: BEM Flow Chart

CHAPTER 3

AERODYNAMICS DESIGN OF WIND TURBINES

The design of wind turbine is an interdisciplinary process that involves many engineering disciplines such as Structures, Aerodynamics and Power systems, etc. The primary focus of this research is on the aerodynamic aspects of the wind turbine design.

The single most important component of wind turbine design is the rotor blade design which relies heavily on the principles of aerodynamics. Horizontal Axis Wind Turbines (HAWT) utilise the generation of lift on aerofoils to produce torque that causes the blades to rotate. Aerofoil selection plays a major role of wind turbine blades as it defines the geometry of the blades as well as its power extraction capabilities. Different aerofoils have different characteristics of lift and drag coefficients. These parameters are largely affected by the Reynolds number at which the turbines are operating

$$\left(\mathrm{Re} = \frac{\rho u l}{\mu} \right) \tag{3.1}$$

For large commercial wind turbines, the Reynolds number is significantly higher than small wind turbines at the same wind speed and tip speed ratio. Other design parameters which have significant level of influence on the efficiency of the blades include is the chord

distribution (how the chord varies with the radius of the blade from root to tip), twist distribution and tip speed ratio (TSR).

3.1 Aerofoil Aerodynamics

As mentioned previously, wind turbine blade heavily relies on the aerodynamic principle of lift to produce torque on the blade which induces a rotational motion. The geometrical shape and cross section of wind turbine blades is defined by the distribution of aerofoils radially. At each blade segment, an aerofoil is stationed with the respect to its chord length. This ultimately defines the cross sectional shape of the blades. The aerodynamic forces and moments which arise as a result of the interaction that occurs between the air or fluid and a solid body, is primarily due to two basic elements in the form of pressure distribution and shear stress distribution. The pressure distribution acts normal or perpendicular to the surface and the shear stress distribution acts tangential to the surface. The pressure variation is mainly due to the changes experienced in air velocity. This can be explained using Bernoulli's principle, which states that the sum of static and dynamic pressure is constant. This is expressed as:

$$P_s + \frac{1}{2}\rho V^2 = P_T \qquad (3.2)$$

Where P_s is the static pressure, P_T is total pressure, ρ is the density of the air and V is the local velocity along the aerofoil surface.

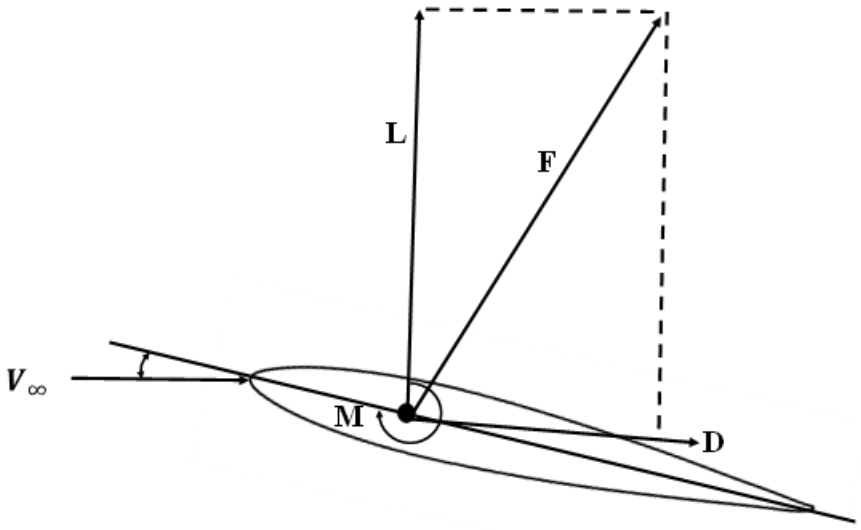

Figure 3.1: Lift and Drag forces on two-dimensional aerofoil

The pressure force exerted above and below the surface varies with changing angle of attack. The pressure differential produces a net force and moment on the aerofoil as shown in Figure 3.1. The net force generated is comprised of two components, lift and drag. Lift is the force component of the net force exerted on the aerofoil which acts perpendicular or normal to the flow direction. Drag, however is the force that resists the motion of an object and that is parallel to the direction of the flow. The magnitude of this forces largely depend on many parameters such as, for a 3D case, the projected area of an object moving through a fluid and velocity. The lift and drag forces are expressed as:

$$L = \frac{1}{2}\rho V^2 A C_L \tag{3.3}$$

$$D = \frac{1}{2}\rho V^2 A C_D \tag{3.4}$$

Where ρ is the density of the fluid, A is the projected area and V is the free stream velocity. The variables of C_D and C_L are a non-dimensional terms that both relate to the characteristics of lift and drag. Both of these terms are dependent on speed and angle of attack. As the angle of Attack increases, the lift force increase and consequently drag also increases. The drag force is not just the result of pressure difference of a body immersed in a fluid. Frictional drag, which is a function of viscosity, also has a significant contribution to the overall drag acting on a solid body.

3.2 Geometry Blade Design

In order to achieve the desired blade shape, a number of parameters have been considered in the design process in this research. The main objective in the design process is to produce a turbine blade that is capable of operating at low wind speeds in built up areas and optimise the aerodynamic performance of the turbine with minimal cost addition into the manufacturing. A wind turbine blade is measured by its performance levels in extracting energy from the wind. Ideally, an optimum blade is preferred but because of the manufacturing cost and the level of difficulty in involved in manufacturing the optimum shape of the blade, we have adopted a linear blade shape. This is further explained in this chapter.

The aerofoil selection is an important step that determines the characteristics of a wind turbine blade. Aerofoils come in many shapes and sizes in terms of camber and thickness to chord ratio. In comparison to aeronautical applications, aerofoils which are specifically

designed for wind turbines are very few in numbers especially for small wind turbines. The most common aerofoils used today for large commercial wind turbines are the National Renewable Energy Laboratory (NREL) aerofoil series. As for small wind turbines, there are a handful of aerofoils that are specifically designed for small wind turbines.

The series of aerofoil considered for this research comes from SG aerofoil family which is designed by Professor Michael Selig and Phillipe Giguere of the University of Illinois at Urbana Champaign. In general, large wind turbine blades are comprised of more than one aerofoil along the entire length of the blade. This is done so to accommodate both the structural and the aerodynamics aspects of the blade. The cross section thickness of the blade tends increases from the tip to the root. However, for small wind turbines, the blade is designed using only one aerofoil through the entire length of the blade. Although large and small horizontal axis wind turbines are very much identical in nature, the difference lies purely in the turbines operating environment. As mentioned earlier in this chapter, large commercial wind turbines operate at a very high Reynolds number compared to small wind turbines which operate at a low Reynolds number. Because of the low Reynolds number at which small wind turbines operate, it is not ideal to make the root of the blade very high in thickness. Although it is desirable from a structural perspective to make the aerofoil thickness at the root bigger, this would ultimately dampen the aerodynamic performance of the turbine (Wood, 2011).

The aerofoils designed by both professor Selig and Giguere were selected based on their high performance at low Reynolds number. Six different aerofoils from the SG family were considered in the design with each having its unique lift and drag characteristics. The main objective in selecting a suitable aerofoil is to find a balance between the aerodynamics performance and the structural needs of the turbine. The SG6040 and SG6050 have a thickness to chord ratio (t/c) of 16% and a camber of 2.5 and 2 respectively as shown in Table 3.1. Due to their high thickness to chord ratio (t/c), both of these aerofoils are suitable for designers which place a lot of emphasis on the structural strength of the blade at the root. The centrifugal load that small wind turbine blades are subjected to at very high rotational speeds is quite significant which makes the SG6040 and the SG6050 aerofoil as good candidates. In order for any wind turbine blade to be reliable, efficient and most importantly safe, especially for small wind turbines which are located at close proximity in residential areas, it is important to accommodate the structural aspects of the blades without compromising the aerodynamics performance.

Table 3.1: SG aerofoil family

Aerofoil	Thickness (t/c) (%)	Camber (%)	Design C_L	Design Reynolds Number (Re)
SG6040	16	2.5	1.1	200,000
SG6041	10	2	0.6	500,000
SG6042	10	3.8	0.9	333,333
SG6043	10	5.5	1.2	250,000
SG6050	16	3.3	1.1	250,000
SG6051	12	3.2	1.2	450,000

From the table above, the SG6041, SG6042 and SG6043 have the same thickness chord ratio but however their design lift coefficient and camber varies. Although these aerofoils provide us with a very low thickness to chord ratio (t/c) that is very much desired for aerodynamic performance, it would present significant problems at the root of the blade where the loads acting on the blade are most critical and thus requires a higher thickness chord ratio aerofoils. A schematic diagram of the SG family aerofoil is illustrated in Figures 3.4 and 3.5 to show how the thickness to chord ratio (t/c) and camber differ on each aerofoil. The choice of aerofoil for the wind turbine of this project ultimately came down to the SG6051. Its 12% thickness to chord ratio (t/c) is sufficiently enough at the root to support the centrifugal loads. The outer section of the blade which is critical for the aerodynamic performance will also utilise the SG6051. The SG6051 was particularly chosen as it satisfies the main objectives of this project of providing adequate strength at the root without compromising the aerodynamic performance of the blade.

Figure 3.2 shows the lift coefficient characteristics of the SG6051 aerofoil as a function angle of attack (AoA) for various Reynolds numbers. An optimum angle of attack of 5.7° which corresponds to the highest lift to drag ratio of the aerofoil is chosen for the design of the blade. The lift coefficient at an optimum angle of attack is found to be 0.90 as shown Figure 3.3. This is utilised to define the optimum twist for best aerodynamic performance of the blade. Once the optimum angle of attack and the best lift coefficient are known, we can determine how the chord will vary with radius.

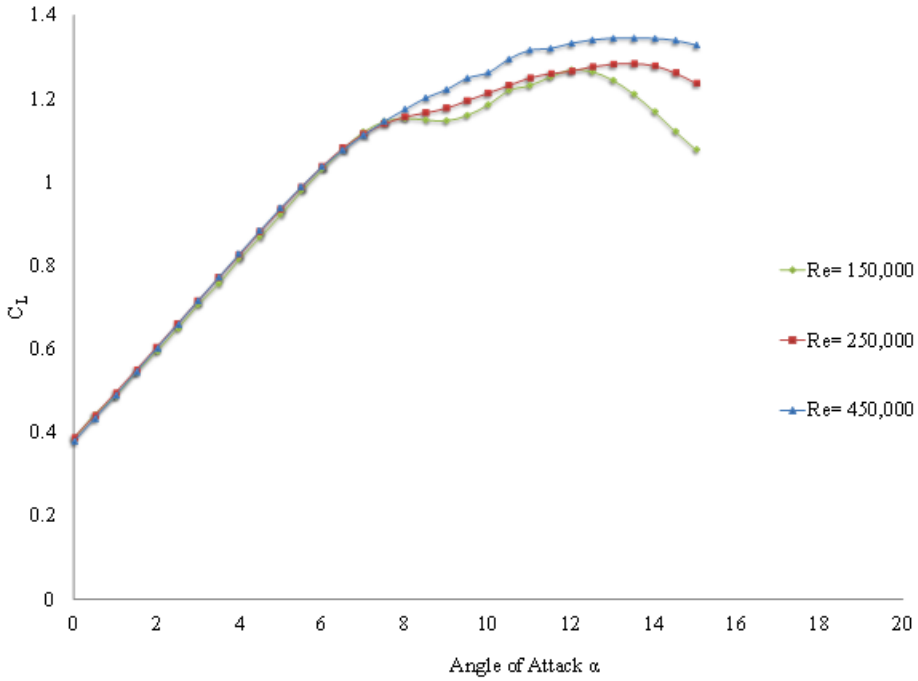

Figure 3.2: Lift coefficient characteristics of SG6051 aerofoil at various angle of attack (AoA) and Reynolds number (UIUC, 2012)

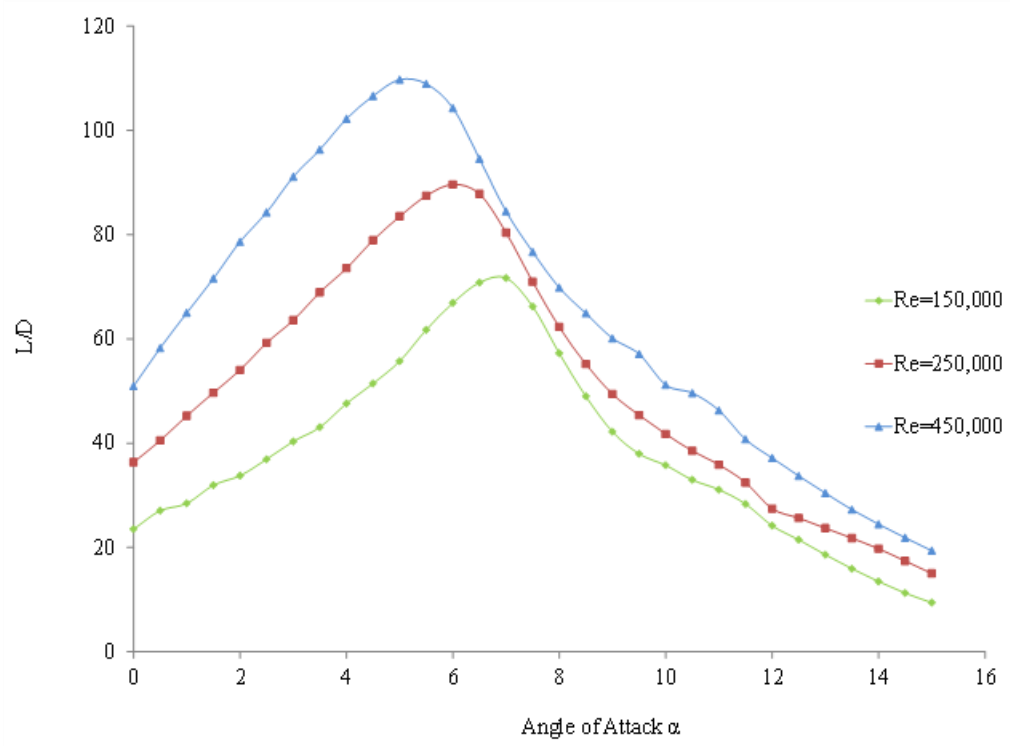

Figure 3.3: Lift to drag ratio (L/D) characteristics of SG6051 aerofoil at various angle of attack (AoA) and Reynolds number (UIUC, 2012)

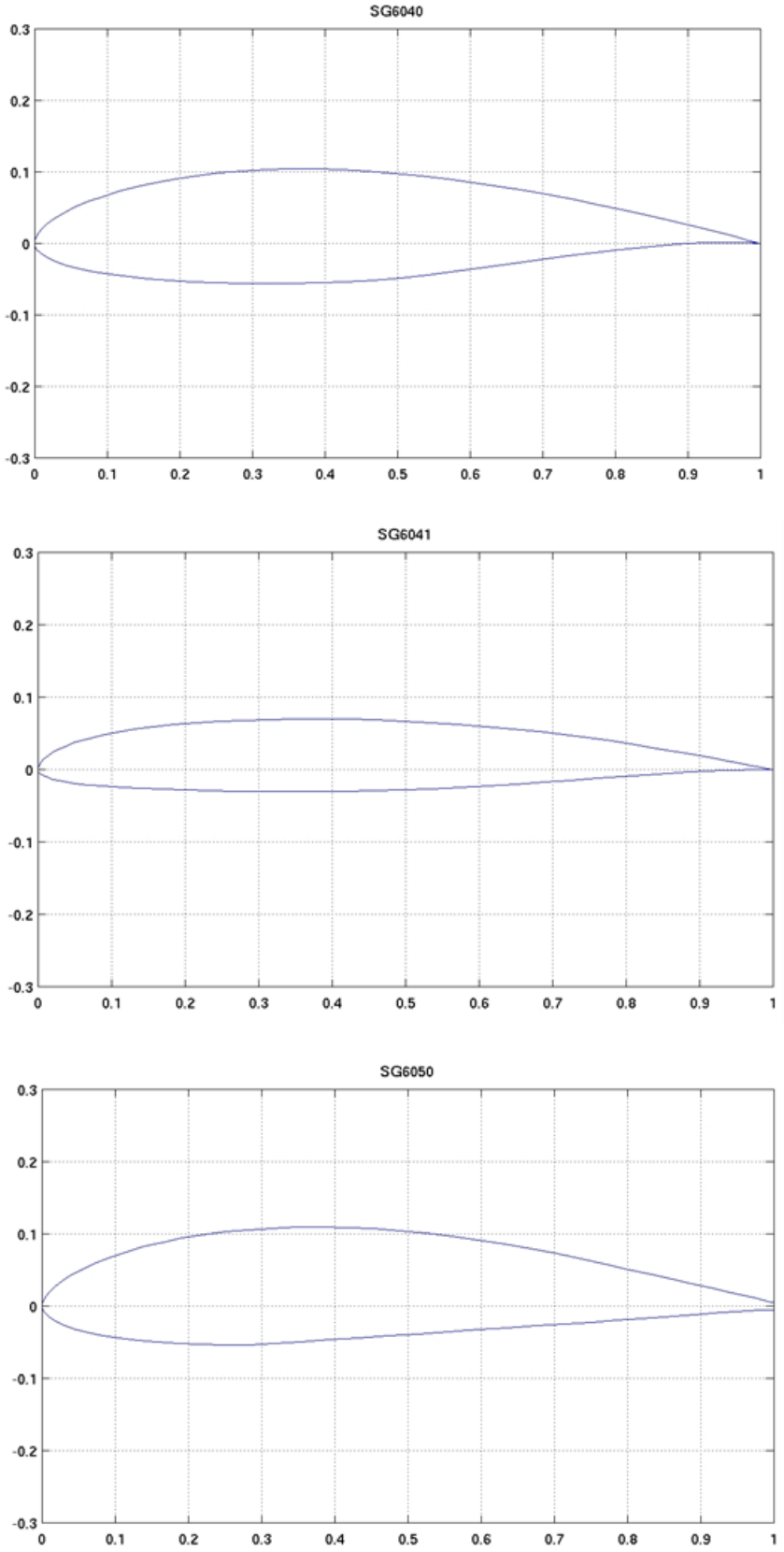

Figure 3.4: SG aerofoil family (UIUC,2012)

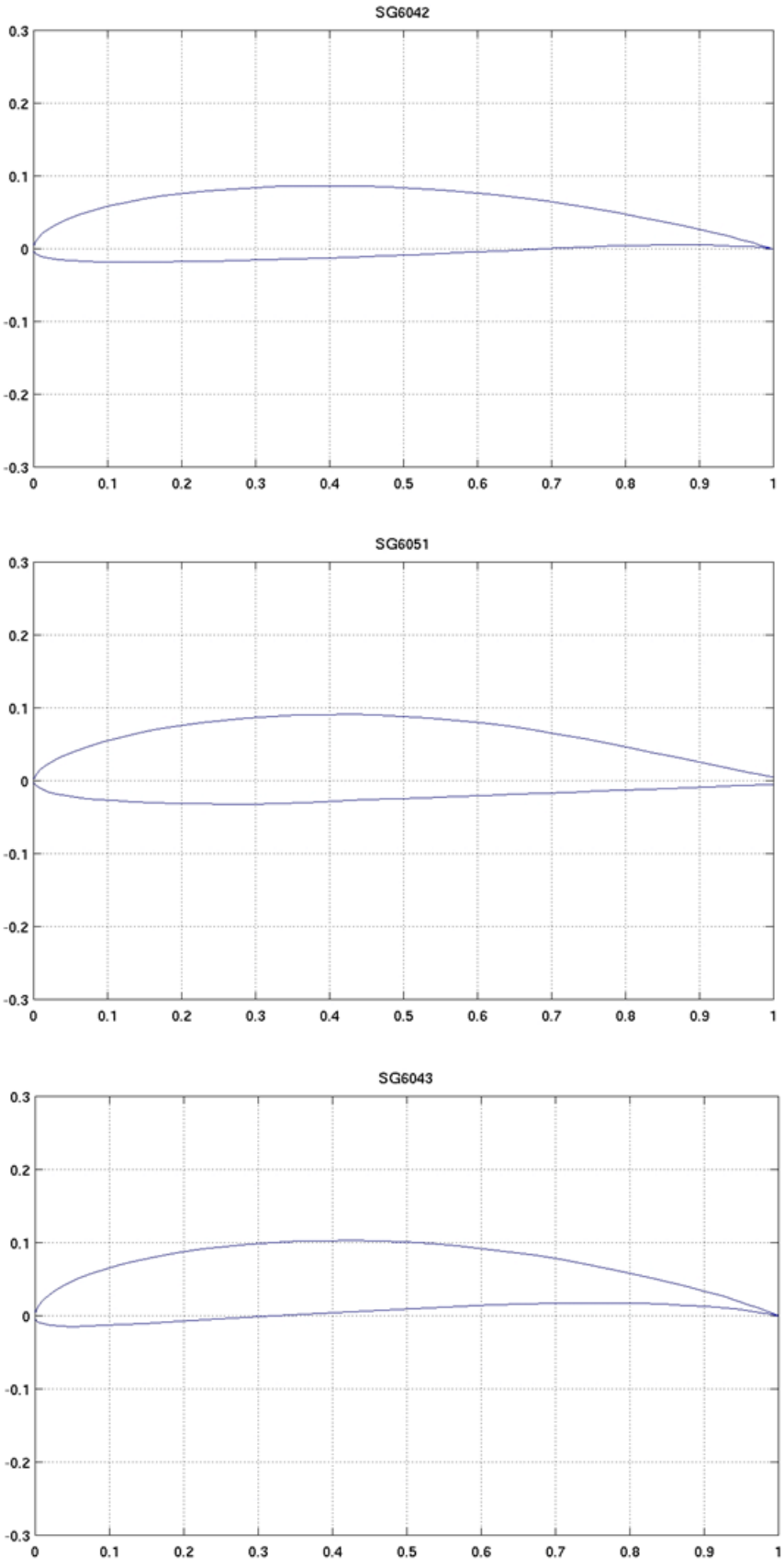

Figure 3.5: SG aerofoil family (UIUC,2012)

3.2.1 Number of Blades

The performance of wind turbines is influenced by many factors and the number of blades integrated in to the system is one of them. The blade number not only affects the solidity ratio of the blade but also the tip speed ratio (TSR). Solidity ratio, which is the ratio of the planform area of the blade and the swept area of the blade, influences the tip speed ratio. A high solidity ratio turbine indicates that there are more blades on the system. This is commonly utilised for low tip speed ratios that require high starting torque. On the other hand, a lower solidity ratio will generate low starting torque. The majority of small horizontal axis wind turbines have a high tip speed ratio and a low solidity ratio.

Generally three bladed design of wind turbines are the most commonly used system both commercially and domestically. The three bladed wind turbines provide a better stability considering that the turbines have to be placed at minimum 10 metres above the ground. As well as a greater stability provided by the three blade design configuration, it is also considered that the aesthetics aspect of a three bladed wind turbine is less disturbing visually. Other important issues that need to be considered in relation to how many blades a wind turbine can have are the environmental impact. This is especially important for small wind turbines used in built up areas.

Figure 3.6 illustrates the influence that the number of blades has on the overall power coefficient. The power increases as a result of increasing the blade from one to two. The percentage increase in power from one blade to two blades is 10 per cent while also increasing the blade number from two to three will increase the power by 3 to 4 per cent. Utilising a four bladed wind turbine will increase the power by 2 per cent compared to the conventional three bladed wind turbines (Hau, 2005). Although there is a 2 per cent power gained by increasing the blade from three to four, the additional weight and cost added to the system is far greater and therefore the three blade configuration is considered as the optimum design configuration for this study.

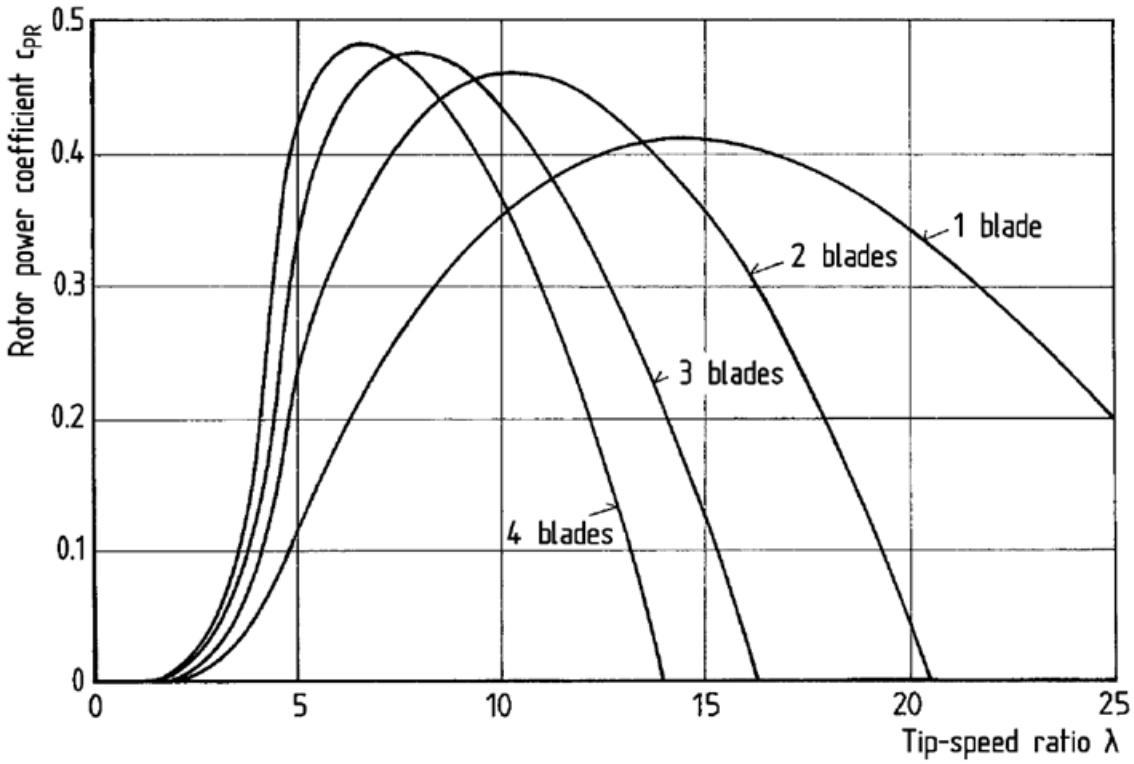

Figure 3.6: Power coefficient and tip speed ratio for different number of blades (Hau, 2005)

3.2.1.1 Blade Radius

The determination of blade radius is fundamental as it significantly affects the power which is proportional to the swept area of the wind turbine. Small wind turbines are generally classified as those having a turbine swept area of less than $200m^2$ which correspond to a rated power of around 50kW (IEC, 2011). For this study, the blades have been designed to have a radius of 0.5 metres. Due to the restriction of space in the wind tunnel test section, the radius was kept at 0.5 metre for all three different designs of the blade.

3.2.1.2 Tip Speed Ratio

The tip speed ratio is an important design parameter commonly used to determine the performance of wind turbines. It is defined as the ratio of rotational tip velocity to the free stream wind as described in equation (2.27). Different wind turbines have different tip speed ratios at which maximum power is achieved.. In determining the blade planform, which is the distribution of chord with radius, the tip speed ratio is an important parameter which governs the variation of the chord from root to tip.

Figure 3.7 shows the power coefficient as a function of tip speed ratio for different rotors. The drag type rotors have a low tip speed ratio compared to the more modern wind turbines. Because of their low power coefficient value, the drag type rotors (VAWT) are not considered as efficient as the lift based rotors. Therefore, it is apparent that the one bladed wind turbine configuration operates at a high tip speed ratio than a three bladed configuration wind turbine.

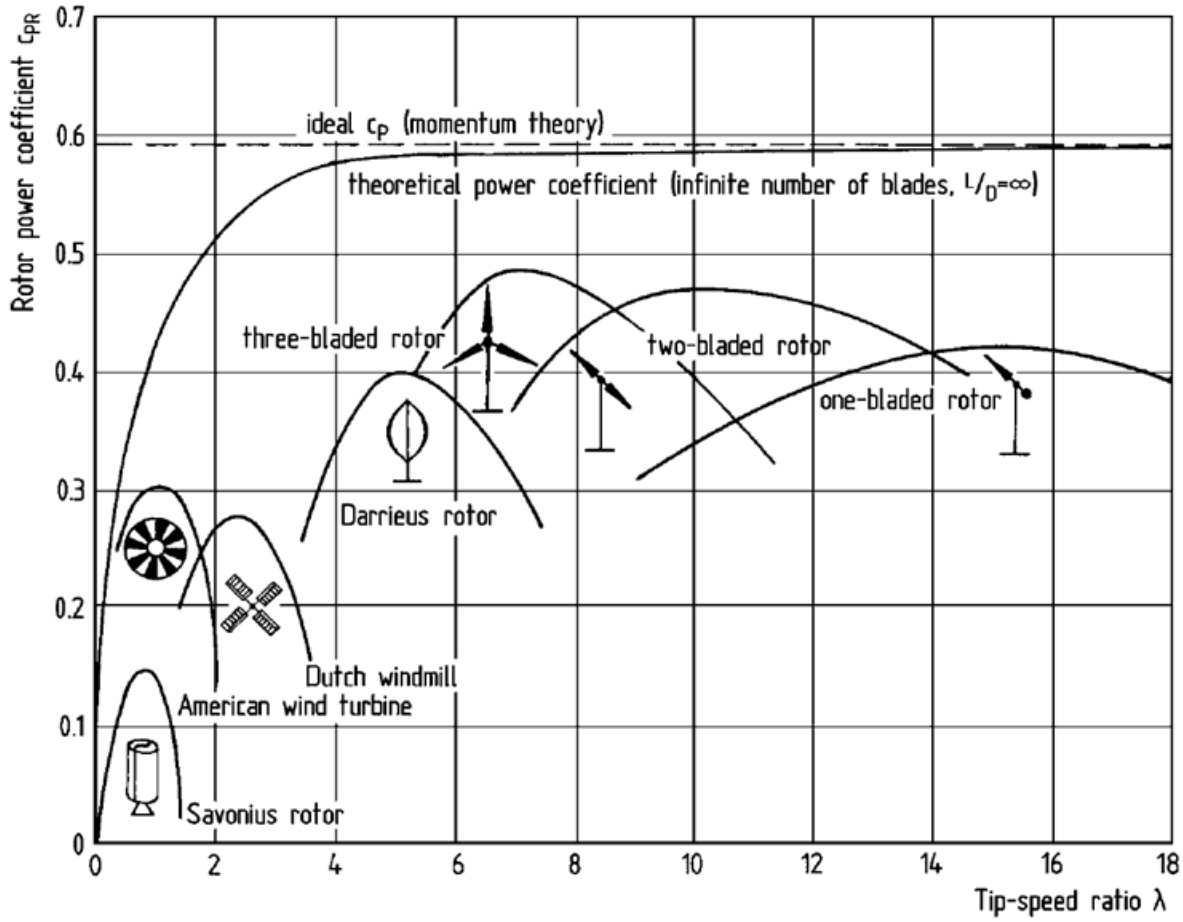

Figure 3.7: Power coefficient of different wind turbine design configuration (Hau, 2005)

.

3.2.2 Chord Distribution

The Chord distribution of the blade is influenced by the tip speed ratio and the optimum lift coefficient which heavily depends upon the type of aerofoil selected. Changing the chord distribution can also affect the axial induction factor (a) as well as the Reynolds number. Small wind turbines have a very short chord length at the root which is primarily used to measure the Reynolds number. The effective aerodynamic area of the blade that is primarily responsible for the majority of kinetic energy extracted from the wind is the outer portion of the blade from a sectional radius of 0.5 to 1. However, as mentioned earlier, the inner section of the blade is generally designed for structural stability as they are relatively insignificant in extracting energy. Figure 3.8 shows both the optimum chord and linear chord distribution along the entire length of blade for the designed blade used in this study. Due to the difficulty involved in the manufacturing process of an optimum chord distribution, a linear chord is adopted in this research instead with greater emphasis put on the outer region of the blade, since the outer section of the blade plays a pivotal role in the extraction of energy. The linear chord is closely matched to the optimum chord only in that region which would yield maximum power for a given operating condition.

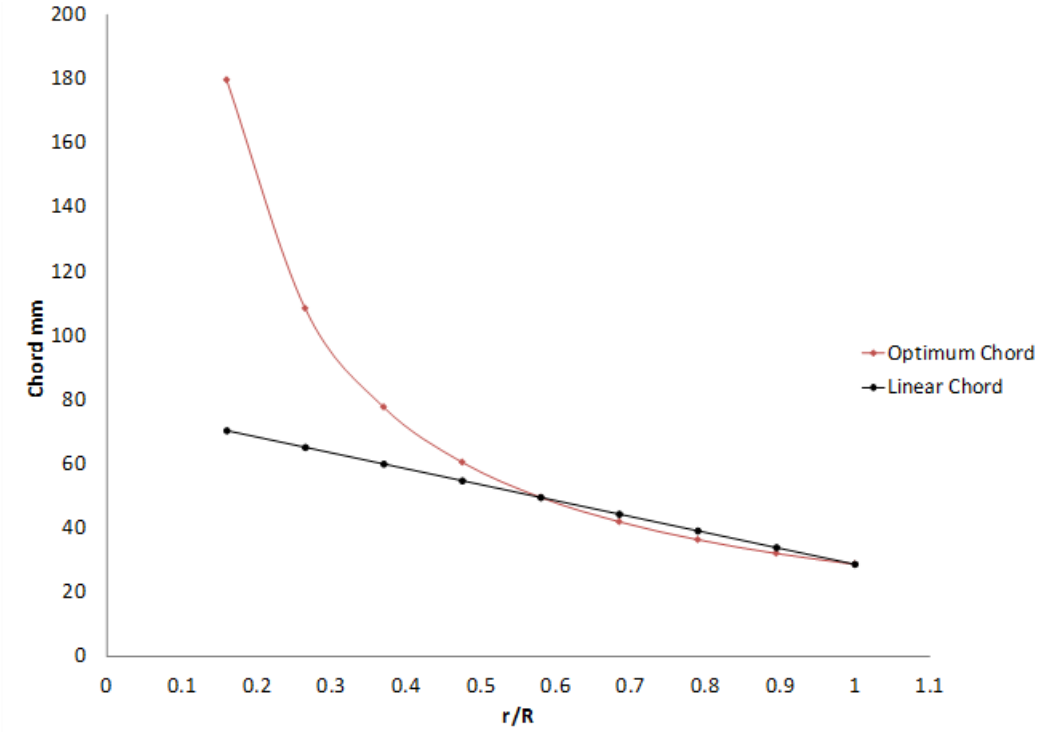

Figure 3.8: Optimum chord and linear chord distribution of 0.5 metre radius wind turbine blade

3.2.3 Twist Distribution

A wind turbine has different rotating speeds at each point along the length of the blade. When compared to the root, the tip section of the blade has the highest rotational speed since it generates a bigger circumference than the point at the root section. As a result of the rotational speed being higher at the tip, the effective flow velocity will no doubt increase from the root to the tip. In order to achieve an optimum twist distribution, the optimum angle of attack of the aerofoil SG6051 and tip speed ratio are utilised as both are critical parameters which define the profile of the blade. Adding twist to a wind turbine, which decreases from the root to the tip, is critical in order to optimise the angle of attack along the entire length of the blade for maximum power output. In addition to optimising the angle of attack, the blade is greatly twisted at the root to increase the torque generated at the root. Figure 3.9 shows the optimum twist distribution that has been determined for the designed blade. The twist variation from the root to the tip is illustrated in Figure 3.10.

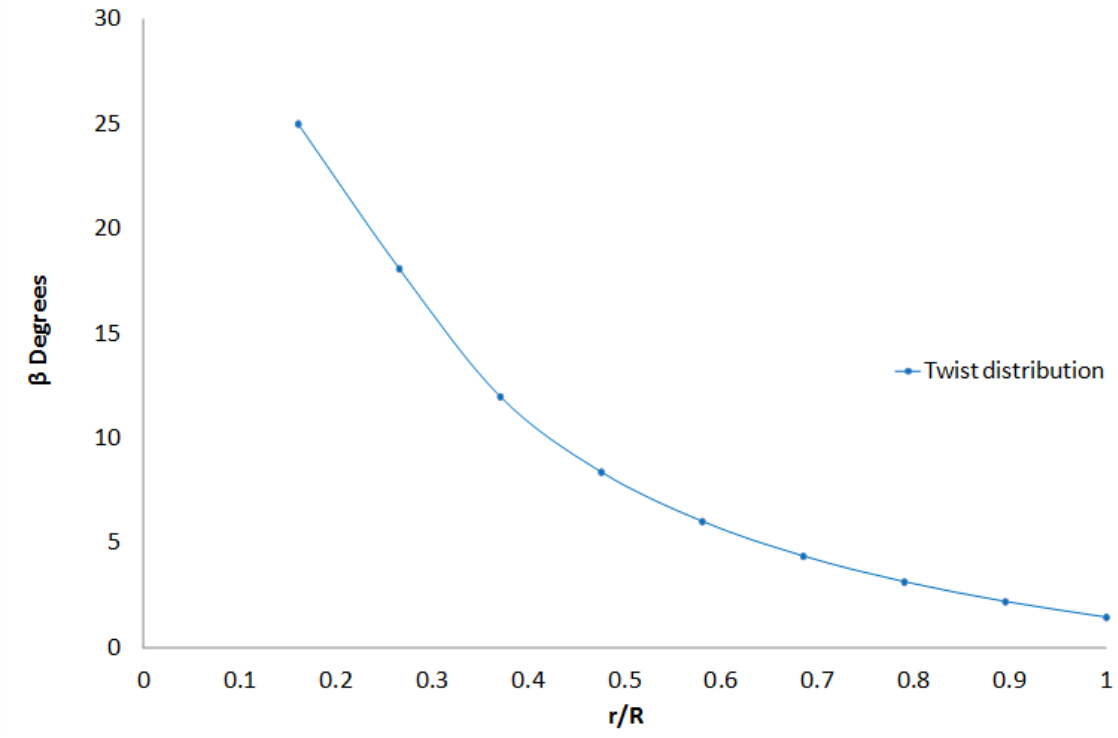

Figure 3.9: Optimum twist distribution of wind turbine blade

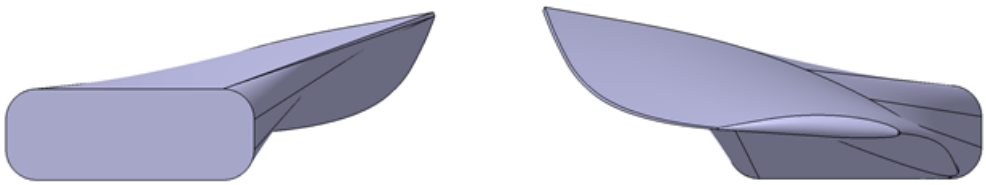

(a) (b)

Figure 3.10: Horizontal axis wind turbine blade (a) back view of the blade twist (b) front view of the blade twist

3.3 The Prototype Wind Turbine

The first set of prototype designed for this project is shown in Figure 3.11. A computer aided design engineering tool, CATIA V5, was utilised in designing the prototype. Due to the space restrictions in the test section of the wind tunnel, the height of the system has been kept at 1300mm to leave sufficient space at the wall of the wind tunnel which has a height of 2 metres. The diameter of wind turbine is approximately 1 metre.

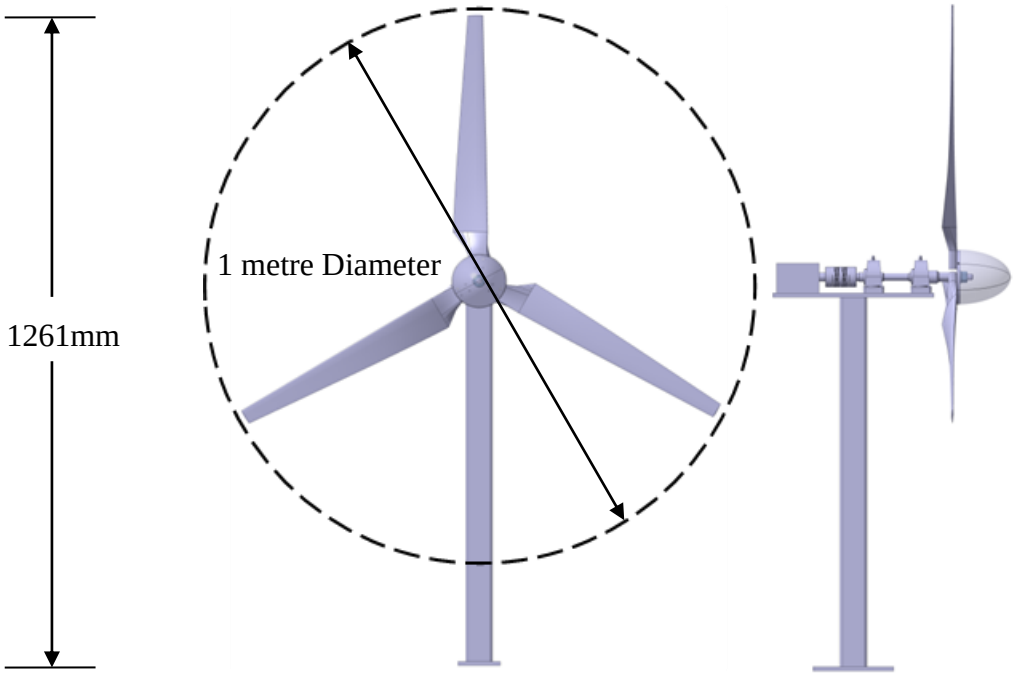

(a) (b)

Figure 3.11: Full assembly horizontal axis wind turbine (a) front view (b) side view

The wind turbine assemble consists of two bearings, a shaft, coupling and a torque sensor which will be further discussed in the next chapter. This design is the baseline design which

will be compared to the other two configurations that is designed to have winglets at the tip of the blade.

3.4 Winglet Geometry Design

Winglets are generally incorporated into an aircraft wing to reduce the vortex generated at the tip of the wing thus increasing the aerodynamic efficiency by reducing the induced drag. The technology of winglets has been investigated and applied in aerospace applications. As the wind energy industry is not as mature as the aeronautical industry, the concepts of winglets are currently being investigated to be implemented for future wind turbine designs. Figure 3.12 illustrates a modern winglet that is defined by its cant angle, twist, sweep, toe, height, chord distribution and the location at which the winglet is attached (Pressure or Suction side). Integrating winglets, whether it is on an aircraft wing or on a wind turbine blade, has its disadvantages. The additional bending moment that is incurred as a result of utilising the winglets is significant and requires additional structural reinforcements to support the bending loads at the root.

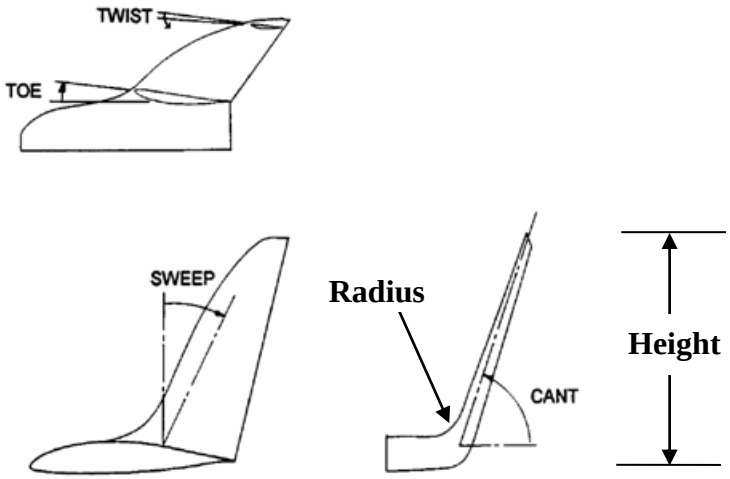

Figure 3.12: Variable parameters of modern winglet (Maughmer, 2001)

Winglets on aircraft wings are predominantly optimised for a particular operating condition such as cruise where the majority of flight time is spent. However, wind turbines operate at different conditions and on a wide range of speeds which complicates the process of optimising winglets for wind turbines. Like wind turbines, sailplanes operate at a wide range of speeds. This is why Maughmer (2001) design method is employed.

Through extensive modelling and flight testing of many winglet designs, (Maughmer, 2001) emphasises the importance of design variables of winglets which heavily influence the performance of winglets. The load distribution of the winglet can be optimised by spanwise twist and platform sweep. Depending on which of this variables matters most in the design, the spanwise twist for example is kept fixed and only the sweep is configured to achieve maximum performance. Increasing the sweep will have the same effect on the load distribution as does adding wash in along the winglet. Another important consideration to make when optimising winglets for a particular operating condition is the chord distribution as well as the height of the winglet. Employing very small chord lengths can result in the winglets to be very ineffective as the drag increases due to the winglet stalling. It is also true that larger chord length will lead to a poor performance of the winglets due to the excessive high loading at the tip. Choosing the ideal chord length is not as straight forward as it may seem. Both the Reynolds number requirements and the wetted area need to be considered. A reduction in Reynolds number will increase the drag coefficient. From equation (3.3), the Reynolds number is directly proportional to the chord length and therefore increasing the chord length would be ideal from a Reynolds number perspective. However, this would result in an increase in drag. In order to reduce the drag, the wetted area is minimised. Since the wetted area is directly proportional to the chord distribution, reducing the chord will result reducing the drag as the wetted area is decreased as well as the Reynolds number.

The complexity involved in designing a winglet is further added by considering the toe angle. The toe angle mainly controls the overall loading on the winglet as well as the overall effect on the load distribution. This parameter can only be optimised for one particular operating condition as the angle of attack of the winglet is a function of lift coefficient. Increasing the toe angle would be very effective at high lift coefficient but it would also be ineffective at low lift coefficients. The toe angle is a critical parameter which determines the performance at a particular operating condition. In general, the toe angle is carefully selected to allow both the wing and the winglet to stall simultaneously. It is important to note that the spanwise chord distribution is chosen such that the loading on the winglet approaches elliptical. This is mainly applied to reduce the induced drag (Maughmer, 2001).

Table 3.2: Winglet design parameters

Winglet Type	Radius mm	Location	Cant Angle	Sweep	Toe	Twist	Height mm
Upwind	5mm	Suction	45°	–	–	–	44.2mm
Downwind	5mm	Pressure	45°	–	–	–	44.2mm

The design and optimisation of winglets is a very complex process that involves many variable parameters. The slightest change to any of these parameters can affect the performance of the winglets. In this study the design process is simplified by considering one variable (cant angle). The majority of literature investigated in this project focused on a cant angle of 90°. In this research however a cant angle of 45° for the winglets has been considered as there are not many existing data for this particular angle both numerically and experimentally. Table 3.2 shows the design parameters used for the winglet design.

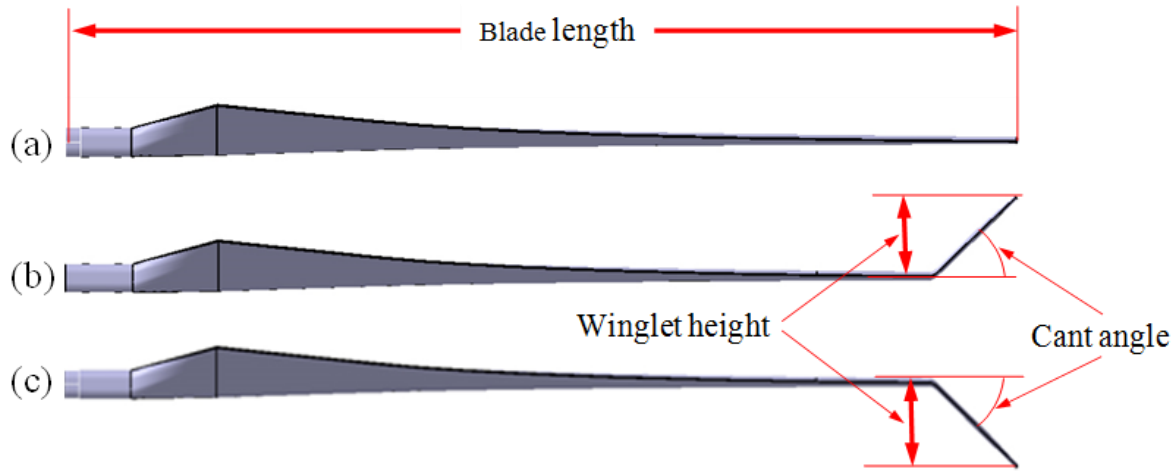

Figure 3.13: Wind turbine blade tip configuration design (a) straight blade without winglet; (b) blade with upwind winglet; (c) blade with downwind winglet

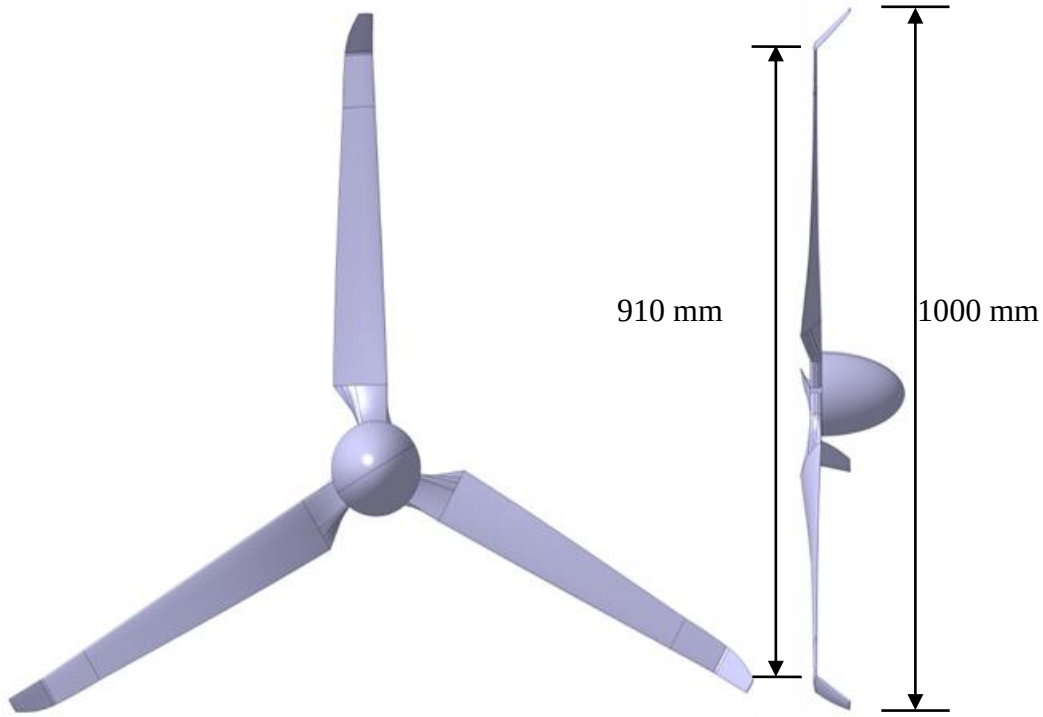

Figure 3.14: Wind turbine with forward facing (upwind) blade tip winglet

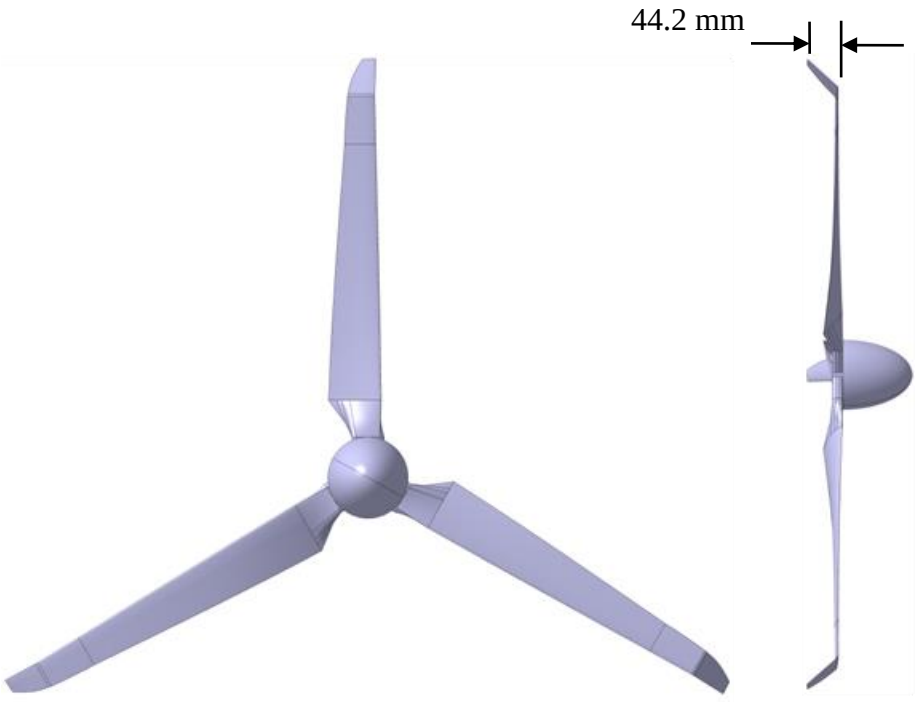

Figure 3.15: Wind turbine with backward facing (downwind) blade tip winglet

.

3.5 Manufacturing of Wind Turbine Blades

There are various materials that can be utilised for the manufacturing of small wind turbine blades. The general criterion of which a material must satisfy is the high strength to weight ratio as well as high stiffness properties of the material. As the turbine blades are subjected to extreme high bending loads as a result of the thrust it produces it becomes very critical for the choice of material selected to have a very high strength property. It is also important to consider the inertia of the blades as it ultimately influences the starting behaviour of the wind turbine (Mishnaevsky Jr et al., 2011). High inertia wind turbine blades have a shorter starting time and the wind turbine will only start to produce useful power at wind speeds above the average. However, a low inertia wind turbine will start rotating at much lower wind speeds than the average wind speed. This places a lot of emphasis not only on the strength of the material but also the weight. Materials such as Radiata Pine and Australian Hoop Pine have been used extensively in many light aircraft propellers due to their excellent strength capabilities and fatigue behaviour (Wood, 2011). These materials are highly suitable for small wind turbine applications for the reasons mentioned above. However, the cost of manufacturing using such materials is very high which only increases with increasing blade length.

Another highly effective material is the use of carbon fibre composites. Carbon fibre composite materials are widely used for its excellent high strength and stiffness to weight ratio and a very good fatigue resistant. Carbon fibre materials are very popular choice of material for large commercial wind turbines as wind turbine blades have increased in size over the last two decades. The increase in size of wind turbine blades significantly adds to the weight of a wind turbine system. Using carbon fibre material for the turbine blades requires moulds to be manufactured for both the upper and lower surfaces of the blade separately. This method can be very challenging as it would have to accommodate for the twist distribution along the entire length of the blade. Without any high precision machining, this method would practically be very difficult to achieve.

Therefore, ABS polycarbonate has been selected in this study for the manufacturing of the wind. Polycarbonate materials are comprised of two groups on the molecular chain known as Methyl and Phenyl which highly influence the stiffness of the material. In comparison to carbon fibre, ABS polycarbonate is slightly less strong but has an excellent heat resistant property. In addition, polycarbonate weighs significantly less than Radiata Pine and

Australian Hoop Pine (Wood, 2011). The wind turbine blades were manufactured at RMIT's Advanced Manufacturing Precinct using 3D printing method. The Fortus 900 MC 3D prototyping machine at the precinct was utilised to manufacture the blades of which the manufacturing process of each set of blades lasted about 22 hours. The disadvantage associated with polycarbonate is that it has low stiffness. Also, the surface finishing of the blades is not ideal. The rough surface finish can be seen in figure in Figure 3.16.

(a) (b) (c)

Figure 3.16: Polycarbonate manufactured wind turbine blade (a) backward facing winglet blade tip (b) straight blade with no winglet (c) forward facing winglet blade tip

CHAPTER 4

EXPERIMENTAL FACILITIES & INSTRUMENTATION

This section details the experimental procedure and equipment that were utilised to acquire the data in the wind turbine as well as data processing. For reliable results to be obtained, it is important that the experiment is conducted professionally and in an efficient manner with the correct procedures and safety precautions taken into account.

4.1 RMIT Industrial Wind Tunnel

Wind tunnels are considered as an essential engineering tool in fluid mechanics. The usage of wind tunnels to conduct experiments enables us to recreate realistic conditions that can be applied in the real world. The RMIT Industrial wind tunnel has been used in this study. The Tunnel is a low subsonic speed wind tunnel with a rectangular test section of 6 square meters. The approximate dimension of the entire rectangular test section is 2 metres in height, 3 meters wide and 9 meters in length. The test section also has an integrated turntable that enables the user to manipulate the yaw angle relative to the wind. For airflow to be generated, the wind tunnel has 7 blades fan of 3 meters in diameter, which is driven by a DC electric motor. To account for noise generation by the motor, the motor is mounted in an isolated area away from the test section. Further reduction in noise is achieved through acoustically treated turning vanes which are designed to absorb some of the noise generated during the testing. As

with every wind tunnel it is important to determine the turbulence intensity, which is a measure of the degree of turbulence in a flow, as it affects the mean wind speed. In our case, the turbulence intensity of the wind tunnel is approximately 1.8%. This makes RMIT's industrial wind tunnel highly suitable for various aerodynamic and aeroacoustic experiments. The wind tunnel can achieve a maximum speed of 145 km/h. A schematic plan view of the tunnel is shown in Figure 4.1.

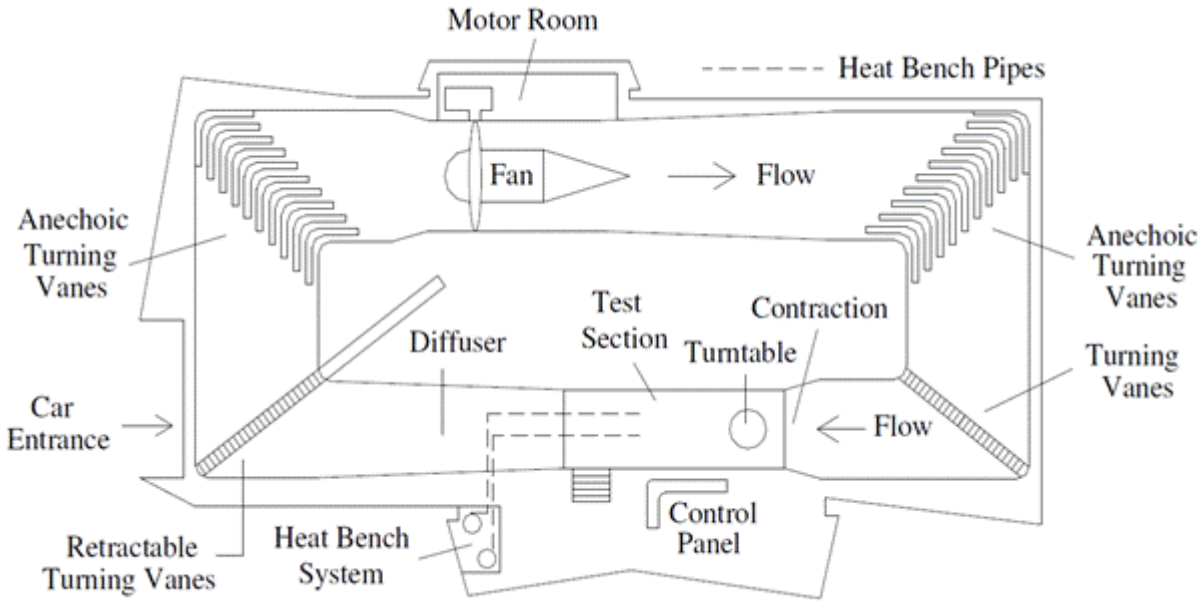

Figure 4.1: A schematic view of RMIT industrial wind tunnel (Alam, 2000)

4.2 Measurements of Dynamic Pressure, Velocity and Temperature

The air speeds inside the wind tunnel were measured with a modified National Physical Laboratory (NPL) ellipsoidal head Pitot-Static tube (located at the entry of the test section) which was connected through flexible tubing with the Baratron pressure sensor (MKS Instruments, USA) as shown in Figure 4.2. The pressure readings from the pressure sensor is fed through to the wind tunnel computers which then computes flow properties such as the local flow speed, dynamic pressure and temperature.

Equation 4.2 represents the components of total pressure, (P_T): static pressure (P_S) and Dynamic pressure, measured by the Pitot - static tube.

$$P_{Static} + P_{Dynamic} = P_{Total} \tag{4.2}$$

The wind speed (V) was calculated using equation 4.3.

$$V = \sqrt{\frac{2(P_{Total} - P_{Static})}{\rho}} \quad \text{(m/s)} \qquad (4.3)$$

4.3 Measurements of Aerodynamics Forces and Moments

To measure the forces and moments in real a time a six component load sensor (JR3) is used. The JR3 load sensor is connected to a strut which is mounted vertically to support the turbine blade. The JR3 load sensor is directly linked to a computer in the wind tunnel which has integrated software that is user friendly and enables the user to retrieve all the forces and moments acting on the blade. The JR3 has a maximum load rating of 200 N. Due to its high stiffness, the load sensor allows minimal degradation of system dynamics position accuracy and high resonant frequency which allows accurate sensor response to rapid force fluctuations. Details of the JR3 sensor are given in Appendix B

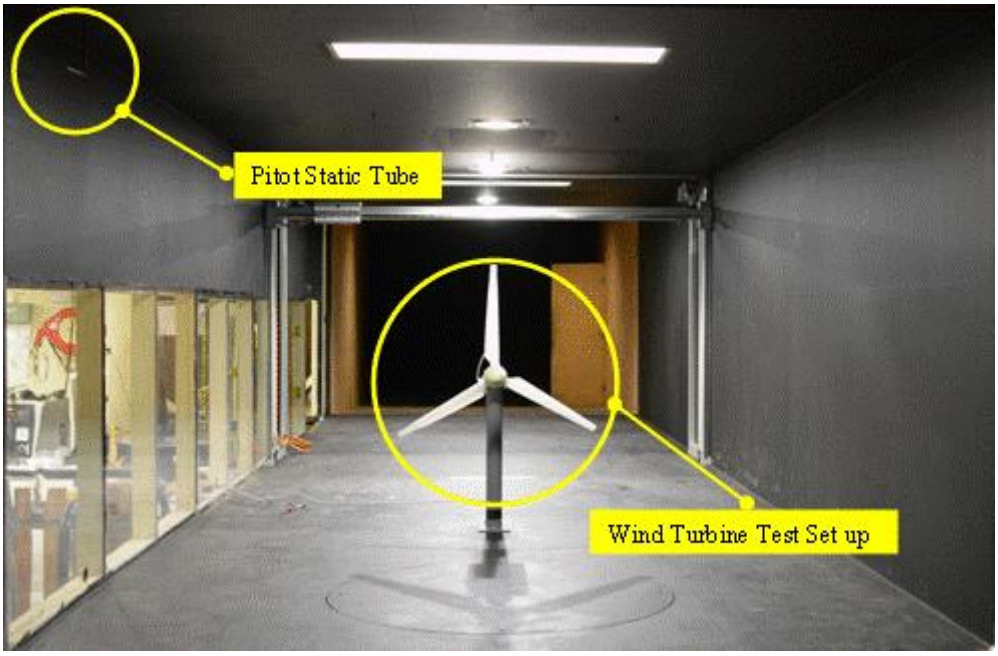

Figure 4.2: RMIT industrial wind tunnel test section

4.4 Wind Tunnel Calibration

Dynamic pressures (*q*) in the wind tunnel were measured vertically from 200 to 1800 mm in an increment of 200 mm from the tunnel floor at the location where the experimental arrangements were mounted. The nominal tunnel air speeds were 20, 40, 80 and 120 km/h with less than ±1% accuracy. The local pressure was normalised by dividing by the wind tunnel reference pressure (*qref*) and plotted against the height for the air speeds as shown in Figure 4.3. This indicated that the local pressure did not vary significantly when referenced to

the tunnel wall-mounted reference pressure for the given speed. However, a small variation of normalised velocity can be seen near the tunnel floor (Figure 4.3). No correction of velocity was deemed necessary as local pressure (*q*) did not vary significantly with wall mounted reference pressure (*qref*) with height. The accuracy of the pressure measured with various speeds across the plane was calculated to be less than ±1%. Hence the tunnel reference pressure was used in the calculation of drag and lift coefficients.

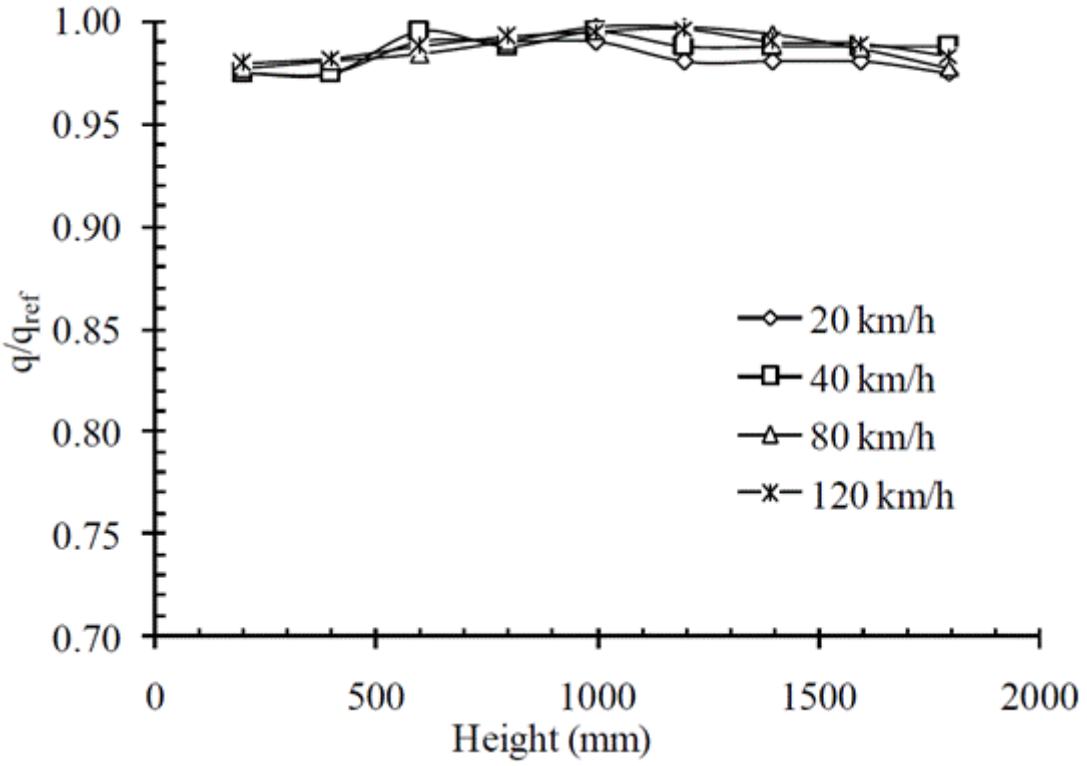

Figure 4.3: Normalised local pressure variation with height in relation to reference pressure

4.5 Torque Measurement

The mechanical power generated by the blade is directly proportional to the torque and angular velocity of the blade. To determine both the torque and angular velocity of the blade, a torque transducer is used. The HBM T20WN was utilised, which is primarily designed for measuring the static, dynamic torque and the rotational speed, consists of an electronic sensor as well as an MX440A amplifier module was used. The torque sensor is connected to a cable that feeds all the information to the MX440A amplifier which computes the torque and rotational velocity of the wind turbine as shown in Figure 4.4 and Figure 4.5 respectively. HBM torque transducer has a nominal rotation speed of 10,000 revolutions per minute (RPM) which is well above the expected maximum rotational speed the wind turbine can reach

during testing. Calibration of the sensor was carried out before and in between the tests. The HBM T20WN is capable of measuring both the torque and rotational speed simultaneously and has a maximum torque range of 5 N.m.

In order to measure the correct torque generated by the wind turbine, a braking device was developed. The braking device is utilised to dampen the rotational energy of the rotating wind turbine. Initially, a bicycle brake shoe was used in the experiment. However, as the break shoe is made off rubber, it did not provide sufficient grip and was deemed inefficient. Alternatively, a simple but smart bicycle disc braking device was used to apply a resistive force which enables us to slowly dampen the rotational energy as shown in Figure 4.4. The resistive force would be applied until the wind turbine came to a complete stop and the torque would be recorded. The mechanical power generated by the wind turbine is proportional to:

$$P = T\omega \tag{4.4}$$

Where:

T= Torque (N.m)

ω= Rotational speed (rad/s)

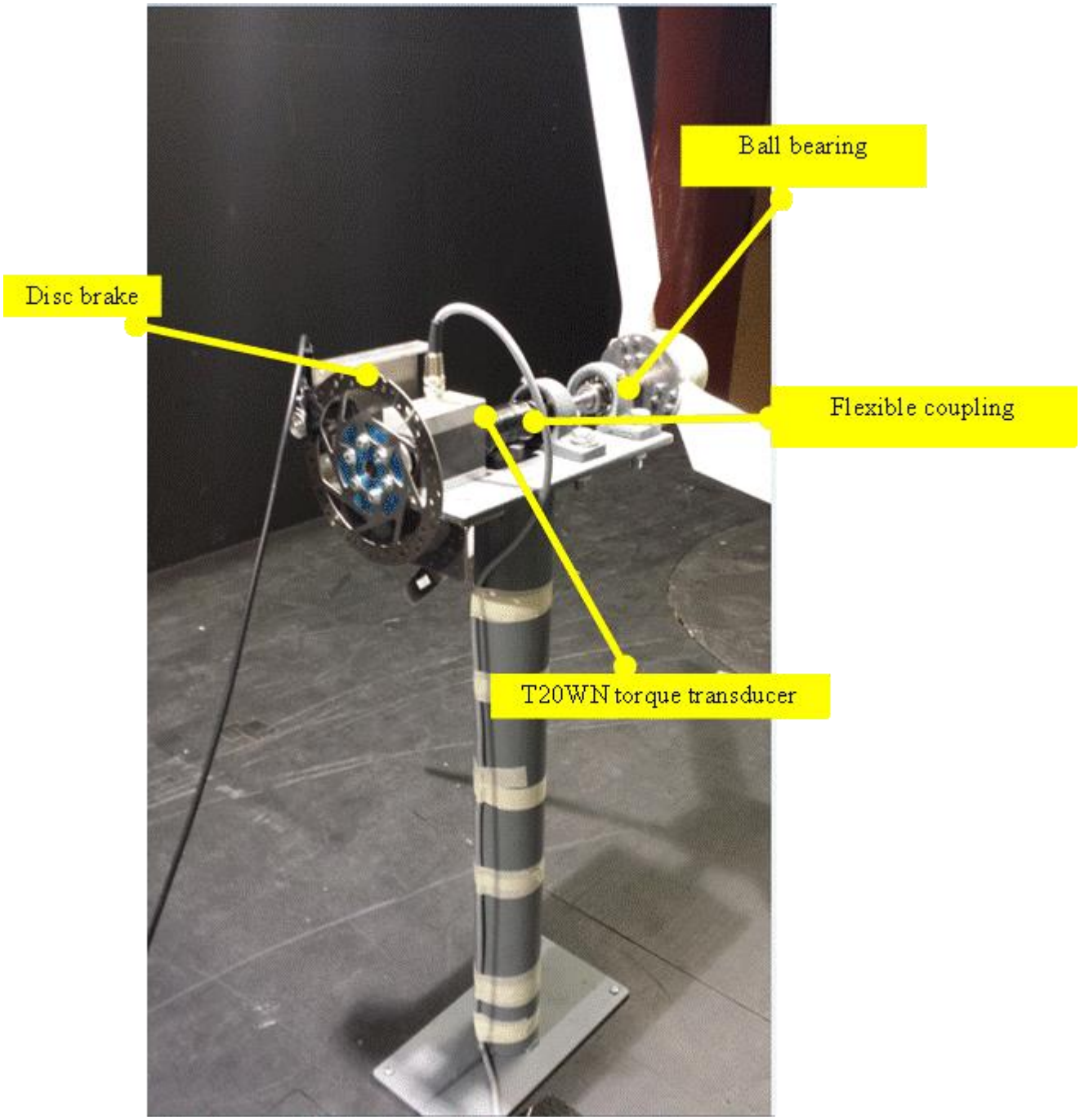

Figure 4.4: HBM torque transducer and disc brake attached to the turbine shaft in RMIT Industrial wind tunnel set up

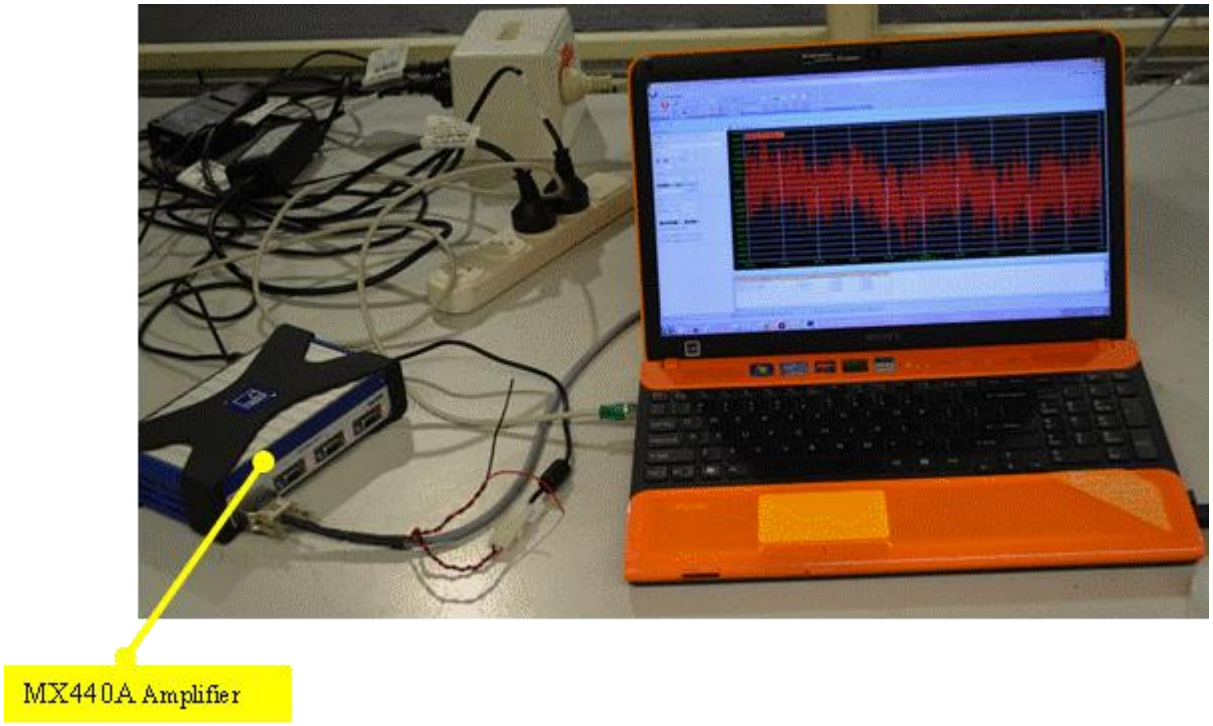

Figure 4.5: MX440A amplifier

4.6 Experimental Procedure

4.6.1 Single Blade Test

The first set of tests was carried out in the wind tunnel investigated the aerodynamic forces exerted on the blade. The blades were vertically mounted to a support strut which was directly aligned to the direction of the flow. To reduce the influence of the strut which supports the blade, on the overall drag and lift force, an aerofoil canopy was utilised to cover the lower of portion of metal strut exposed to the flow, thereby reducing the interference drag. The strut is vertically connected to a six component load sensor JR3 underneath the wind tunnel floor with a load rating of 200N (Newtons). This test was carried out for all three design configurations of the blade. Figure 4.6 illustrates the experimental set up of the blade in the wind tunnel test section.

The blades were tested at speeds starting from 30 km/h to 90 km/h with an increment of 10 km/h. Through close observation, the blade began vibrating violently at speeds of 100 km/h. For safety precautions, all blades were tested at wind speeds not more than 90 km/h.

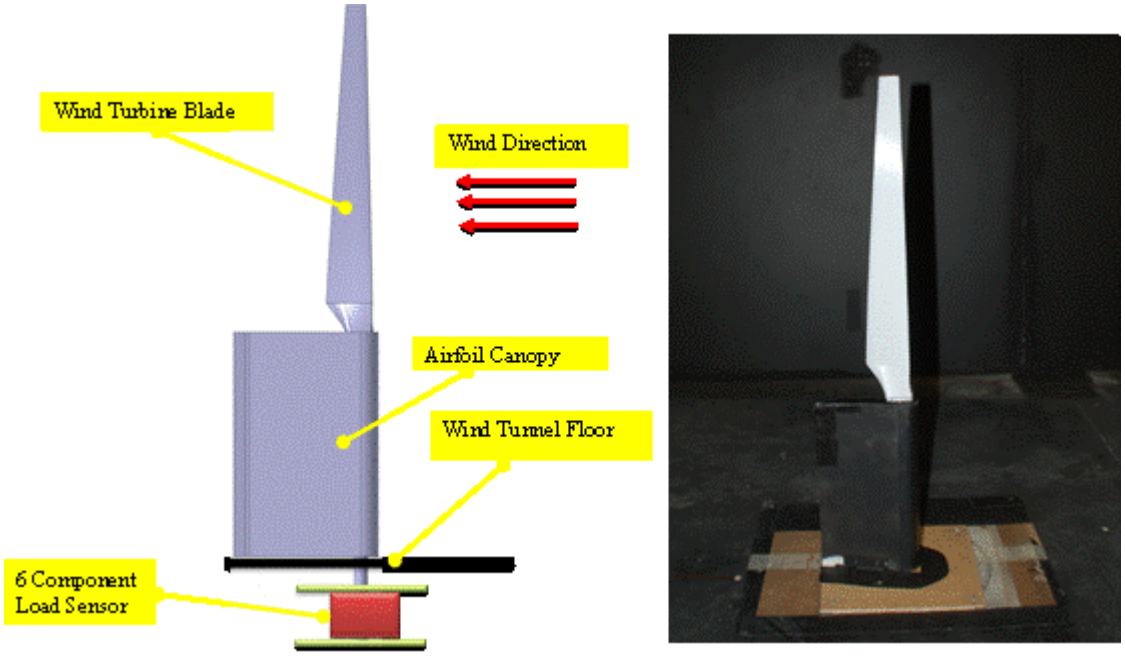

(a) (b)

Figure 4.6: Vertically mounted single blade in the wind tunnel. (a) CATIA model (b) Wind tunnel setup

4.6.1.1 Yaw Angle Orientation

To better understand the significance of the aerodynamic forces acting on the turbine blade, the wind turbine blade was tested in the wind tunnel at different yaw angles ranging between -90° to +90° at an increment of 15°. Figure 4.7 shows the top view of the experimental set up. It was anticipated that the aerodynamic drag force on the blade would reach maximum when the blade is positioned at a yaw angle of 90°. This can theoretically be explained by the fact that the pressure gradient on the blade is significantly high. Positioning the blade at different yaw angles enables for the evaluation of the aerodynamic forces exerted on the blade and also on the flow separation from the blade.

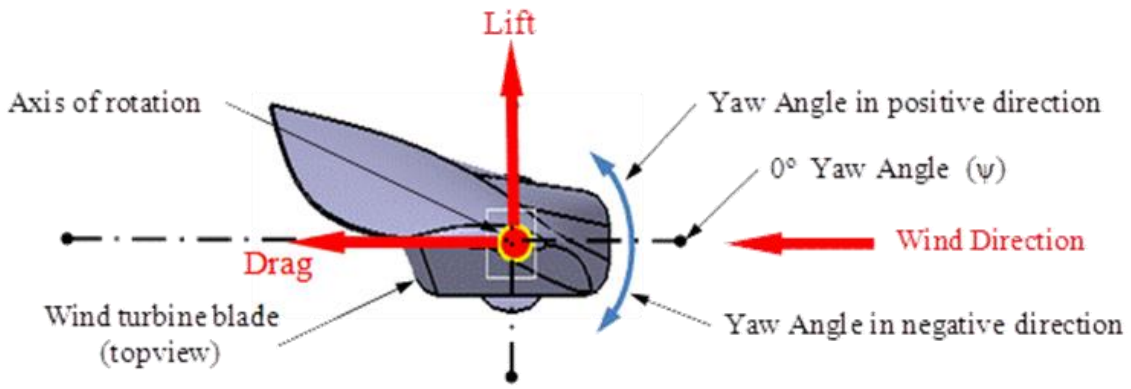

Figure 4.7: Top view of vertically mounted blade

4.6.2 Full Scale Wind Turbine Test

The full scale wind turbine test was carried out to determine its power extraction capabilities. In order to execute this test safely and accurately, it is important to consider the structural support of the wind turbine. The wind turbine blades are supported by a circular structural hollow beam of 700mm in length. Allowing the beam to remain hollow reinforces its structural strength and support the significant bending loads exerted on the beam as a result of the thrust produced from the wind turbine during operation. A rectangular flat plate was welded to the base of the beam to provide stability and more resistive to vibration. Similarly, an additional rectangular flat plate is also welded at the top section of the beam to support the other components of the system such as the bearing, coupling and torque sensor.

A number of different types of bearings were considered to be integrated with the wind turbine system. The bearing which was considered to be competent for this type of application is the self-aligning ball bearing. The self-aligning bearing is robust in operation and is highly suitable for high speed applications such as small wind turbines. These type of bearings generate less friction and enable them to function at high speeds. Two self-aligning ball bearings supported by P204 cast iron housing were utilised in this study. To mechanically attach the shaft of the wind turbine and the shaft of the torque sensor, both being 16mm in diameter, a stainless steel flexible coupling is used as shown in Figure 4.4. The coupling has 3° angular misalignment and can support loads of up to 10.73Nm. As the scale of the wind turbine in this study is relatively small, it is highly expected that the maximum torque generated will not exceed 4 Nm. Therefore, the coupling selected for this task is more than sufficient to support the torsional loads subjected on the shaft.

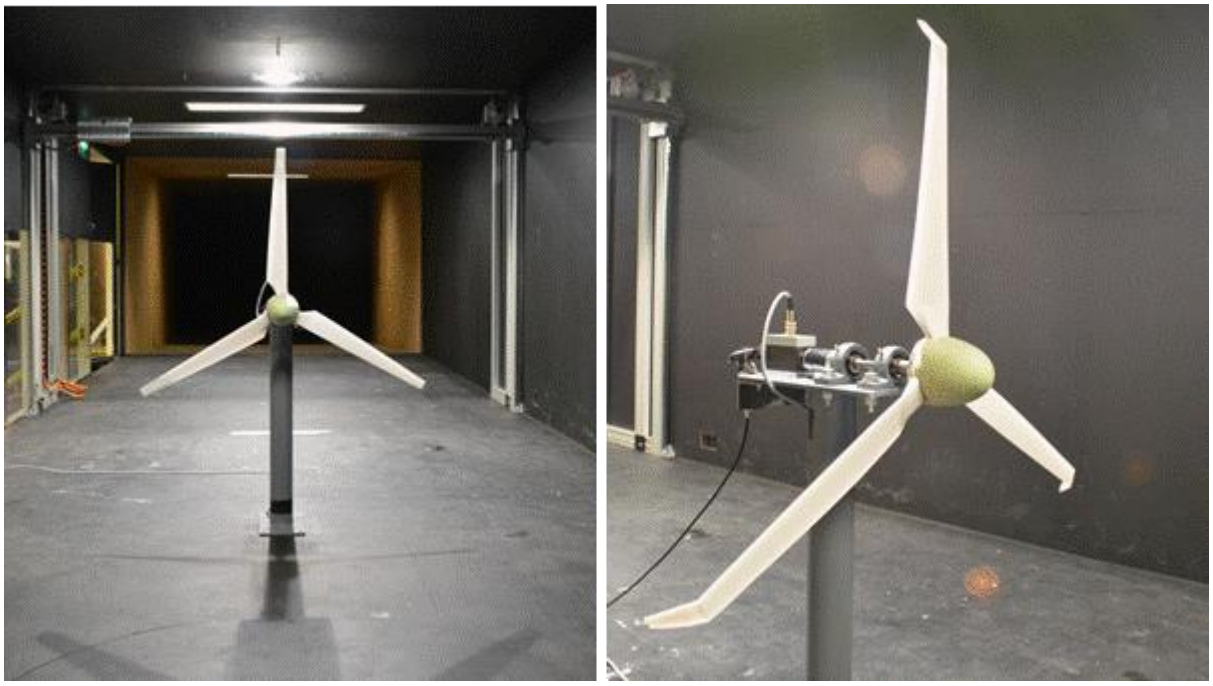

(a) (b)

Figure 4.8: Full scale wind turbine (a) Plain configuration blades (b) Backward facing (downwind) winglet blades

One of the main objectives of this research is to determine the power curve of all three wind turbine design configurations. In order to achieve this, the wind turbine was tested in the wind tunnel at a maximum wind speed of 40 km/h at an increment of 2 km/h. Further experiments were conducted to investigate the influence of the nacelle, which in this case are flat plate, bearings, coupling and the torque sensor. The nacelle causes significant turbulence in the wake which increases the interference drag of the overall wind turbine. In order to investigate the level of influence the nacelle has on the aerodynamic performance of the blades, the gap between the nearest bearing and the hub is extended. To simplify the experimental test and process of the wind turbine, external hollow shafts in the desired size (100mm and 150mm) were designed and integrated with the main shaft using corkscrews. This method presented an attractive alternative which significantly reduced the rigorous process involved in the set up without having the need to entirely remove the main shaft, carefully aligned with the wind turbine, at each interval of the experiment. Three different gap (distances) of 36.8mm, 100mm and 150mm were studied as shown in Figure 4.9. A maximum extension of 150mm gap could only be achieved as it was not feasible to extend the gap beyond this point due to the high level of bending loads and stresses exerted on to the

bearing. All three different design configurations of the wind turbine blade were tested for each gap extension.

It is important to note that the full scale wind turbine experiment was conducted to determine and evaluate the turbines power curve characteristics only. The power curve to be obtained from the experiments would be based on the mechanical power of the turbine due to the applied torque on the shaft by the rotating blades.

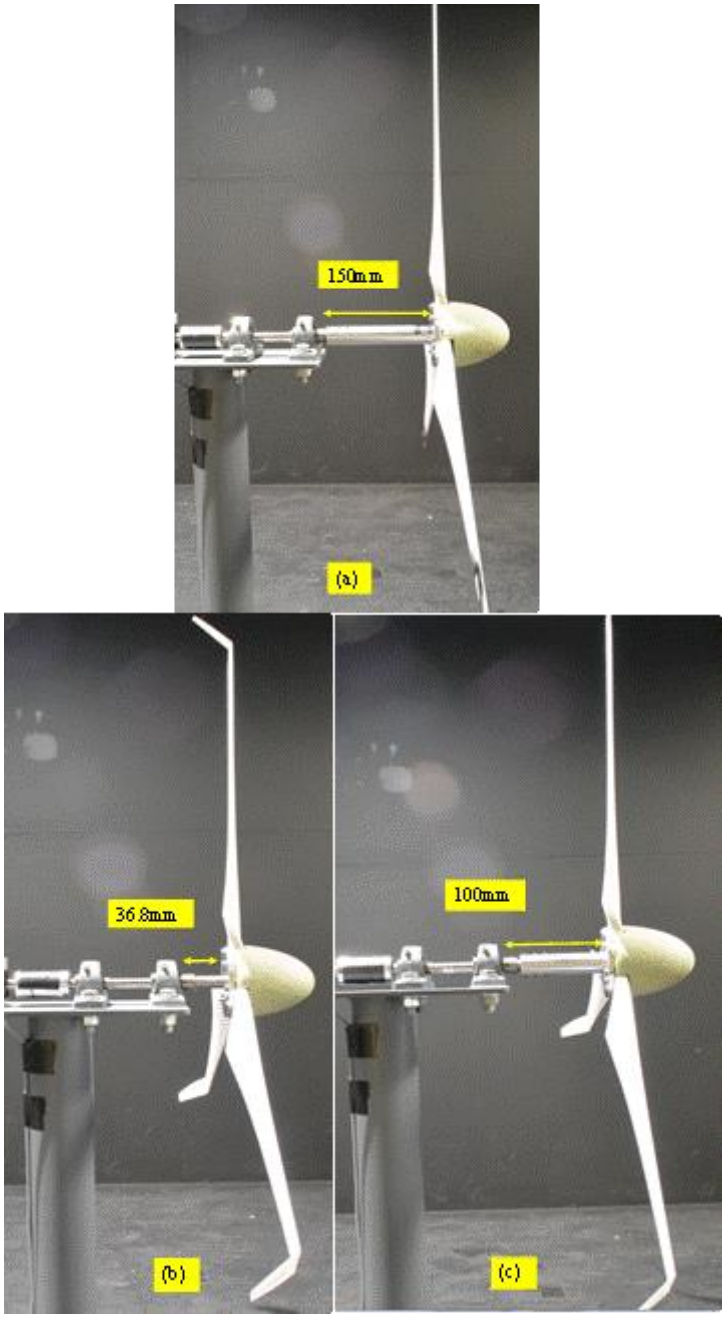

Figure 4.9: Full scale wind turbine with different shaft extensions (a) 150mm gap (b) 36.8mm gap (c) 100mm gap

4.7 Calibration and Accuracy

It is essential to determine the degree of influence the errors associated with the experiment may have upon the overall results acquired. The acquisition such as dynamic pressure, velocity, forces and moments in the wind tunnel are influenced by many factors such as air fluctuations. Therefore it is necessary to address these errors and apply correct measures to minimize the consequences of these errors.

4.7.1 Repeatability of Results

In order to verify the repeatability of the experimental data and increase the confidence level in the data, every single test conducted in the wind tunnel was performed three times. The data had a maximum variation of less than 1%. This was a good indication of the accuracy possessed by the measuring equipments.

4.7.2 Temperature and Pressure Errors

Running the wind tunnel for a period of time can significantly affect both the temperature and pressure in the tunnel due to temperature rise in the tunnel caused by the hub of the tunnel fan due to friction. Close observation of these two properties indicated that there was a slight fluctuation in the readings. The fluctuation in both the temperature and pressure were accounted for in the acquisition of the data and correct measures were taken to rectify the problem.

4.7.3 Wind Tunnel Speed Errors

The air speed in the wind tunnel was measured using an ellipsoidal head Pitot-static tube which is connected to a MKS Baratron reference pressure transducer. In order to verify the readings obtained from the MKS Baratron pressure transducer, the air speed was also measured with a Honeywell (160 PC) pressure transducer. The variation of the wind tunnel air speed was found to be less than 1%.

4.7.4 Blockage Correction

Blockage effects can significantly influence the flow speed around the test section and therefore causes the data acquired to be incorrect. The presence of the wind tunnel walls as well as the test model effectively reduces the cross sectional area of the test section and as a result of this blockage, the flow distorts and gains momentum at close proximity to the model. It is essential to take correct measure to minimize the influence of the blockages which has the ability to contaminate the experimental data. The blockage ratio (BR) is defined as the projected frontal area of the test model and the cross sectional area of the wind tunnel.

$$\left(BR = \frac{A_{Model}}{A_{Tunnel\,Test\,Section}} \times 100\% \right)$$

(4.5)

A blockage ratio of less than 5% can be neglected as the distortion in the flow is not significant (Cermak & Isyumov, 1998). However, a blockage ratio between 5% and 10% can significantly influence the experimental data and as a result additional tests is necessary but at a much smaller scale. The blockage ratio of the single blade test model was less than 1% which is quite below the threshold limit of 5%.

CHAPTER 5

COMPUTATIONAL FLUID DYNAMICS (CFD) MODELLING

Rapid advancements of computer processing power have enabled the use of Computational Fluid Dynamics (CFD) to become an integral part of engineering design and analysis. CFD is employed to better understand the physical process and events that take place in the flow of fluids such as the external flow of aircraft wings and cars. CFD is also widely used as a tool to complement experimental approaches by providing a cost effective means of simulating real fluid flows. This research solely employs CFD as a means of validating the results which are obtained through experimental work.

5.1 Governing Equations

The concept of CFD is fundamentally based on the governing equations of fluid dynamics which are famously known as the Navier Stokes equation. The Navier Stokes equations are based on the principles that the properties of fluids such as pressure and velocity can be define by the laws of conservation. The conservations laws such as the conservation of mass, momentum and energy are defined by the following physical laws:

- The mass of a fluid is conserved.

- The rate of change of momentum equals to the sum of forces acting on a fluid particle (Newton's second law).
- The rate of change of energy is equal to the sum of the rate of heat addition to and the rate of work done on a fluid particle (first law of thermodynamics).

The mathematical expression of the governing equations is expressed in equation 5.1.

Equation (5.1) represents the mass conservation or better known as the continuity equation for a three dimensional at a point in an incompressible fluid

$$\frac{\partial u}{\partial x} + \frac{\partial v}{\partial y} + \frac{\partial w}{\partial z} = 0 \tag{5.1}$$

The momentum equation in all three directions x, y and z coupled with the stress equation of a Newtonian fluid yields what is known as the Navier Stokes equation, which is given in equation (5.2).

$$\begin{aligned}
\rho\left(\frac{\partial u}{\partial t} + u\frac{\partial u}{\partial x} + v\frac{\partial u}{\partial y} + w\frac{\partial u}{\partial z}\right) &= \rho g_x - \frac{\partial p}{\partial x} + \mu\left(\frac{\partial^2 u}{\partial x^2} + \frac{\partial^2 u}{\partial y^2} + \frac{\partial^2 u}{\partial z^2}\right) \\
\rho\left(\frac{\partial v}{\partial t} + u\frac{\partial v}{\partial x} + v\frac{\partial v}{\partial y} + w\frac{\partial v}{\partial z}\right) &= \rho g_y - \frac{\partial p}{\partial y} + \mu\left(\frac{\partial^2 v}{\partial x^2} + \frac{\partial^2 v}{\partial y^2} + \frac{\partial^2 v}{\partial z^2}\right) \\
\rho\left(\frac{\partial w}{\partial t} + u\frac{\partial w}{\partial x} + v\frac{\partial w}{\partial y} + w\frac{\partial w}{\partial z}\right) &= \rho g_z - \frac{\partial p}{\partial z} + \mu\left(\frac{\partial^2 w}{\partial x^2} + \frac{\partial^2 w}{\partial y^2} + \frac{\partial^2 w}{\partial z^2}\right)
\end{aligned} \tag{5.2}$$

A basic form of the energy equation is given in equation (5.3). Where, K is the thermal conductivity.

$$u\frac{\partial T}{\partial x} + v\frac{\partial T}{\partial y} = K\left(\frac{\partial^2 T}{\partial x^2} + \frac{\partial^2 T}{\partial y^2}\right) \tag{5.3}$$

5.2 Turbulence modelling

The majority of flows encountered in real life are turbulent in nature. Turbulence flow is an unsteady periodic motion in which the velocity components in all three directions fluctuate and as a result there is a significant change in mass and momentum interchange that takes place between each neighbouring layers of fluid. The motion of a turbulence flow is predominantly rotational which are produced by the viscous effects of boundaries and the separation of fluid from the surface. Due to the irregularity nature of turbulent flows which makes the flow increasingly complex, a modelling approach using the Navier Stokes equation alone in an attempt to describe the flow behaviour of turbulent flows becomes practically impossible. As the Navier Stokes equation is not capable of predicting the behaviour of turbulent flows, additional equation is developed that is capable of predicting the time averaged velocity, pressure and temperature fields without entirely solving the complete turbulent flow over time and as a result it significantly reduces the computational resources.

Several turbulence models have been developed in the past specifically aimed at predicting turbulent flows. The method adopted by each of the turbulence model varies and the complexity of each model depends on the objectives of the simulation. One of the most widely used turbulence models is the Reynolds Averaged Navier Stokes model as it offers the most economic approach for solving complex turbulent flows. The RANS turbulence model is subdivided into many different models such as the one equation turbulence model of Spalart – Allmaras and the two equation turbulence model such as the κ-ω, κ-ε and the SST model.

5.2.1 Spalart Allmaras Model

The Spalart-Allmaras (SA) is a one equation turbulence model which was designed for aeronautical applications that involved wall bounded flows. In contrast to other models, this turbulence model is relatively simple as it solves a modelled transport equation for the kinematic eddy viscosity (Versteeg & Malalasekera, 1995). This model is a low Reynolds number model and as a result it is highly affected by the changes in the viscous areas of the boundary layer. As the SA model is generally used to predict turbulence in near wall regions, the vortices generated in a turbulent flow may cause difficulty in approximating the flow behaviour in that region. As this model does have the capability to accurately predict the flow

fields that shear flow and separated flow, it is considered not suitable for the application of this study.

5.2.2 k-Epsilon Model

The two equation turbulence models are widely the most used model as it is robust, economical and yields rapid stable solutions. The two transport equation solved in this model are the turbulent kinetic energy (κ) and the rate of dissipation of turbulence (ε).This model is manly used to predict the flow in areas that are away from the walls. However, this model is not efficient for flows that exhibit swirling behaviour as well as flows with very strong flow separation. Improved models have been developed based on the κ ε turbulence model which accounts for the aforementioned incapability of the model.

5.2.3 Wilcox k-Omega Model

The κ ω which is also a two equation turbulence model is based on the turbulent kinetic energy and the turbulent frequency. The Wilcox κ ω is primarily aimed at predicting the free shear flow separation rates. Through extensive experiments, it was found that these measurements were in close agreement with for far wakes, mixing layers, planes and round and radial jets. As a result of this agreement, this model is accepted for determining wall bounded flows and free shear flows. The most notable advantage of this model compared to the previous models, is that the turbulent frequency equation can be integrated without additional terms through the viscous sublayer which makes it an ideal turbulence model for near wall treatment.

5.2.4 Shear Stress Transport (SST) k-Omega Model

The shear stress transport (SST) k-omega model was developed recently to manage the freestream sensitivity of the κ ω model. This is achieved by combining the turbulent frequency equation (ω) and the rate of dissipation of turbulence (ε). The major advantage of the SST k-omega model is its accuracy in predicting the flow behaviour of the wall boundary layer. It is also capable of capturing regions of recirculation in the flow. However, it is often difficult for the model to achieve quick convergence. Rajendran et al. (2011) utilised the SST turbulence model for the aerodynamic analysis of a horizontal axis wind turbine. The study revealed that the SST turbulence model presented a more accurate solution than the κ ε

turbulence model. As the SST κ ω model is more robust and accurate in its predictions than the aforementioned models the SST is employed in this research for the analysis of the wind turbine.

5.3 CAD Geometry

All CFD codes follow an identical systematic process to successfully simulate a problem. The main elements of the process are: Pre-processing, Solver execution and post processing. Each of these elements is dependent on each other and can significantly influence the solution of the simulation. In order to execute any simulation, Computer Aided Design (CAD) geometry is required as it defines the objectives of the simulation. In this research, the wind turbine was designed in CATIA V5 which is compatible with the CFD software package employed, ANSYS CFX. To transfer the CAD model to ANSYS CFX, the model was converted to a step file. As result of this conversion some elements of the model were divided into many faces and vertices. The increased number of faces in the model is highly undesirable as it would increase the number of mesh elements in the meshing process. It also adds to the complexity involved in meshing faces of small area. The general aim of any CAD model is to minimise the number of faces and any unnecessary features to reduce the meshing elements. Features such as the support stand, bearings and shaft that did not serve any significance in the analysis were eliminated.

5.4 Mesh Generation

One of the most critical steps in CFD is the generation of a mesh. The partial differential equations that govern fluid flow are very complex to solve and as a result an approximation method is used to solve the properties of fluid numerically in a control volume. The majority of time spent in CFD is devoted to generating a quality mesh as it significantly influences the stability of the numerical solution. The type of mesh employed in this analysis is an unstructured mesh composed of 2D triangles and quadrilaterals as well as 3D tetrahedral. The benefit of using an unstructured mesh is that it is automated and requires less time and effort. The drawbacks of this type of mesh is that the elements of triangle and tetrahedral do not blend well which results in the elements to have the same size and shape. A finer mesh is required of the entire domain to achieve satisfactory level of density in the mesh at particular region of interest.

The wind turbine blades were meshed using a face size of 0.02m as well as applying an additional edge sizing along the edges of the blade of 0.0001m. One of the elements that determine the accuracy of the solution is the level of mesh density. A higher mesh density increases the accuracy of the solution whilst contributing to the stability numerical equations. However, excessive refinements in the mesh will yield inaccurate results and cause the solution to diverge significantly. The mesh density was increased from coarse to very fine mesh in the fluid domain. Since the region of interest in the analysis is near by the blade tip, further increase in mesh was required to accurately predict the flow behaviour in that region. In order to increase the mesh density around the blade tip without necessarily increasing the number of elements in the outer regions of domain, a body of influenced is applied with a body size of 0.01m. Figure 5.1 illustrates the fine unstructured mesh applied in the cylindrical fluid domain.

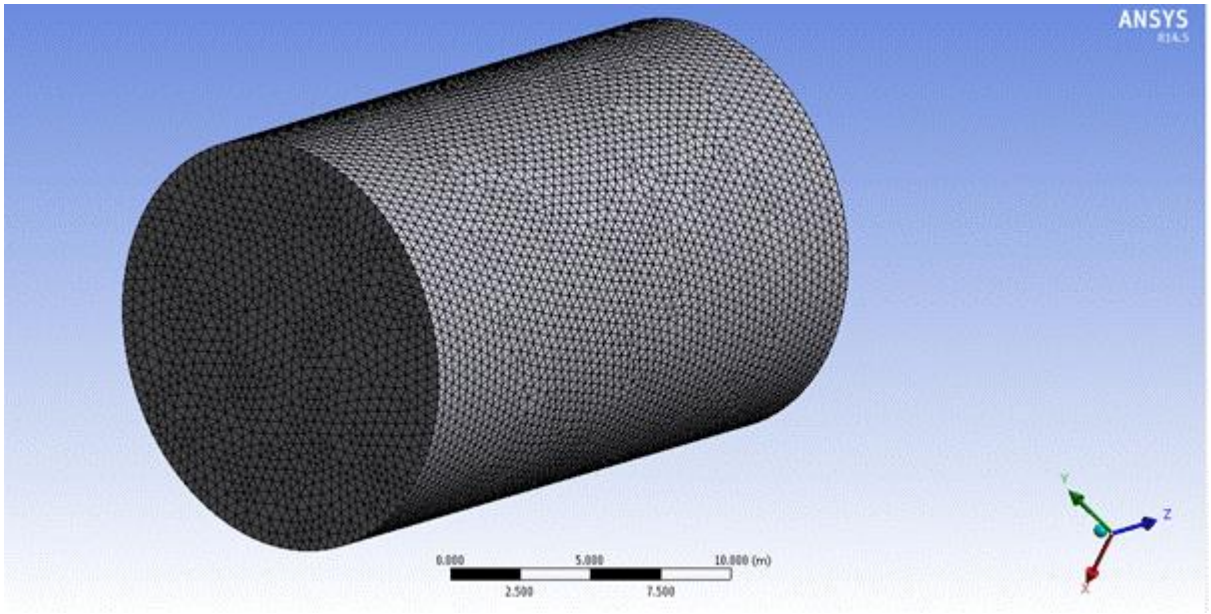

Figure 5.1: Unstructred mesh of fluid domain

.

Table 5.1 shows the number of elements and nodes in the refined mesh of all the different configuration of the wind turbine. As the table indicates, there is a slight variation in the number of elements and nodes even though all three configurations were given the same size functions. There is a possibility this could of have risen as a result of the number faces on the blades. As mentioned previously, some faces on the blade were merged in order to minimise the meshing process and reduce the number of mesh elements. However, not all faces could

be merged for all three wind turbine blades and this effectively resulted in the blades to have different number of faces.

Table 5.1: Number of elements and nodes for different configuration wind turbine.

	Number of Elements	Number of Nodes
Wind Turbine (Baseline)	4,433,448	1,017,574
Wind Turbine (suction side facing winglet)	4.420,215	1,001,153
Wind Turbine (pressure side facing winglet)	4,430,347	1,015,529

5.4.1 Grid Quality Evaluation

A good grid quality is essential in order to achieve an accurate solution and numerical stability. To evaluate the quality of the grid, a number of diagnostic tools are utilised. One of the tools used to assess the quality of the grid is the skewness. Skewness determines the proximity of the cell size to an ideal size (equilateral or equiangular). A higher value of skewness close to 1 corresponds to a very poor mesh whereas a skewness value near zero corresponds to a very good mesh As shown in Table 5.2. Therefore it is essential the skewness value do not exceed 0.50 to achieve convergence of the solution. The skewness value in the mesh generated is found to be 0.75 which is reasonably accurate, although not desirable, to yield a good solution. Another tool that is used that is used to assess the quality of the mesh is the orthogonal quality. An orthogonal value of 1 indicates the mesh is of high quality, however if the value approaches zero it is considered to be very poor. Generally, it is recommended that the minimum orthogonal value is kept above 0.05.

Table 5.2: Grid quality evaluation

Cell quality	Excellent	Very good	Good	Acceptable	Bad	Inacceptable
Skewness	0.25-0.50	0.50-0.80	0.80-0.94	0.95-0.97	0.98-1.00	0.98-1.00
Orthogonal	0.95-1.00	0.70-0.95	0.20-0.69	0.15-0.20	0.001-0.14	0-0.001

5.4.2 Boundary Layer

In order to accurately capture the flow behaviour at the near wall region, wall function approach is utilised. As the fluid comes into contact with a solid surface, the fluid velocity decreases non-linearly towards the surface and eventually the first layer of fluid just above the surface will have zero velocity. This phenomenon is called the no slip condition as the fluid is completely stationary and not in motion. To accurately resolve the boundary layer without having the need to extensively refine the mesh, which would significantly add to the computational cost, an inflation layer mesh is used to capture the near wall region. It is essential to determine the placement of the first node above the wall. A non-dimensional distance parameter that is based on the local fluid velocity from the wall to the first node is used, known as Y plus. Figure 5.2 shows the velocity distribution near the wall region. It is important to ensure that the first node point falls within the boundary layer region to correctly capture the flow behaviour.

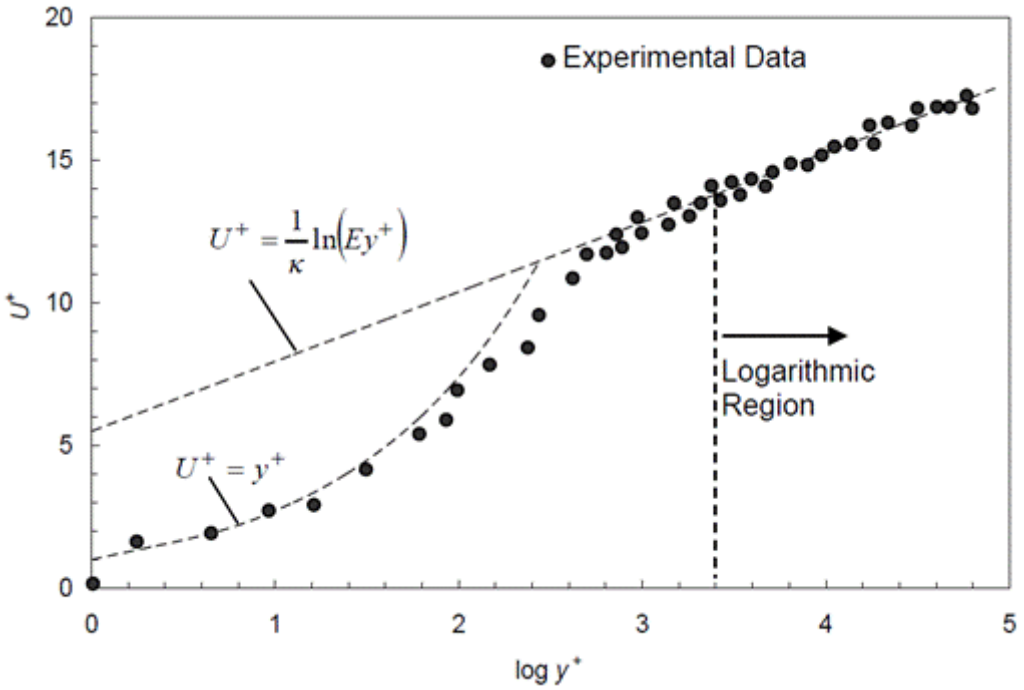

Figure 5.2: Velocity distribution of near wall region (Tu, 2008)

In order to determine the first layer thickness, a Y plus value of one is used which is suitable for the SST turbulence model as the flow is expected to experience an adverse pressure gradients and separation at the root of the blades. A first layer thickness of 0.0001895m is used for the wall region of the turbine blades with a growth rate of 15 per cent. The

maximum layers in the boundary were chosen to be 19 layers. Figure 5.3 shows the mesh of the fluid domain as well as inflation layer applied at the wall. The mesh density increases in the location of interest and gradually decreases in the far away areas from the blade.

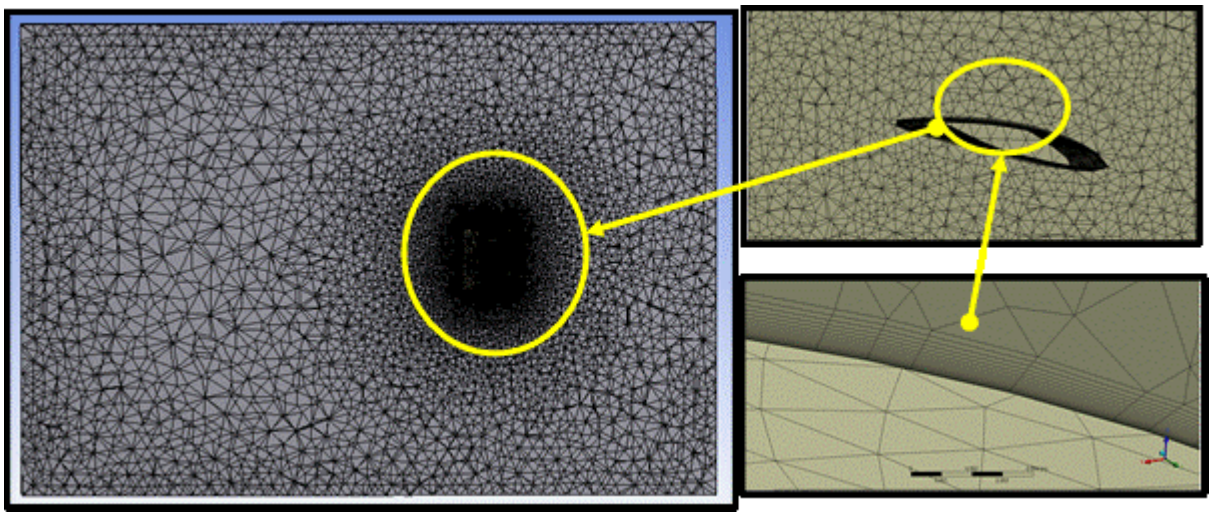

Figure 5.3: Boundary layer mesh of wind turbine blade

5.5 Boundary Conditions

Applying correct boundary conditions is important to provide meaningful values at the boundary of the calculation domain. Since the flow is considered as incompressible in the simulation, an inlet velocity is applied with a medium turbulence intensity of 5 per cent. An outlet pressure of zero was applied at the outlet so that no pressure differential is created at the outlet and as a result the outlet pressure is made to equal the atmospheric pressure. The fluid used in this analysis is a standard air of 25° Celsius with a density of 1.185 kg/m^3 and a dynamic viscosity of 1.183×10^{-5} kg/m s. The wind turbine is applied as a wall boundary with a rotating frame type. An inlet velocity that represents the wind speed and with a corresponding rotational speed obtained in the experiment is used in this simulation. The fluid domain is divided into components, a stationary and a rotating domain. As the name implies, the stationary domain is assumed stationary and the rotating domain is rotating. This method is utilised to simulate the rotation of the wind turbine in the fluid domain. This is further explained in the next section. The far field component of the boundary is applied as a free slip wall. Lastly, the wind turbine blades are applied as a no slip wall. Table 5.3 illustrates the type of boundary used for each component of the fluid domain. A maximum iteration of 900 was selected with a residual RMS value of 10^{-4} . The physical timescale selected for the simulation was 0.001 which lead to convergence in the solution.

Table 5.3: Boundary conditions applied

Boundary Conditions	
Component	**Boundary type**
Inlet	Inlet velocity
Outlet	Pressure outlet
Stationary domain	Stationary
Rotating domain	Rotating
Far field	Wall – Free slip wall
Wind turbine	Wall – No slip wall

5.5.1 Multiple Reference Frame (MRF)

Rotating machines such as a wind turbine are best described by a Multiple Reference Frame (MRF). The flow of air around a rotating wind turbine assumes the fluid flows in an inertial frame of reference while the wind turbine blades rotate in non-inertial reference frame. In a Multiple Reference Frame (MRF) the fluid flow is solved in a rotating reference frame. The Navier Stokes equations are solved in a rotating reference frame that rotates the blade. Mathematically the transformation from a stationary frame to a rotating frame can be achieved in two different methods. The first method of transformation can be obtained through the momentum equations which are expressed in terms of the velocity relative to the moving frame. The second method is achieved by making use of the velocities in the absolute frame of reference in the momentum equations (Liu & Hill, 2000). There are several other methods that can be utilised to model moving components such as a moving mesh. The moving mesh method is quite complex and require high computational resources.

Table 5.4: Fluid domain dimensions

	Rotating Domain	Stationary Domain
Cylinder radius	2m	15m
Cylinder length	1.5m	22m
Upstream	0.5m	7m
Downstream	1m	15m

Table 5.4 shows the dimensions of both the rotating domain and the stationary domain. Sufficient distance in the downstream is important to allow the flow to develop at the wake. A distance of 15 meters is applied in the downstream as well as a distance of 7 metres in the

upstream. Figure 5.4 shows the Multiple Reference Frame (MRF) fluid domain applied in the computational modelling.

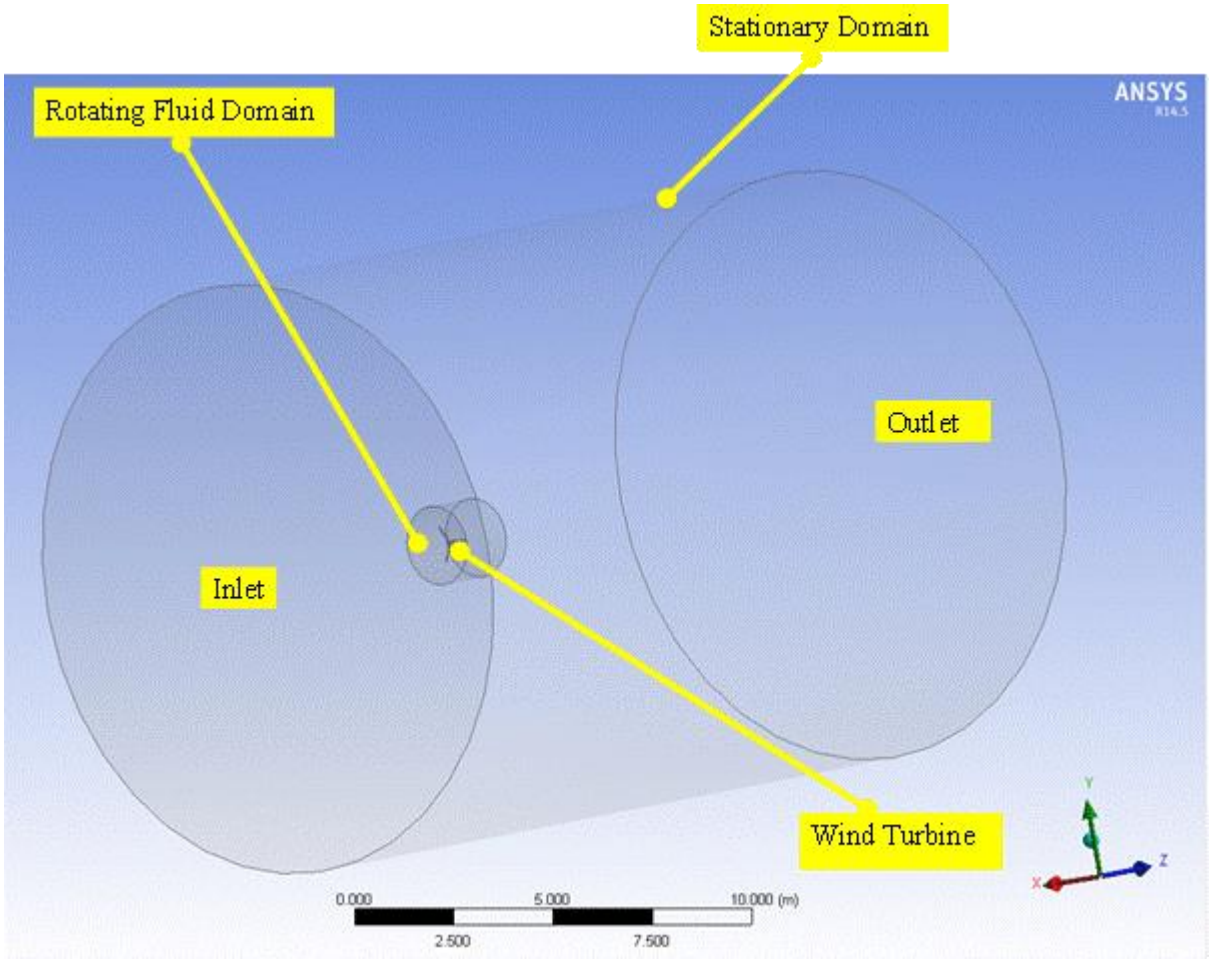

Figure 5.4: Multiple reference frame fluid domain

CHAPTER 6

RESULTS & DISCUSSION

This section outlines the results obtained from experimental work and numerical analysis. A comparison of numerical and the experimental results for the power output of the wind turbine is made. The computational modelling is also utilised to provide qualitative information about the state of flow around the blade tip. Initially tests were conducted followed by the full scale wind turbine test to determine the mechanical power output of the system.

6.1 Initial Test

The initial test was performed in order to better understand the behaviour and characteristics of the aerodynamic forces (i.e. drag and lift) subjected on the blades. To evaluate the effects of a winglet integrated on a wind turbine blade, a single blade from all three different blade tip configuration was tested (i.e. straight blade, forward facing winglet blade and backward facing winglet blade). The drag and lift coefficients were computed with varying yaw angles for each blade using the following equations:

$$C_D = \frac{D}{\frac{1}{2}\rho V^2 A} \tag{6.1}$$

$$C_L = \frac{D}{\frac{1}{2}\rho V^2 A} \tag{6.2}$$

As mentioned earlier, each set of data was taken three times. The blades were tested over range of wind speeds from 30 km/h to 90 km/h with an increment of 10km/h.

6.1.1 Straight Blade (Baseline)

Initial tests were performed for the baseline blade with no winglets integrated into the tip of the blades. In order to determine the influence winglets have on the performance of the blades, it is essential to determine the aerodynamic characteristics of the straight (baseline) blade first which can be used as a reference for the other two design configurations. Figures 6.2 and 6.3 illustrate the lift coefficient and drag coefficient as a function of yaw angle and speed. As the blade twist is distributed along the entire length of the blade radius, the highest twist is located at the root of the blade and subsequently reduces towards the tip of the blade where twist is almost zero at the tip. Due to the twist on the blade, the yaw angle is taken in reference to the blade tip relative to the direction of the airflow. The blades were tested at varying yaw angles of -90° and +90° at an increment of 15° because the geometrical shape of the blade is not symmetrical due to the twist and most importantly the shape of the aerofoil selected for the blades, which is a non-symmetrical aerofoil (SG6051).

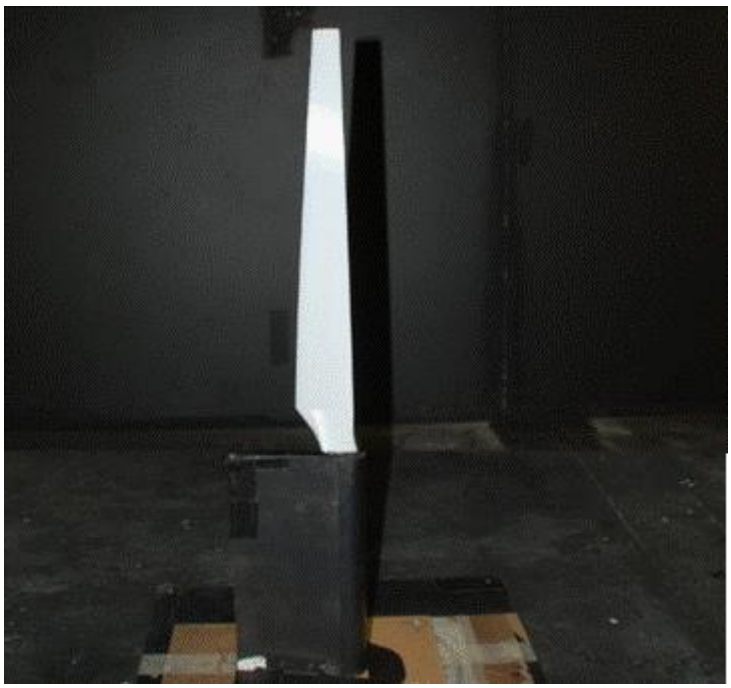

Figure 6.1: Wind tunnel test set up for baseline blade at 0° yaw angle.

From Figure 6.2, the straight blade (no winglets) is found to have an average lift coefficient (C_L) of 0.29 at 0° yaw angle. The lift coefficient (C_L) slightly increases with increasing yaw angle and wind speed, reaching a maximum average value of 0.49 at 30° yaw angle. Above 30° yaw angle, the lift coefficient drops sharply. Similar trend can be observed on the leeward side of the blade (negative yaw angles), where the maximum lift coefficient is 0.78 at -30° yaw angle. Theoretically as the yaw angle is increased to 30° on the windward side, the flow separation from the blade immediately takes effect and the adverse pressure gradient becomes dominant and thus contributes to the loss of lift force on the blade.

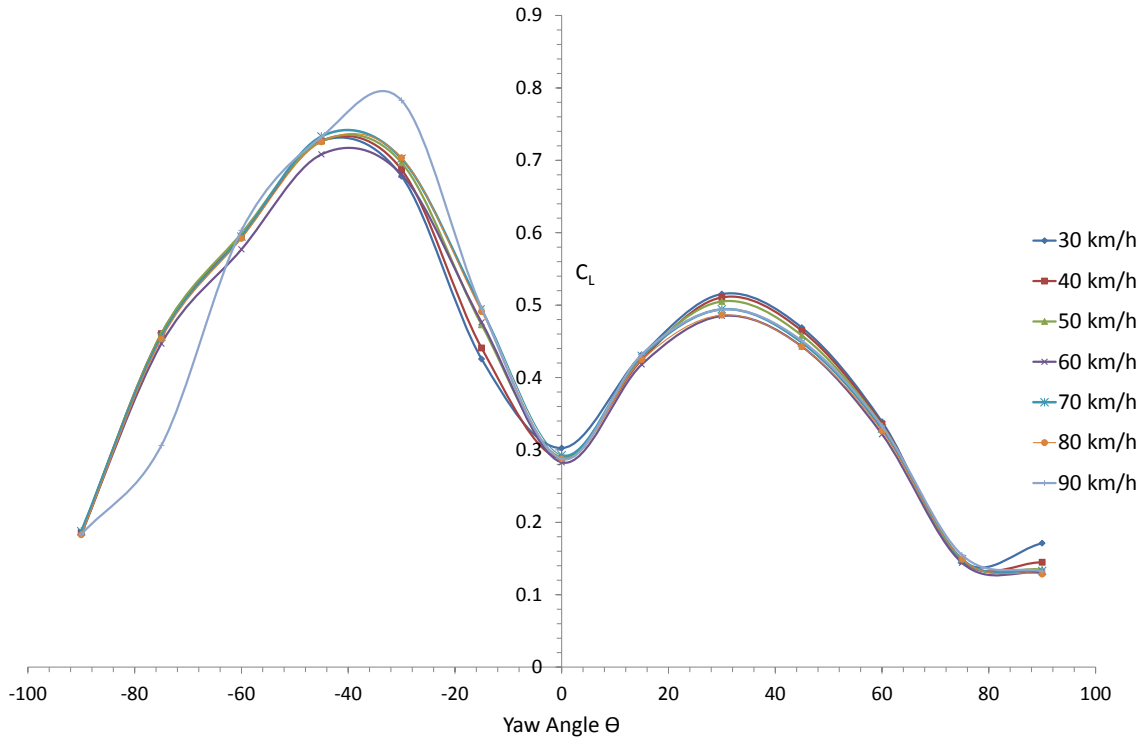

Figure 6.2: Lift coefficient (C_L) as a function of yaw angle and speed for baseline blade.

In comparison to the lift coefficient (C_L) on the blade, the drag coefficient (C_D) increases with increasing speed and yaw angle as shown in Figure 6.3. At 0° yaw angle, the average drag coefficient (C_D) is 0.19. The C_D value steadily increases up to a yaw angle of 75° and then slightly drops as illustrated in Figure 6.2. The average C_D value is found to be 1.07 at 75° yaw angle. A slight variation in C_D value can be observed for the leeward side of the blade. At -15°, the drag coefficient drops to an average of 0.12 in comparison to the C_D value of 0.45 at +15° yaw angle. The drop in C_D value can be attributed to the twist distribution of the blade as the twist varies at every station on the blade. As a result this causes the flow separation to occur around the tip portion of the blade while the flow still remains attached to the inner section of the blade. A notable difference in C_D between the negative and positive yaw angle can be observed at -90° and +90°. The average drag coefficient at +90° yaw angle reduces to 0.95 while the average C_D value at -90° is higher at 1.12.

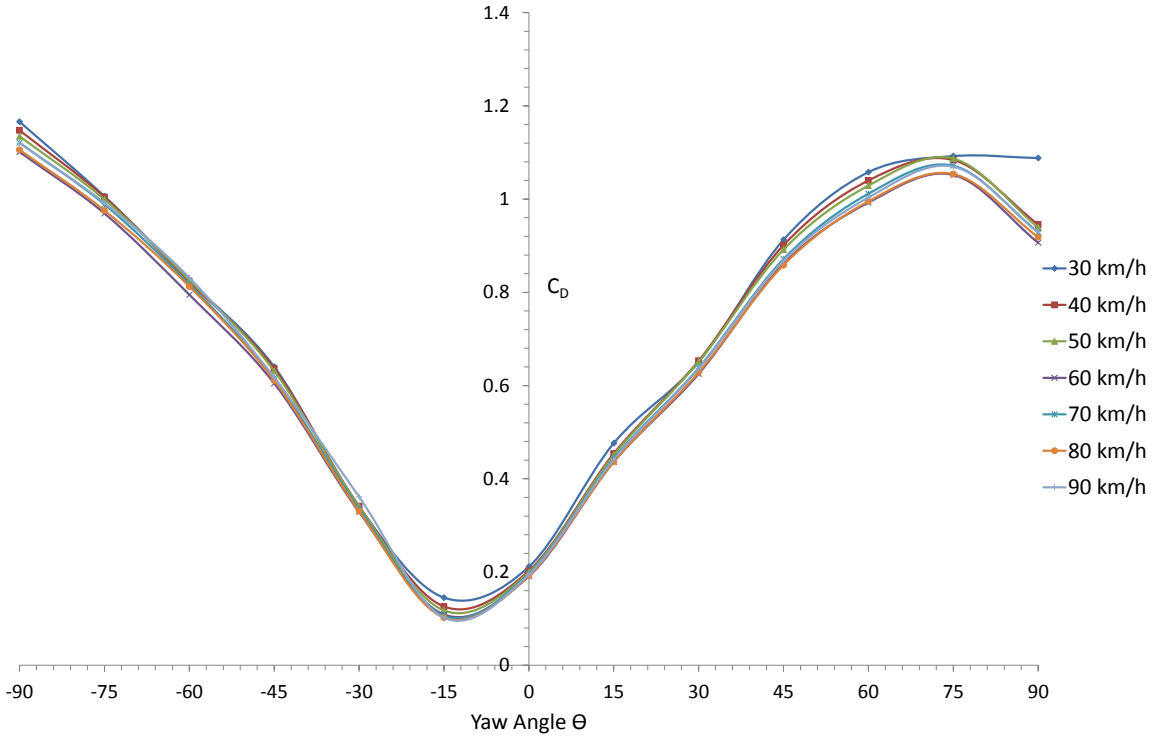

Figure 6.3: Drag coefficient (C_D) as a function of yaw angle and speed for baseline blade.

6.1.2 Forward Facing Winglet Blade (Upwind)

Based on the design of the baseline blade, a forward facing winglet at the suction of the blade was integrated at the blade tip. The suction side of the blade can be considered as the region which has relatively high flow velocity and low pressure. The winglets are designed to reduce the spanwise flow at the tip of the blade by reducing the downwash and thus reducing the induced drag on the blade. As shown in Figure 6.5, the average lift coefficient (C_L) at 0° yaw angle is found to be 0.35. In comparison to the baseline blade with no winglet attached, the lift coefficient for the forward facing winglet blade had increased by 20.7 per cent at 0° yaw angle.

Figure 6.4: Wind tunnel test set up for forward facing winglet blade at 0 yaw angle.

Further increase in lift coefficient is observed as the yaw angle is varied from 0° to 30° and the wind speed is increased simultaneously. Above 30°, the flow initiates to detach itself from the blade and as a result the $C_L$value significantly drops to a minimum value of 0.13 at 90° yaw angle. The results indicate that the flow separation from the blade occurs at two distinct yaw angles for both the negative and positive yaw angle variation. At the leeward side of the blade (negative yaw angle), the flow separation occurs at -45° and as for the variation in the positive yaw angle, the flow separates at +30°.

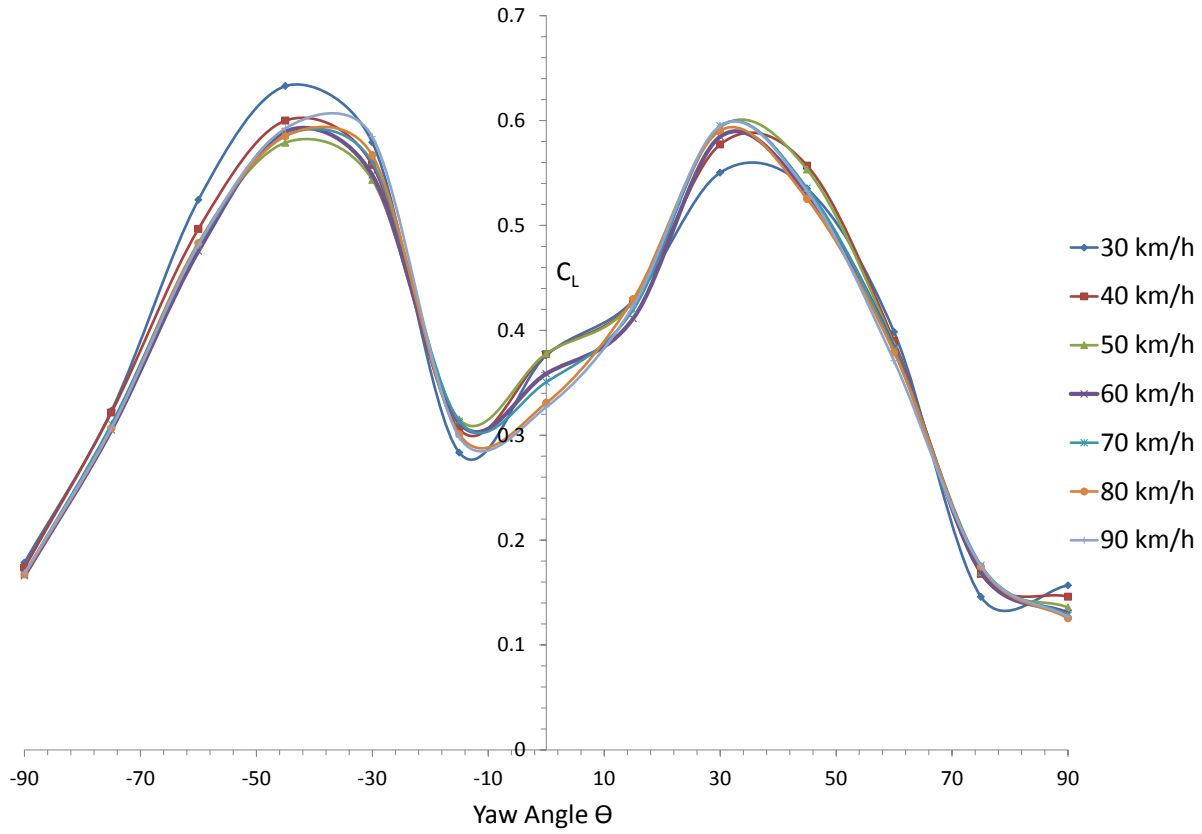

Figure 6.5: Lift coefficient (C_L) as a function of yaw angle and speed for forward facing winglet blade (upwind).

Adding a winglet into a wind turbine results in additional drag on the overall drag exerted on the blade. The additional drag generated by the presence of the winglet must be less than the induced drag in order to improve the aerodynamic performance of the blades. From Figure 6.6, the drag coefficient (C_D) at 0° yaw angle is slightly higher than that of the baseline blade for the same yaw angle. At 0° yaw angle, the drag coefficient is found to be 0.24. The drag coefficient increases with increase in yaw angle and speed. An average C_D value of 1.39 is found at 90° yaw angle. The forward facing winglet blade displayed a higher C_D value when compared to the baseline blade at a yaw angle of 90°. As shown in the graph below the C_D value significantly differs from -90° to +90°. Although the drag drastically increases from 0° to 90°, there is a notable difference in the leeward side of the blade from 0° to -90°. The average C_D value is at -90° yaw angle is found to be 1.01 which is considerably less than that of +90°.

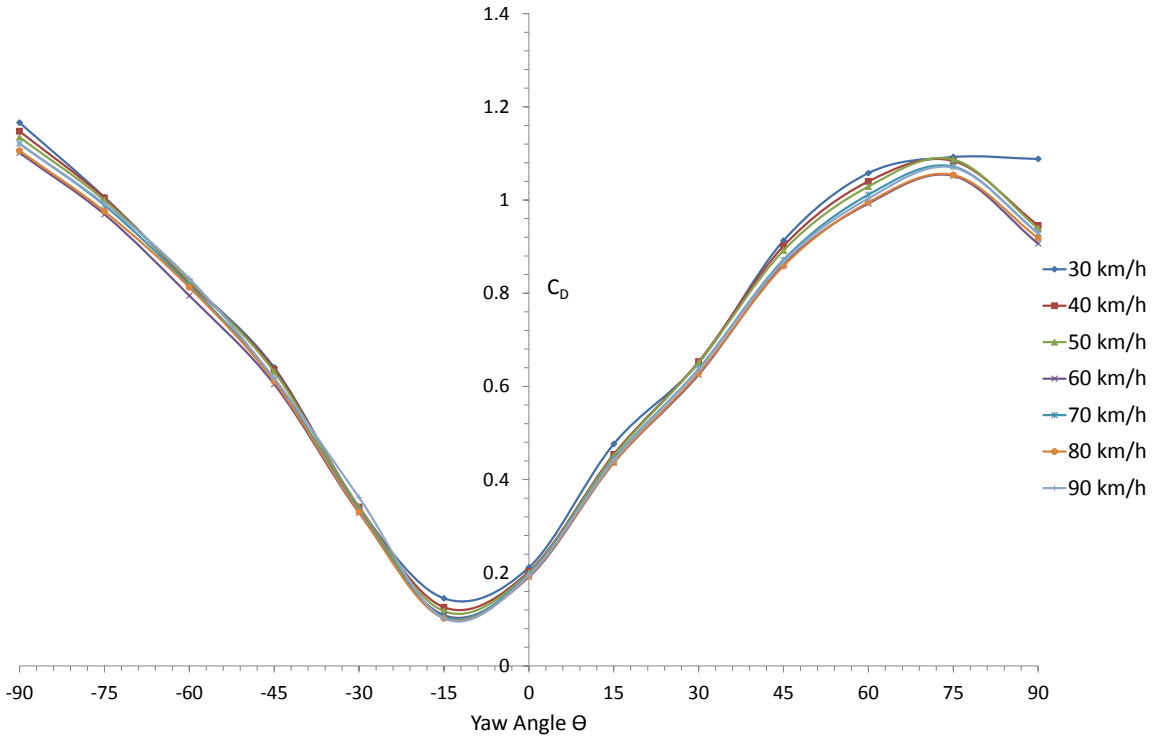

Figure 6.6: Lift coefficient (C_D) as a function of yaw angle and speed for forward facing winglet blade (upwind).

6.1.3 Backward Facing Winglet Blade (Downwind)

The third blade used in this study is the backward facing winglet blade. In this design, the winglet is configured to face in the region of the blade that comprises of low velocity and high pressure which is predominantly known as a pressure facing winglet. As shown in Figure 6.8, the average lift coefficient (C_L) at 0° yaw angle is found to be 0.22, which is considerably less than the forward facing winglet but slightly higher than the baseline blade. The results indicate that the lift coefficient (C_L) reaches an average of 0.67 at 45° yaw angle before the flow separates from the blade and eventually causes the C_L value to drop. However, at the leeward side of the blade, the flow separation occurs at above -30° yaw angle. Further observation in the variation C_L value with yaw angle shows that at -15° yaw angle, the pressure facing winglet blade produces a signi0ficantly high lift coefficient magnitude than the previous two design blades (baseline and forward facing winglet blade).

Figure 6.7: Wind tunnel test set up for Pressure facing winglet blade (downwind) at 0° yaw angle.

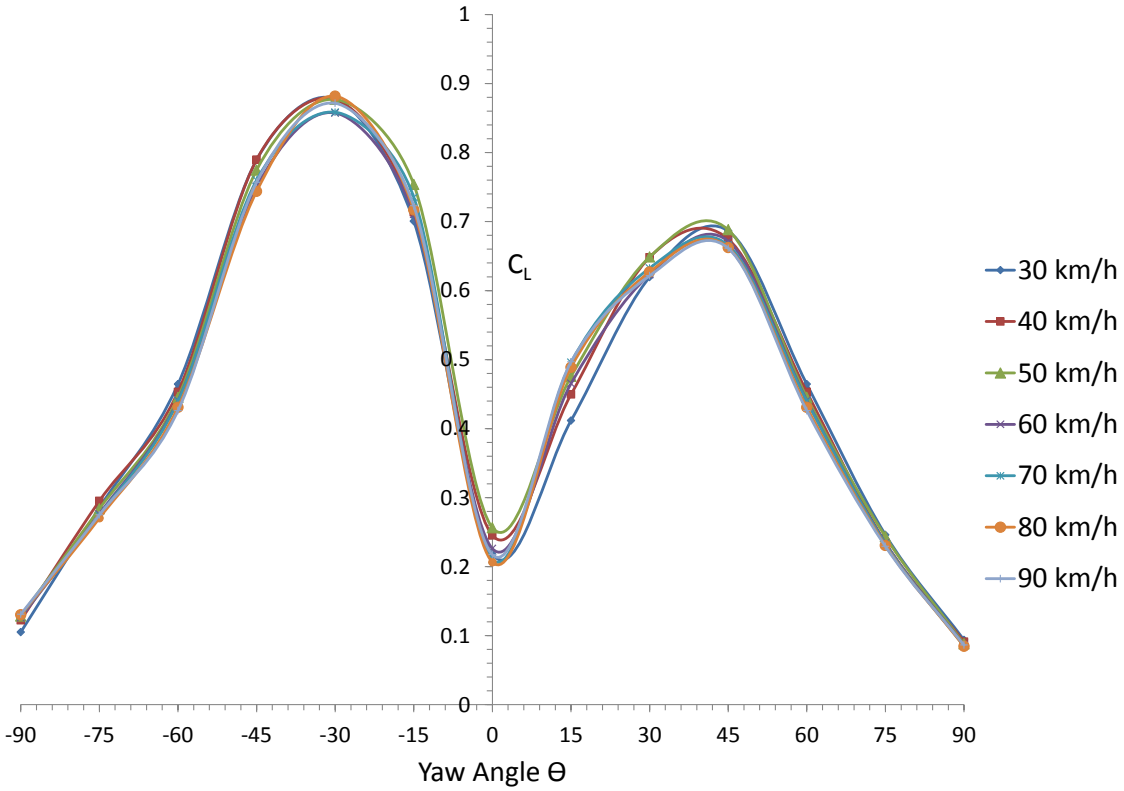

Figure 6.8: Lift coefficient (C_L) as a function of yaw angle and speed for pressure facing winglet blade (downwind).

In Figure 6.9, the pressure facing winglet displayed a similar drag coefficient from -90° to +90° yaw angle. The magnitude of the average C_D value at 0° yaw angle is 0.20. In comparison to the forward facing winglet, the pressure facing winglet produced a slightly lower drag coefficient for the same yaw angle of 0°. As the flow separates from the blade, the drag forces continue to rise until an average C_D value of 1.27 and 1.25 is found for both +90° and -90° yaw angle respectively. Figure 6.9 also indicates that the pressure facing winglet had generated a greater drag coefficient magnitude at lower yaw angles than the previous blades.

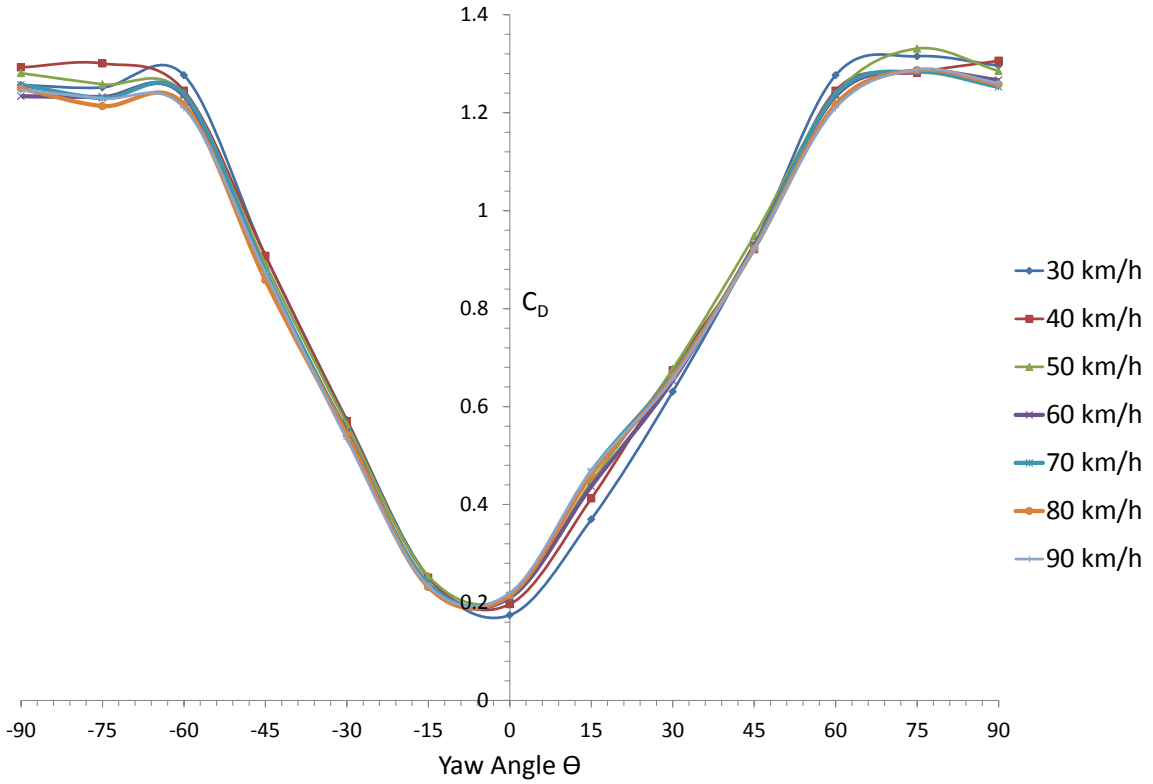

Figure 6.9: Drag coefficient (C_D) as a function of yaw angle and speed for pressure facing winglet blade (downwind..

6.1.4 Comparison of Lift to Drag Ratio (L/D)

To determine the effectiveness of the wind turbine blades with and without the winglets, the lift to drag ratio of each blade is evaluated. Figure 6.10 represents the lift to drag ratio obtained for the baseline blade, forward facing winglet blade and the pressure facing winglet blade. A comparative analysis was conducted to determine the influence of the winglets on the overall aerodynamic properties such as the ratio of lift and drag. The results indicate that the lift to drag ratio varies significantly for the three blades. The forward facing winglet blade produced the highest lift to drag ratio with a value of 5.15 at 0° yaw angle when compared to the straight blade with a value of 4.08. The lowest lift to drag ratio was produced by the backward facing winglet with a value of 2.98 at -15° yaw angle. The forward facing winglet corresponded to an increase in lift to drag (L/D) ratio of 26% from the baseline blade. The backward facing winglet however, resulted in a decrease of lift to drag ratio of 27%. It is apparent that the utilisation of the winglets in the suction side of the blade resulted in an overall increase in lift to drag ratio. It is anticipated that the increase in L/D will yield a greater power output for the forward facing winglet blade than the baseline blade and backward facing winglet.

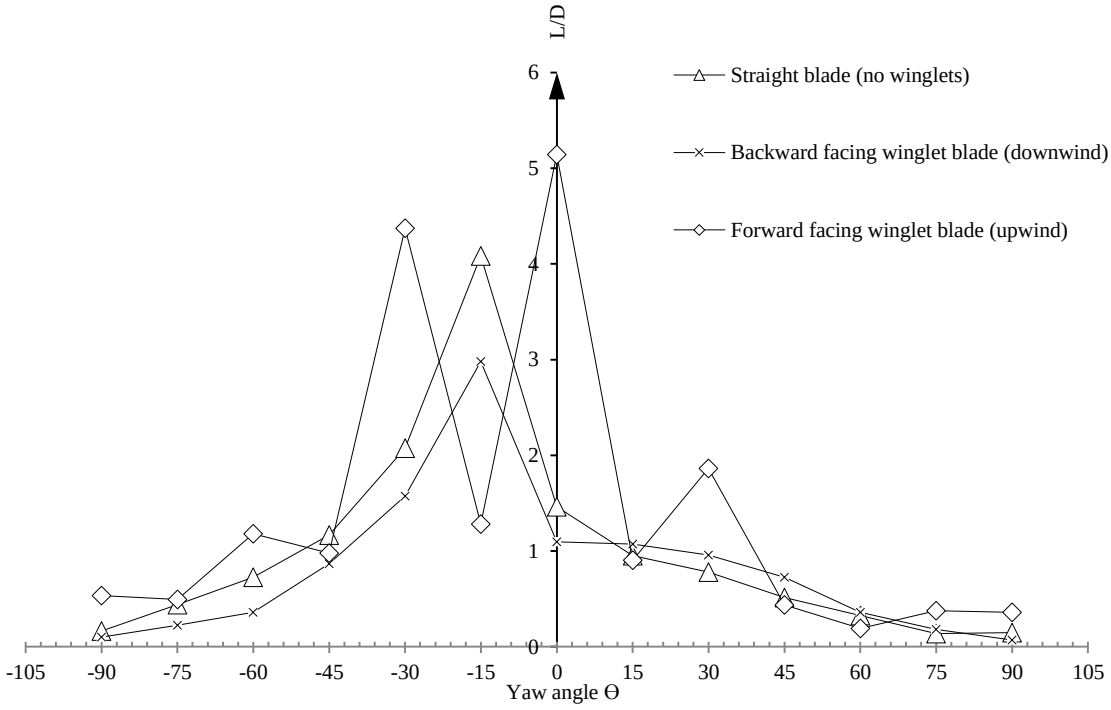

Figure 6.10: Lift to drag ratio for different blade configuration

6.1.5 Side Force Comparison

Winglets are integrated into wind turbine blades with the sole purpose enhancing the aerodynamic performance of the blades and thus ultimately improving the energy extraction from the wind. However, in order for a winglet to be effective it must generate a side force that would divert the inflow air. Figure 6.11 illustrates the side force generated by the blade as a function of speed. At low speeds the side force variation is very small for all three blades. However at above 50 km/h, the side force varies significantly. The results indicate that, the forward facing winglet blade produced a higher magnitude side force at 90 km/h at a magnitude of 1.05 N. The backward facing winglet blade produced a side force of 0.27 N which is noticeably less than the baseline blade of 0.40 N at 90 km/h. From these results, it is apparent that by positioning the winglet in the suction (low pressure and high velocity) side of the blade, it significantly influences the side force exerted on the blades by increasing the side force. A less desirable effect is observed for when the winglet is positioned in the pressure dominated region of the blade.

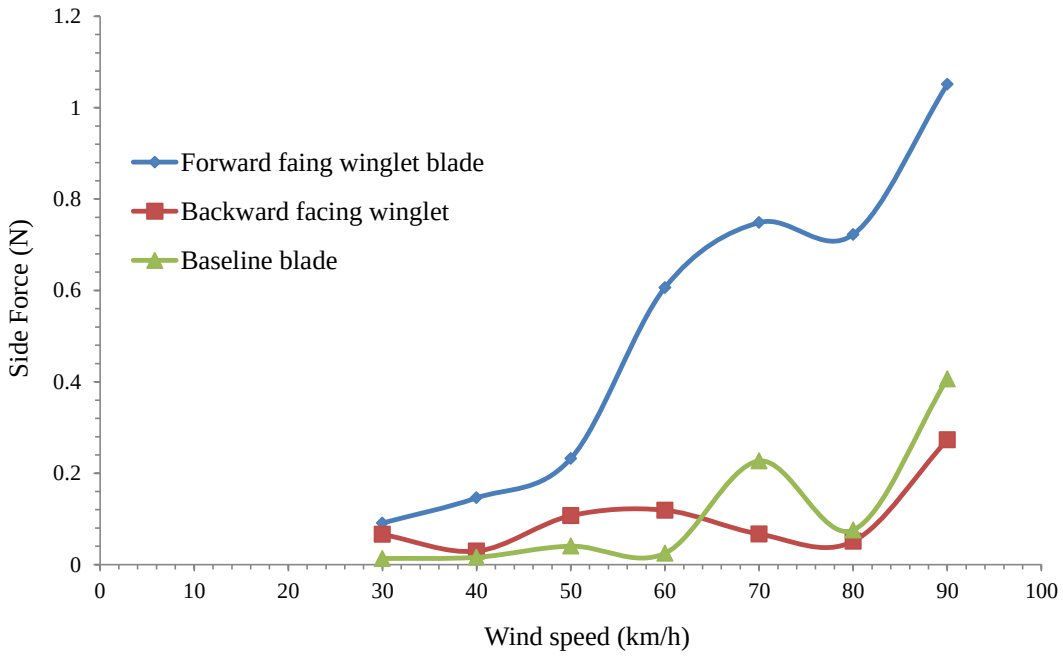

Figure 6.11: Side force variation as a function of speed for all three blade design configuration.

6.2 Wind Turbine Performance Curve

In order to determine the performance of wind turbines, there are several parameters which must be known and are used to evaluate the wind turbine performance characteristics. The tip speed ratio which is defined as the ratio of blade tip rotational speed and wind speed is an essential parameter which is used to determine the performance of wind turbines in a normalised form (C_PVs. λ). Wind tunnel experiments were conducted for all three blade design configurations at varying shaft length (36.8mm, 100mm and 150mm) for all three sets of blade configuration as described in Section 4.5.2.

6.2.1 36.8mm Shaft Length

Each set of wind turbine was evaluated for its power extraction capabilities and compared by determining the performance curve or otherwise known as the power curve. Figure 6.13, represents the performance curve of all three wind turbine design configuration as function of tip speed ratio. During the experimental wind tunnel test, it was observed that the starting speed for which the wind turbines began rotating varied for all three designs. The baseline wind turbine began to rotate at a speed of 18 km/h whereas for the forward facing winglet and the pressure facing winglet started rotating at a wind speed of 18 km/h and 20.5 km/h respectively.

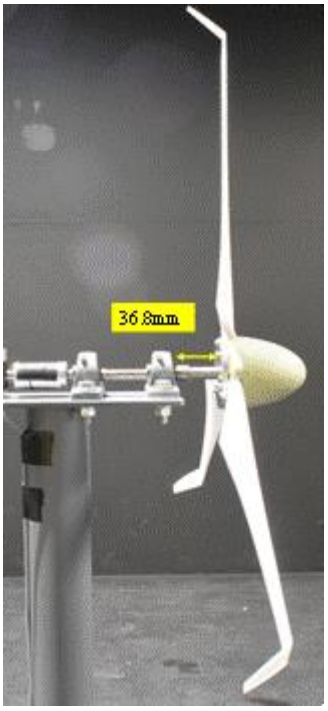

Figure 6.12: Wind turbine test setup with 36.8mm shaft length extension

As shown in Figure 6.13, the power coefficient (C_P) of all three wind turbine design configuration varied. The results revealed that the forward facing winglet blade produced a higher power output than compared to the backward facing winglet and straight blade. The maximum power output generated by the forward facing winglet blade is found to be 252.6 Watts. This resulted in an increase of 21.2 W when compared to the straight blade which produced a power output of 231.4 W. In contrast to the forward facing winglet blade, the backward facing winglet produced the opposite effect. The power output produced by the backward facing winglet is found to be 213.2 W. This is significantly lower than the other two blade design configurations. As indicated in Figure 6.13, the power coefficient (C_P) of the forward facing winglet blade is found to be 0.48 which is higher than the power coefficient of the backward facing winglet blade and the straight blade with a value of 0.41 and 0.45 respectively. During the testing phase of the wind turbines, it was observed that the intensity of the noise generated by the blades varied. Not only did the backward facing winglet blade produce the least power coefficient(C_P), it also generated an undesired level of noise at higher wind speeds compared to the straight blade and forward facing winglet blade.

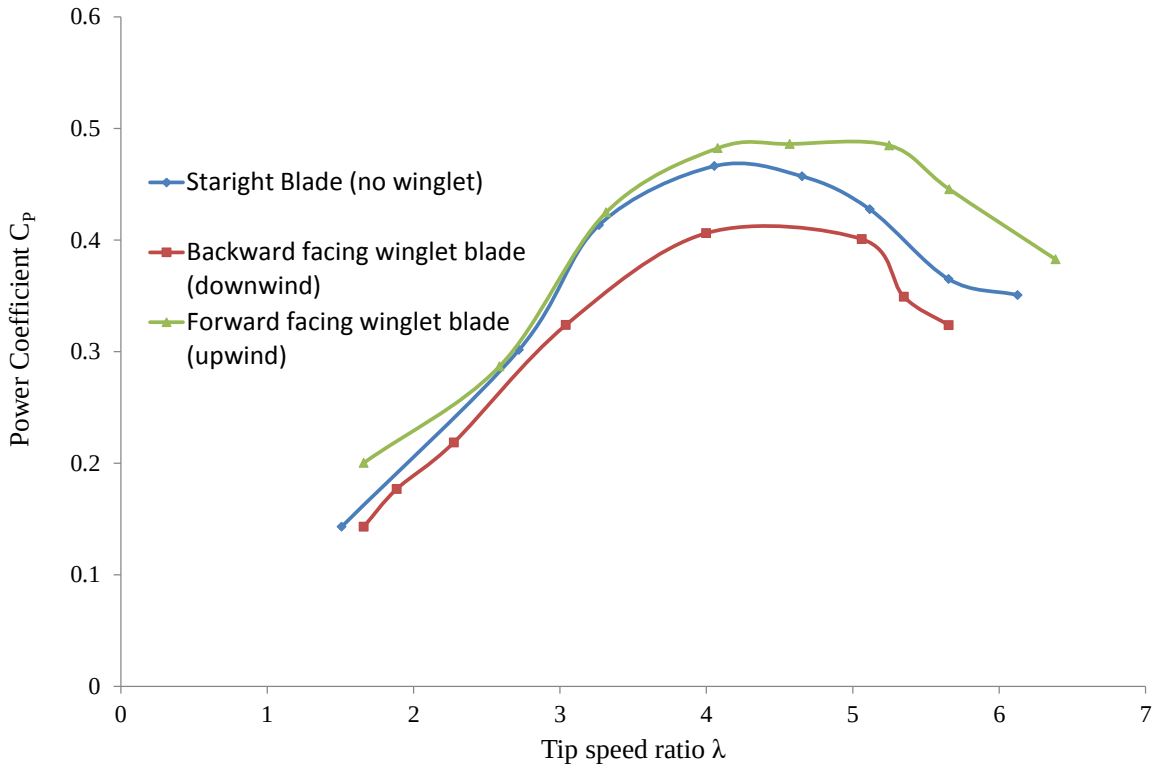

Figure 6.13: Wind turbine performance curve for three different blade design configuration at 36.8mm shaft length.

6.2.2 100mm Shaft Length

The gap between the nearest bearing unit and the hub is extended by a distance of 100mm, as shown in Figure 6.14, in order to evaluate the effects of the interference drag caused by the nacelle. Increasing the shaft length would increase the moment arm and as a result the shaft would be subjected to greater bending loads which would put the bearing units and coupling under significant amount of stress. Therefore, it is essential the 100mm shaft length is tested with extreme care. It was observed during the testing that, extending the shaft by 100mm altered the starting speed of all three wind turbine blade design configuration. The straight blade with no winglets attached began rotating at a wind speed of 20km/h whilst the forward facing winglet blade and backward facing blade started to rotate at 21 km/h and 23 km/h. respectively. All three set of wind turbines were tested over a range of wind speeds from 18km/h to 40km/h at an increment of 2km/h.

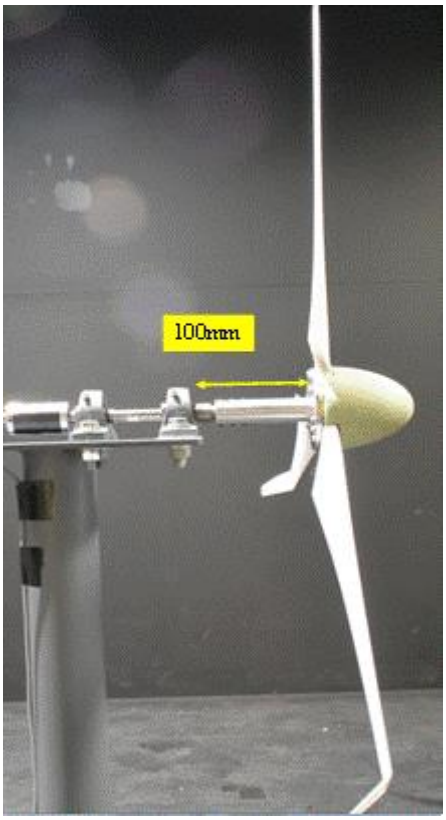

Figure 6.14: Wind turbine test setup with 100mm shaft length extension

Figure 6.15 shows the performance curve obtained from the test of 100mm shaft extension of all three wind turbine blade design configuration. It is evident from Figure 6.15 that the forward facing winglet blade performed better yet again when compared to the other two wind turbine design configuration. On the other hand, the backward facing winglet blade

performed poorly in comparison to the forward facing winglet blade and the straight blade. A power output of 253.6 W was produced by the straight blade with no winglets. This was an increase of 22.2 W when compared to the shaft length of 36.8mm. The maximum coefficient of performance of the straight blade is found to be 0.47. This is obtained at a tip speed ratio of around 4. Although the backward facing winglet blade produced the least power output compared to the other two blade design configuration for a 100mm shaft length, an increase in power output was still obtained when the shaft length is varied from 36.8mm to 100mm. A maximum power output of 217.8 W is found for the backward facing wing blade with a coefficient of performance of 0.41 which is the same as that obtained for the backward facing winglet at 36.8 shaft length. It is clearly indicated in Figure 6.15 that the forward facing winglet resulted in a higher power output in comparison to the straight blade and backward facing winglet blade. The results indicate that a peak coefficient of performance of 0.49 was achieved at a tip speed ratio of 4.5 for the forward facing winglet blade with a maximum power output of 264.3 W. This is an increase of 11.7 W from the 36.8mm shaft length.

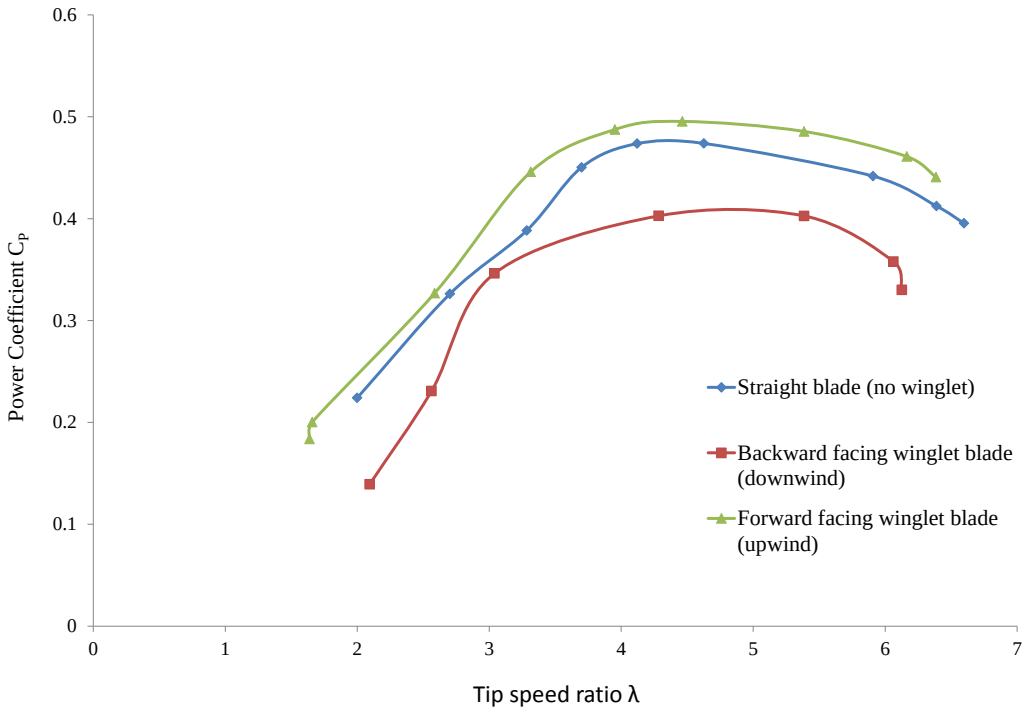

Figure 6.15: Wind turbine performance curve for three different blade design configuration at 100mm shaft length.

6.2.3 150mm Shaft Length

A shaft length of 150mm was also developed to evaluate the effects of interference drag cause by the nacelle. Initially a shaft length of 200mm was proposed, but after taking into consideration the stress that would be exerted on the bearing and coupling due to the thrust of the wind turbine during operation, it was considered a shaft length of 150mm would be appropriate for the experiment. Figure 6.16 illustrates the 150mm shaft length employed in the experiment. All three wind turbine blade design configuration were tested over a range of wind speeds from 18km/h to 40km/h. All three wind turbine blade tip design configuration displayed high rotational speeds at high wind speeds when compared at 36.8mm and 100mm shaft length. The wind turbines, in particular the backward facing winglet blade exhibited undesirable vibration as well noise at high wind speeds. This could potentially explain the discrepancies in the results obtained for the power output.

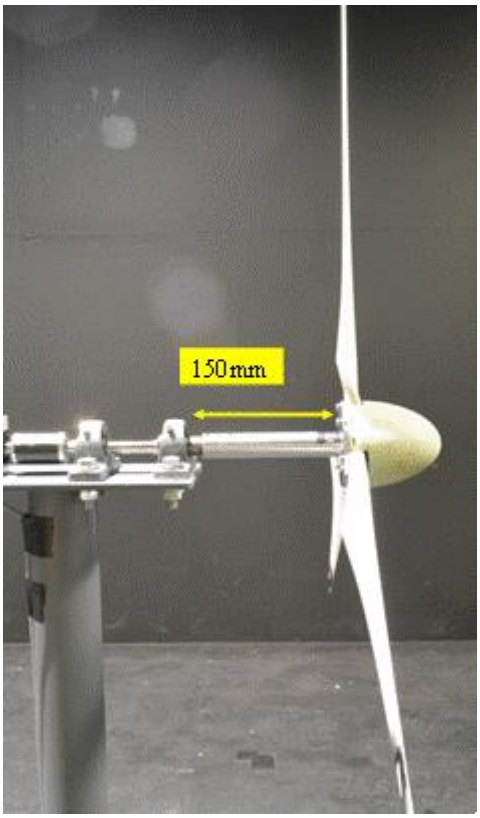

Figure 6.16: Wind turbine test setup with 150mm shaft length extension

As shown in Figure 6.17, the forward facing winglet has had a significant influence on the overall performance of the turbine by generating a higher power coefficient than the other blade tip designs. A power coefficient value of 0.51 is obtained for the forward facing winglet blade at a tip speed ratio of 5.5. The maximum power output recorded for the forward

facing winglet was 237.4 W, an overall increase of 11.1 W from the 100mm shaft length. Although the backward facing winglet blade performed relatively poor compared to the other two blade design configuration, it was observed during the testing the backward facing winglet blade had a low starting speed of 18km/h compared to the forward facing winglet and straight blade of 20km/h and 22km/h respectively. The maximum power output obtained for the backward facing winglet blade was 228.2 W and the maximum power coefficient of the turbine blade is achieved at a tip speed ratio of 5 with a value of 0.43. This is slightly higher than the power coefficient obtained at 100mm shaft length. The straight blade without winglets performed better than the backward facing winglet blade as expected. The maximum power coefficient attained by the straight blade with no winglets attached is 0.48 at a tip speed ratio of 5.2 as shown in Figure 6.17. A maximum power output of 261.4 W was generated by the straight blade.

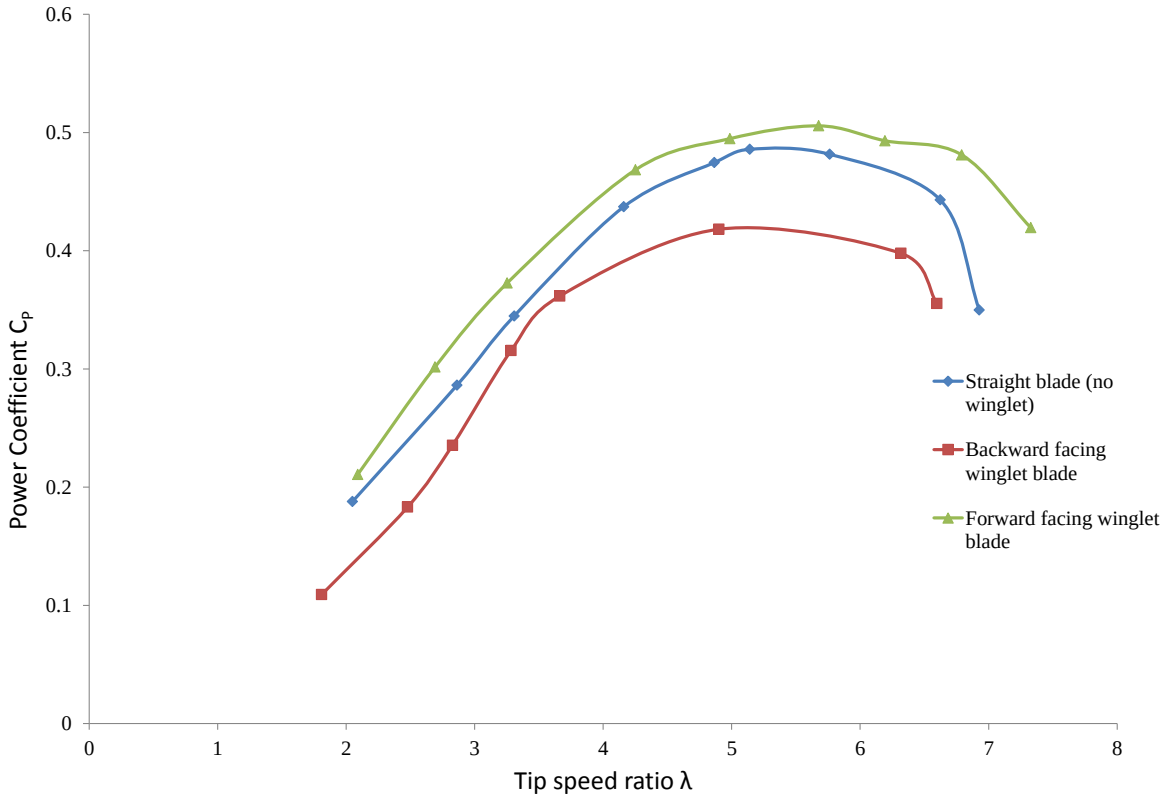

Figure 6.17: Wind turbine performance curve for three different blade design configuration at 150mm shaft length.

6.3 Computational Fluid Dynamics Analysis

The numerical simulation through CFD modelling was primarily employed to understand the power output potential of all three wind turbine blade design configuration at a shaft length of 36.8mm. The experimental data obtained for all three blade design configuration are used to validate the simulation results. Fluid flow analysis of rotating machines such as a wind turbine exhibit complex flow behaviours and therefore in order to achieve a stable solution in the simulation, it is essential that the turbine blades are modelled the correctly. For this analysis a multiple reference frame is utilised to predict and analyse the performance of wind turbine blades. As mentioned previously, the Multiple Reference Frame (MRF) method breaks down the fluid domain into two components, a stationary fluid domain and a rotating fluid domain. The advantage of the MRF method is that it enables us to model rotating components such as wind turbines in a steady state time averaged flow field instead of a transient approach. Ideally wind turbines or any other rotating machines are modelled using a transient approach method. However this method is very complex to achieve convergence and yield a stable solution. It also requires a higher computational resource to simulate the problem. In order to obtain a stable solution in the numerical equations, it is essential that convergence is achieved. A number of variable parameters are monitored such as the torque and thrust produced by the turbines, to ensure that convergence is reached.

6.3.1 Post Processing

Figures 6.18 to 6.23 show the pressure variation of all three wind turbine design configuration (straight blade, forward facing winglet blade and backward facing winglet). It is noticeable that the magnitude of the pressure on the wind turbine blades is higher at the front than at the back. As the airflow approaches the wind turbine, the flow velocity of the air gradually reduces as it is affected by the presence of the wind turbine for which it extracts the kinetic energy of the air. The reduction in airflow velocity gives rise to pressure, hence high pressure is obtained at the front section of the turbine blades. The airflow that immediately passes through the turbine blades, gains momentum and increases in velocity downstream. Due to the increase in velocity of the air downstream, the pressure decreases. As shown in Figure 6.18, the straight blade produced the highest pressure compared to the other two design configuration. The location of maximum and minimum pressure is found at the tip of the blades (leading edge) for both the front and back of turbine blades of all three wind turbine design configuration. The introduction of winglets at the tip of the blades resulted in a

decrease in pressure as shown in Figure 6.20 and Figure 6.22. This may be attributed to the fact that the outward spanwise flow and inward spanwise flow at the blade tip caused by the pressure differences of the front and back surface of the blade is minimised. It is evident that the presence of the winglets at the tip has had an effect in reducing the pressure.

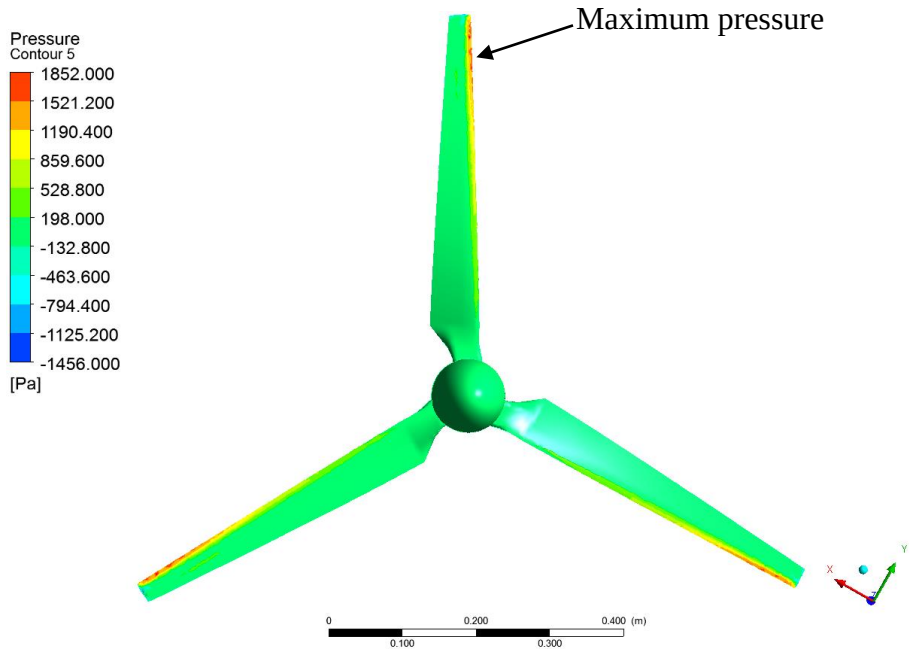

Figure 6.18: Pressure variation contour plot of straight blade no winglet (front view)

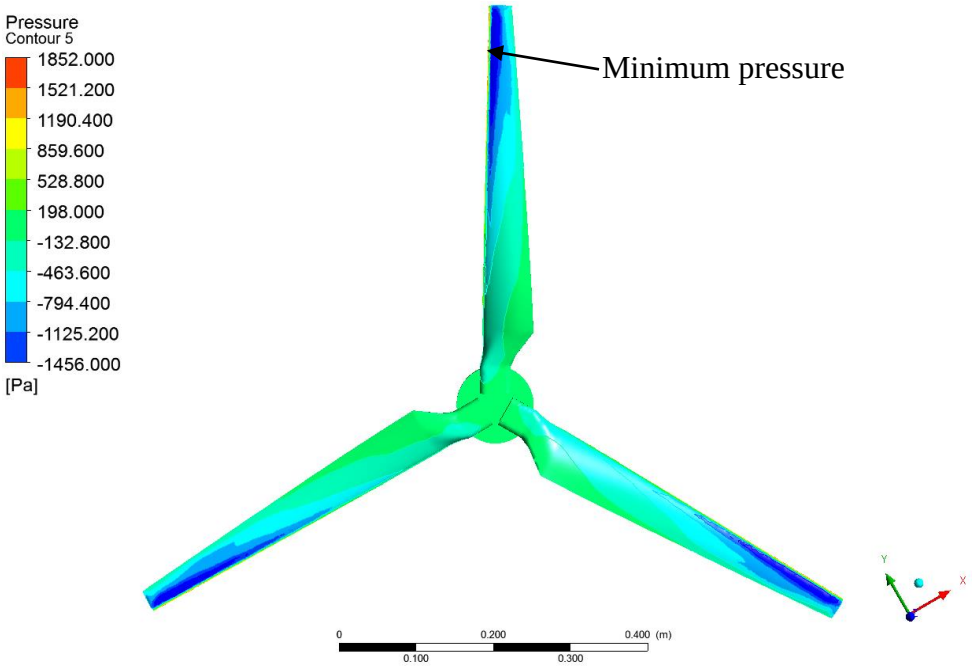

Figure 6.19: Pressure variation contour plot of straight blade no winglet (back view)

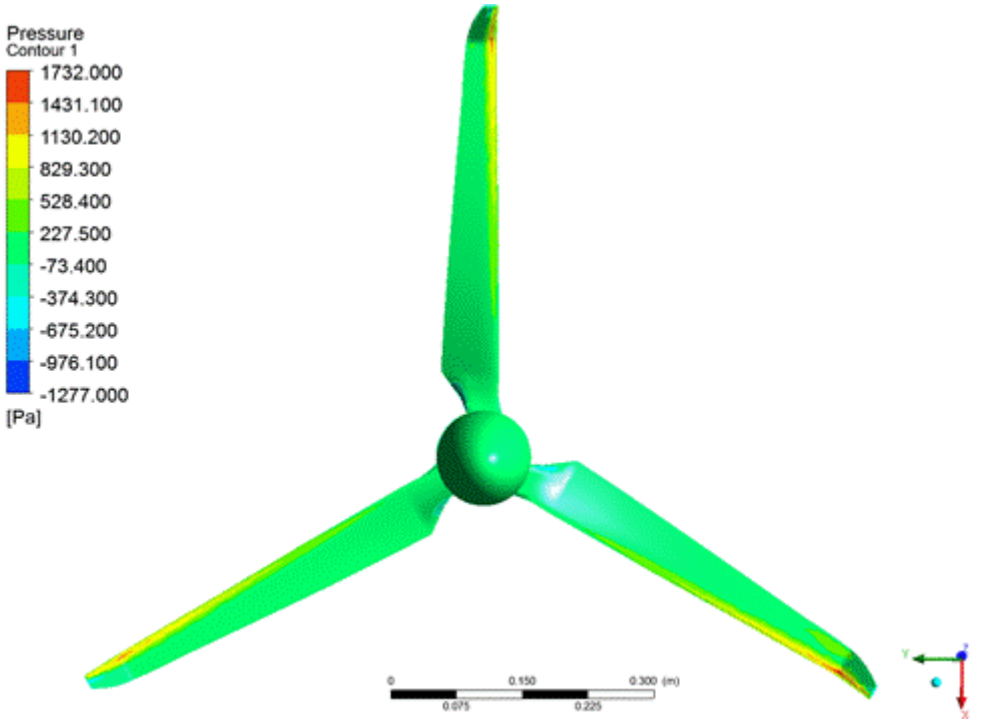

Figure 6.20: Pressure variation contour plot of forward facing winglet blade (front view)

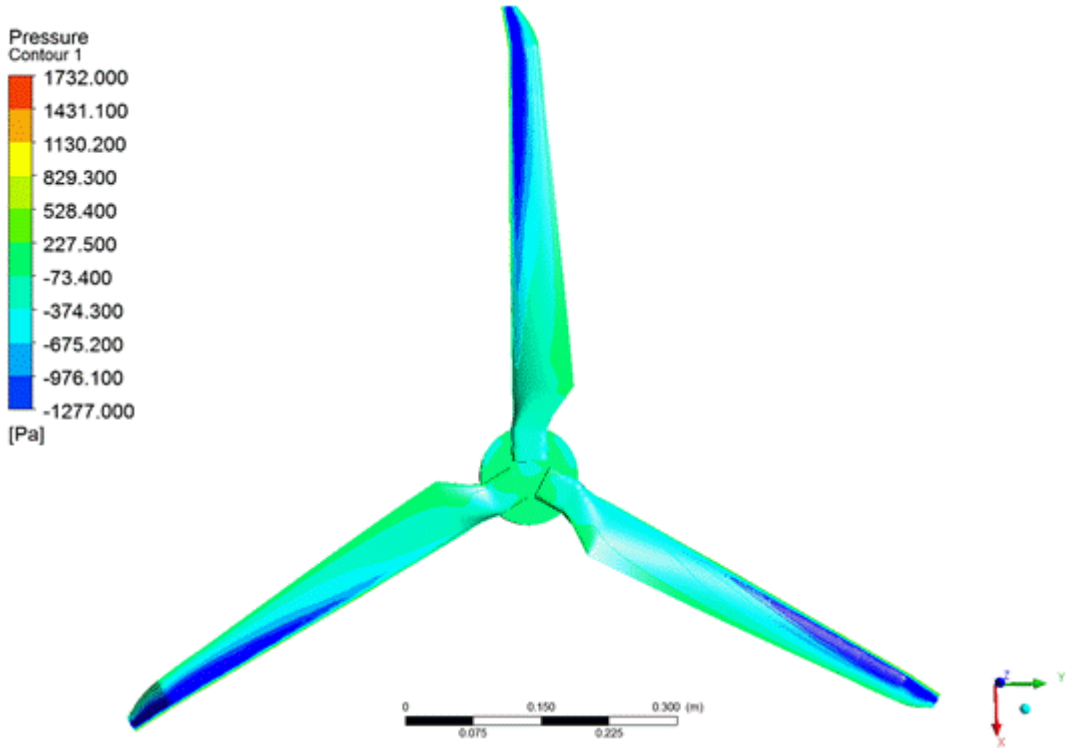

Figure 6.21: Pressure variation contour plot of forward facing winglet blade (back view)

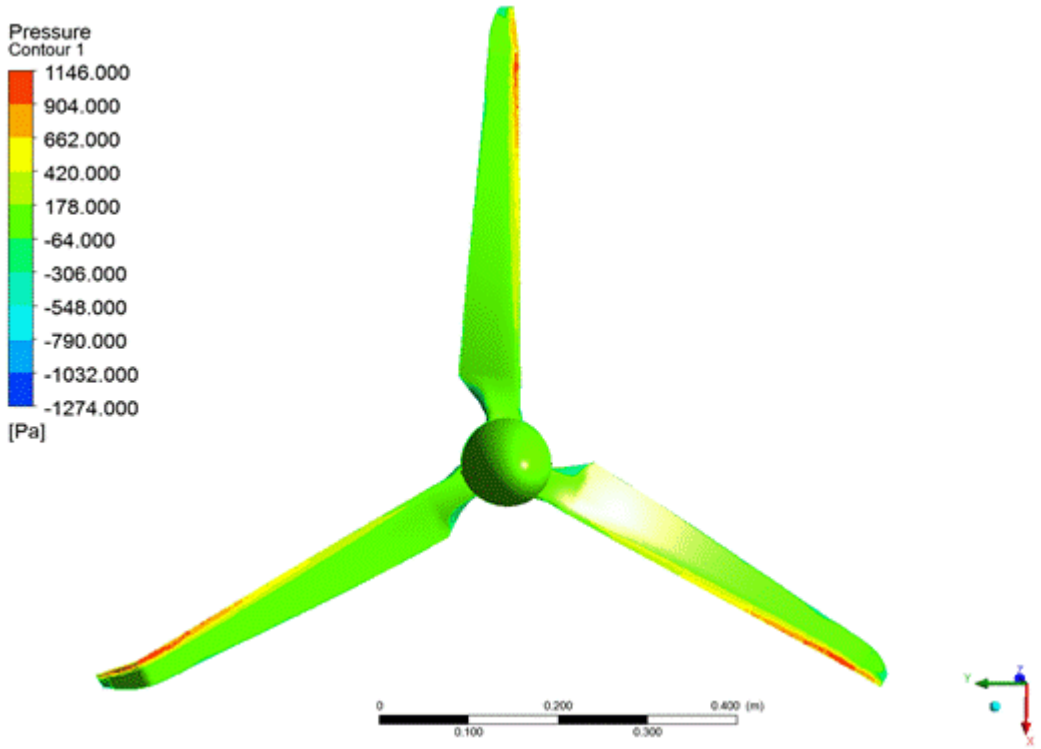

Figure 6.22: Pressure variation contour plot of backward facing winglet blade (front view)

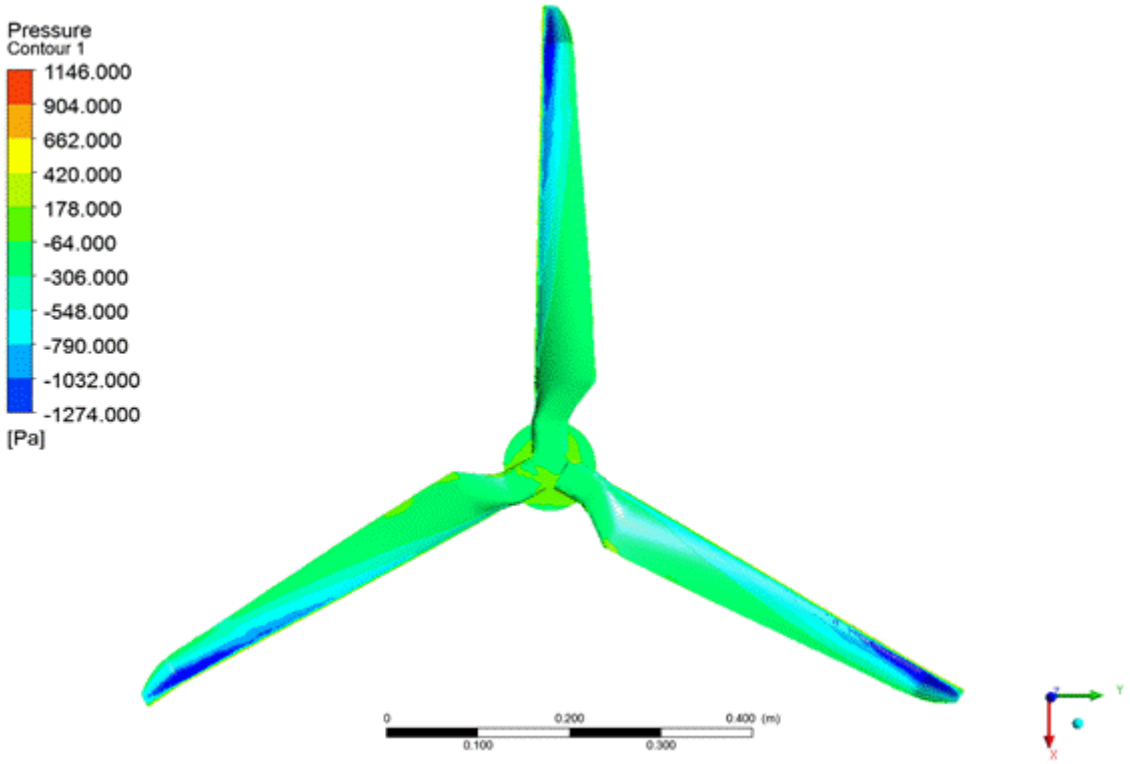

Figure 6.23: Pressure variation contour plot of backward facing winglet blade (back view)

The main objective of employing winglets is to minimise the vortices generated at the tip of the blade due to the pressure differences at the tip. The vortex induces drag on the blade that adversely impacts on the performance of wind turbines. Figure 6.24, illustrates the flow field velocity vector at the tip region of the blade for all three blade tip design configuration. It is clearly shown that the straight blade with no winglets significantly contributes to the formation of vortices at the blade tip. The pressure gradient force drives the high pressure airflow at the pressure side of the turbine outwardly at the blade tip which merges with the low pressure air at the suction side of the blade tip, as illustrated in Figure 6.24. A close inspection of Figure 6.24 reveals that a reduction in the rapid circulation of the flow at the blade tip is achieved with the presence of the winglet. Both the forward facing and backward facing winglet blade successfully achieved in reducing the vortices at the tip. However, the backward facing winglet displays strong presence of turbulence in the flow in comparison to the forward facing winglet blade.

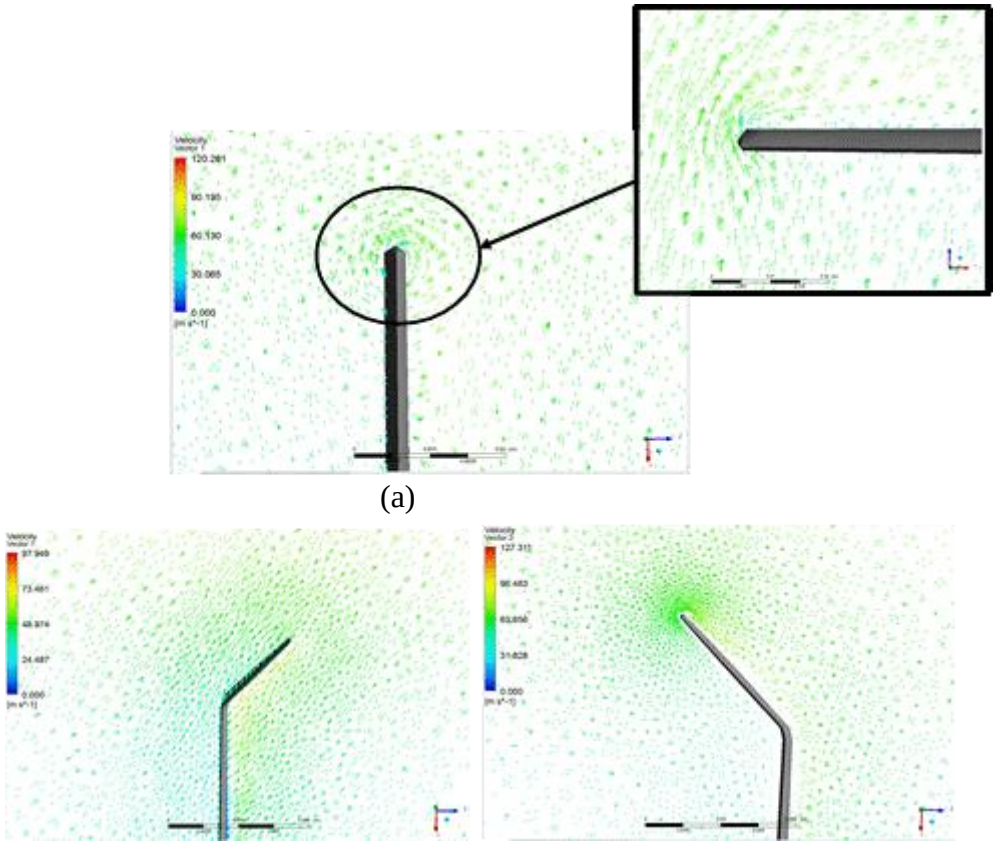

(a)

(b) (c)

Figure 6.24: Velocity vector contour plot (a) straight blade (no winglet) (b) backward facing winglet blade (c) forward facing winglet blade

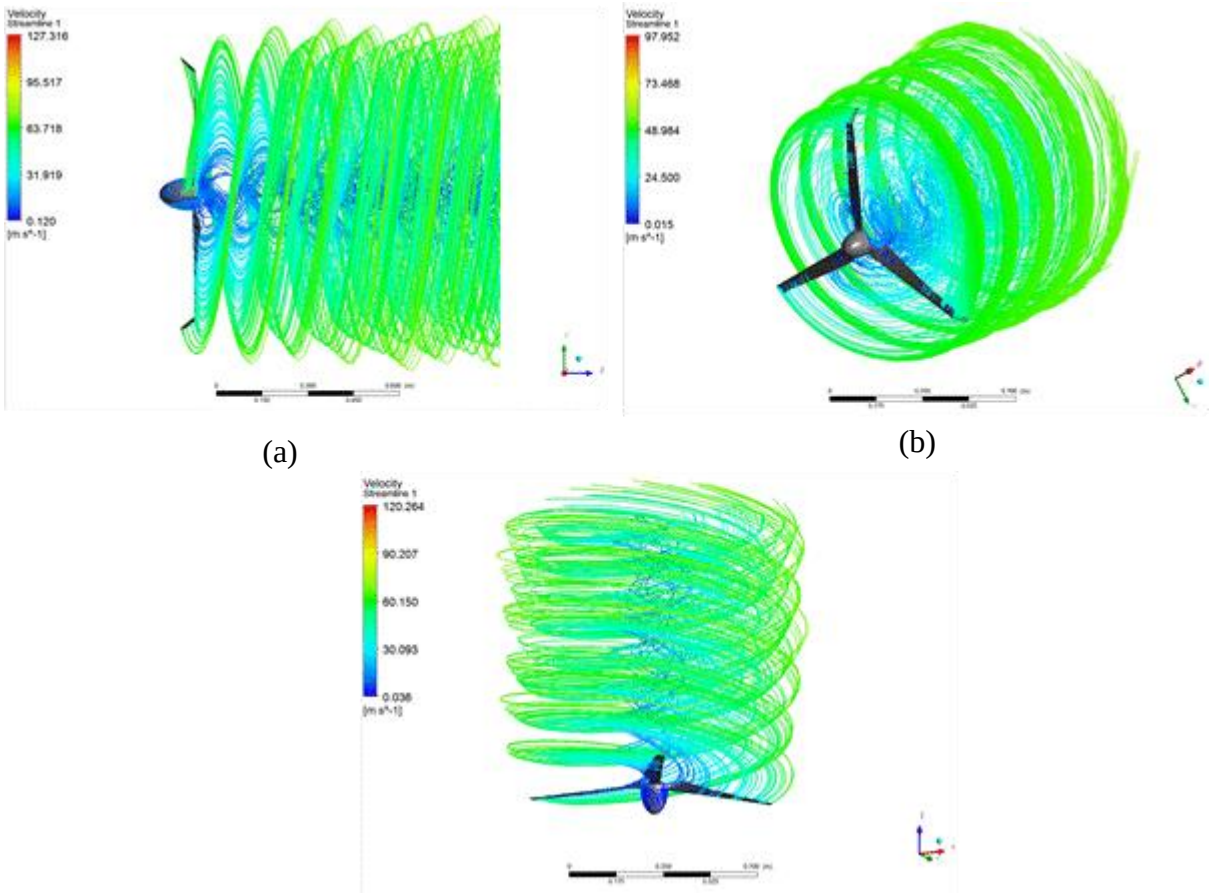

Figure 6.25: Streamline velocity flow path (a) forward facing winglet (b) backward facing winglet blade (c) straight blade (no winglet)

Figure 6.25 illustrates the flow path downstream of the wind turbine for all three blade design configuration. It can be observed that the flow velocity is minimum right through the middle downstream of the wind turbine. As expected, high flow velocity occurs near the tip region of the blade where the tip speed is greater relative to the root section of the blade. The backward facing winglet blade displayed a low flow velocity at the tip as the rotational speed of the turbine decreased when configuring the winglet in that position. The airflow at the tip of the blades imposes torque on the blade that leads to an equal and opposite torque imposed on the air itself. This eventually causes the air to rotate in the opposite direction relative to the wind turbine. As a result the vortex generated at the tip induces a bigger drag magnitude which affects the performance of the turbine blades. It is evident that the forward facing winglet enhanced the rotational speed of the turbine, hence a high power output is generated by the blade.

6.4 Performance Curve (Numerical)

In order to establish the power curve of the turbine blades, the torque generated through numerical simulation is monitored and extracted. It is important to note that the numerical simulation of the wind turbines was performed only for the case of the 36.8mm shaft length. The experimental data obtained for the 36.8mm shaft length was utilised to validate the numerical solution. The power curve obtained through numerical modelling displayed a similar trend to that of the experiment. Figure 6.26 shows the performance curve of all three wind turbine design configuration obtained from the numerical simulation. As expected, the forward facing winglet blade produced a higher power coefficient than the other turbines. A maximum power coefficient of 0.42 is found for the forward facing winglet blade. This is relatively lower than the power coefficient obtained in the experiment. As indicated in the Figure 6.26, the backward facing winglet blade is the least efficient with a power coefficient value of 0.34. This is achieved at a tip speed ratio of 4.2. At low tip speed ratios, the straight blade achieves a higher power coefficient compared to the forward facing and backward facing winglet. However the blades do not generate any sufficient power at these tip speed ratio. A maximum power coefficient of 0.40 was obtained for the straight blade with no winglets.

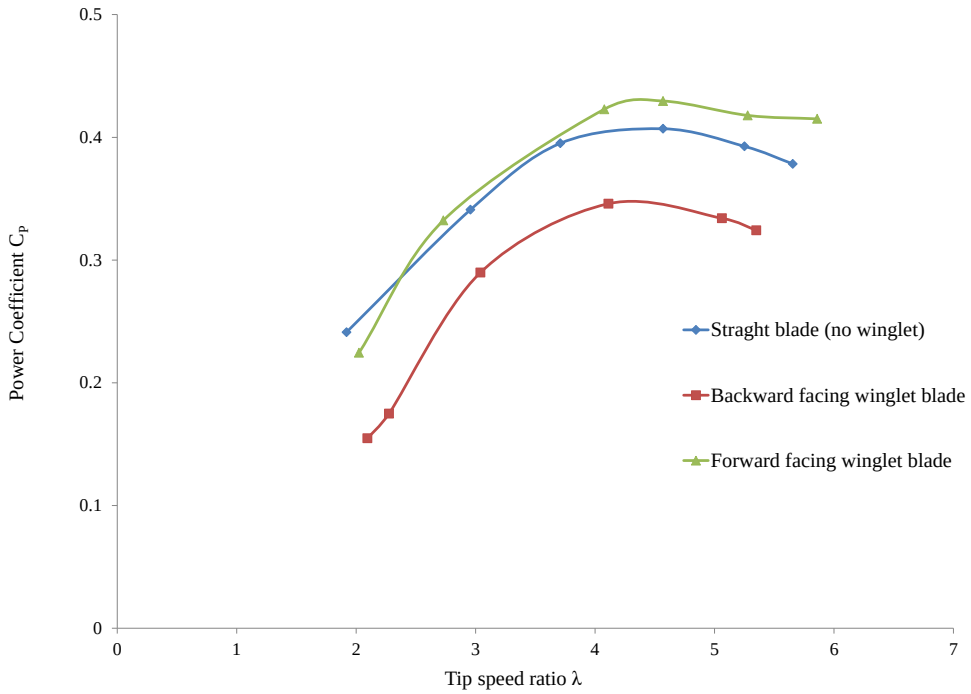

Figure 6.26: Wind turbine performance curve for all three blade design configuration

6.5 Summary of Results

Table 6.1 shows a summary of the wind turbine performance obtained through wind tunnel tests. As shown, the forward facing winglet contributed heavily in the performance of the wind turbine compared to the backward facing winglet and turbine blade with no winglet. It is also shown that increasing the shaft length to reduce interference drag improves the overall performance of the turbine. All three wind turbine blade configuration resulted in an increase in the performance of the turbine as the shaft length is increased from 36.8mm to 150mm.

Table 6.1: Summary of experimental wind turbine performance

Wind turbine design configuration	Shaft Length	Maximum C_P	Maximum power output (Watts)
Straight blade (no winglet)	36.8	0.45	231.4
	100	0.47	253.6
	150	0.48	261.4
Backward facing winglet (downwind)	36.8	0.41	213.2
	100	0.41	217.8
	150	0.43	228.2
Forward facing winglet (upwind)	36.8	0.48	252.6
	100	0.49	264.3
	150	0.51	275.4

Table 6.2 shows a summary of the numerical results of the wind turbine performance for all three wind turbine configuration. As mentioned previously, the simulations were performed for the case of 36.8mm shaft length for comparison with the experimental findings.

Table 6.2: Summary of CFD wind turbine performance at 36.8mm shaft length

Wind turbine design configuration	Maximum C_P	Maximum power output (Watts)
Straight blade (no winglet)	0.40	191.7
Backward facing winglet blade	0.34	149.1
Forward facing winglet blade	0.42	224.7

6.6 General Discussion

In this work, three wind turbine blades (one with no winglet and two with winglets) have been designed, manufactured and investigated. The study was undertaken experimentally using RMIT Industrial Wind Tunnel. The computational modelling was also undertaken using CFX commercial software. The blades have been tested at speeds (30 to 90 km/h) under a range of yaw angles (±90°). The turbine assembly was tested at speeds (15 to 40 km/h). A braking device has been designed and utilised in the experimental investigation to develop the power curve of the turbine with 3 different types of blades.

The aerodynamic properties such as drag, lift and side forces were measured for each type of blades. The mechanical power generated by the turbine with each blade type was measured via a torque sensor over a range of speeds mentioned earlier. The forward facing winglet was positioned at the suction region of the blade. It was noted that such positioning helps diffusing the span-wise vortex flow at the blade tip and consequently improved the aerodynamic lift and reduced the drag (i.e., increased the L/D ratio). The backward facing blades produced more drag than lift. A strong correlation between the lift to drag ratio (L/D) and the power produced by the turbine blade was observed. The power output was direct proportional to the L/D ratio.

It was noted that the effect of nacelle could be controlled by adjusting the gap between the nacelle and the hub. The minimisation of interference drag caused by the nacelle has resulted in power increase.

The results obtained through numerical modelling of the turbine blades slightly differed in comparison to the experimental data. Despite the variation, the overall trend of the data is similar to the experimental findings. Some errors were associated with the computational modelling such as the discretisation error and the modelling error. These errors influenced the numerical solution and caused the variation. Further refinement of the mesh could improve the accuracy of the solution. However, this was not attempted in this study due to time constraint.

In order to obtain the benefit of winglet utilisation in wind turbines, the winglet needs to be structurally well integrated with the turbine blade. One of the major implications of findings from this research is that small scale horizontal axis wind turbines with winglets can be used

in built up areas to harness the wind energy for power generation. This will reduce the dependency on the grid power and contribute to the reduction of greenhouse gas emission.

CHAPTER 7

Conclusion & Recommendations for Future Work

7.1 Conclusions

The main objective of this research were to enhance the power generation capabilities of a small horizontal axis wind turbine utilised in built up areas. An alternative blade tip configuration using winglets was employed and integrated at the tip of the turbine blade for the purpose of enhancing the performance of the wind turbines. This research also investigated the influence of interference drag caused by the presence of the nacelle on the overall performance of the turbine. The following conclusions were therefore drawn from the research work presented here

7.1.1 General Conclusions

Three sets of small full scale horizontal axis wind turbine blades with varied blade tips of approximately 1 metre in diameter were designed and manufactured. A series of test was performed at RMIT Industrial Wind Tunnel in order to evaluate: (a) aerodynamic characteristics of the turbine blades with and without winglets at varied yaw angles (Θ = -90° to +90° with an increment of 15°) and (b) performance of the turbine blades and its power generation capabilities. The turbine blades that were developed and investigated in this research have the same design characteristics and could only be distinguished by their blade tips. A straight blade with no winglet at the tip has been developed and used as a benchmark

to evaluate the performance of both backward facing winglet (downwind) and forward facing winglet (upwind) blade. As the design of winglets is highly complex, the winglet employed in this study was optimised for a cant angle of 45°.

Based on the experimental investigation and computational modelling the following conclusions have been drawn:

The effect of winglets on the aerodynamic properties (drag coefficient, lift coefficient and side force coefficient) is significant. The forward facing winglet produced a significantly higher side force coefficient than the other two blade designs.

The integration of winglets on wind turbine baldes significantly influences the aerodynamic behaviour of the blade regardless of the positioning (suction or pressure side) of the winglet on the blade. The forward facing winglet blade contributed to a high lift coefficient (C_L) compared to the straight blade with no winglets and the backward facing winglet blade.

The forward facing winglet generates a significant increase lift to drag ratio (L/D) in reference to the straight blade (baseline). However, the backward facing winglet generates adverse L/D ratio as the winglet positioning had an adverse effect on the lift to drag ratio (L/D).

The performance of wind turbines has been enhanced through utilisation of winglets. This can be achieved by positioning the winglet on the suction side of the blade where the static pressure of the air is low and the air speed is relatively high. The forward facing winglet blade produced a substantially higher power output in comparison to the straight blade with no winglets and the backward facing winglet blade.

The power output is significantly influenced by the interference drag caused by the presence of the nacelle. Establishing a gap between the nacelle and the turbine hub helps reduces the turbulence in the airflow encountered immediately.

The experimental study revealed that the aerodynamic noise level of the blade varied for all the three blade tip configurations. Minimal noise was found to be affiliated with the forward facing winglet.

A comparative analysis of the numerical modelling results and the experimental findings (based on 36.8mm shaft length) was undertaken. Although there were slight variation in the numerically obtained results compared to the experimental findings, both methods have

shown agreement that the forward facing winglet is the most efficient design in enhancing the performance of the turbine blades. With rapid advancement of computer capabilities, it is feasible and viable to predict the performance of wind turbines through a numerical approach.

7.1.2 Specific Conclusions

The aerodynamic characteristics of each blade design configuration varied with varying yaw angle. At 0° yaw angle, the forward facing winglet blade produced an average lift coefficient (C_L) of 0.35. In comparison to the straight blade with no winglets, the forward facing winglet provided 20.7% increase in lift coefficient (C_L). Although the forward facing winglet blade provided a significant improvement in lift coefficient, it displayed a higher drag coefficient (C_D).

Augmentation of the power output produced by the wind turbine is achieved by positioning the winglet at the suction region of the turbine blade. Placing the winglet at the suction region contributes to the reduction of spanwise flow at the tip of blade and as a result the magnitude of the vortex is minimised. The forward facing winglet blade produced a greater power output compared to both the straight blade and the backward facing winglet blade. A maximum power coefficient value of 0.51 is achieved for the forward facing winglet blade at a shaft length of 150mm. This is an increase of 6.25% from a shaft length of 36.8mm. It is evident that expanding the gap between the nacelle and the wind turbine hub affects the overall performance of the turbine blade. Power enhancement is achieved for all three blade tip design configurations as the shaft length is increased. This is mainly attributed to the reduction in interference drag of the nacelle.

Numerical modelling of wind turbines through CFD simulation provided quantitative information about the state of the flow around the turbine blades. This can be utilised to aid in understanding the aerodynamic behaviour of the turbine blades.

7.2 Recommendations for Future Work

After conducting the work presented here and reviewing the literature review available in the public domain, the following areas have been identified for future work:

1. One of the major limitations of this research is the choice of material selected to construct the wind turbine blades. An ABS polycarbonate material provides sufficient strength to resist the centrifugal forces exerted on the blades during operation however they have a very poor stiffness. Due to the lack of adequate stiffness in ABS polycarbonate materials the turbine blades experienced excessive vibration at high wind speeds. Alternative materials to polycarbonate are carbon fibre composites, Australian hoop pine wood and radiata wood. All of the aforementioned materials provide good strength and stiffness.

2. The performance curve obtained in this study is based on the mechanical power output and not the electrical power. It would be extremely useful to evaluate the power generation capabilities of the turbine using an electric generator.

3. Winglets are highly sensitive devices that can influence the aerodynamic forces and the performance of wind turbines. Further optimisation of the winglet is required that evaluates the effects of sweep angle, toe angle and twist.

4. As the wind speed is highly unpredictable in built up areas, in situ measurements are required to evaluate the turbine performance.

5. More comprehensive CFD modelling is imperative in order to understand better and establish an accurate correlation with the experimental findings.

REFERENCES

Alam, F. (2000). *The effects of car A-pillar and windshield geometry on local flow and noise.* (PhD Thesis), Royal Melbourne Institute of Technology.

AviationPartners. (2012). Blended Winglet Technology. Retrieved 12th November, 2012, from http://www.aviationpartners.com/technology.html

Barlow, J., Rae Jr., W. H., & Pope, A. (1999). *Low-speed wind tunnel testing*. New York: John Wiley & Sons Inc.

Blocken, B., & Carmeliet, J. (2004). Pedestrian wind environment around buildings: literature review and practical examples. *Journal of Thermal Envelope and Building Science, 28*(2), 107-159.

Breitsamter, C. (2011). Wake vortex characteristics of transport aircraft. *Progress in Aerospace Sciences, 47*(2), 89-134.

Burton T., Sharpe D., Jenkins N., Bossanyi E.,. (2001). *Wind Energy Handbook* (1st ed.): John Wiley & Sons.

Capeluto, G., Yezioro, A., & Shaviv, E. (2003). Climatic aspects in urban design - a case study. *Building and Environment, 38*(6), 827-835.

Cermak, J.E. & Isyumov, N. (1998). Wind Tunnel Studies of Buildings and Structures (Asce Manual and Reports on Engineering Practice). American Society of Civil Engineers.

Charlier, R. H., & Justus, J. R. (1993). *Ocean energies: environmental, economic and technological aspects of alternative power sources*: Elsevier.

Chattot, J. (2009). Effects of blade tip modifications on wind turbine performance using vortex model. *Computers & Fluids, 38*(7), 1405-1410.

Cui, P., & Han, J. (2012). Prediction of flutter characteristics for a transport wing with wingtip devices. *Aerospace Science and Technology, 23*(1), 461-468.

Dopita, M., Williamson, R. (2009). Australia's Renewable Energy Future (pp. 8-15): Australian Academy of Science.

Døssing, M. (2007). Vortex lattice modelling of winglets on wind turbine blades. *Master's thesis. Risø National Laboratory, Technical University of Denmark, Roskilde, Denmark.*

Eggleston, D., & Stoddard, F. (1987). *Wind turbine engineering design*. New York: Van Nostrand Reinhold.

Eriksson, S., Bernhoff, H., & Leijon, M. (2008). Evaluation of different turbine concepts for wind power. *Renewable and Sustainable Energy Reviews, 12*(5), 1419-1434.

Etkin, B. (2012). *Dynamics of atmospheric flight*: Courier Dover Publications.

Gertz, D. (2011). *An Evaluation Testbed for Alternative Wind Turbine Blade Tip Design.* (Masters Thesis), University of Waterloo.

Gillard, J., Swan, W., & Combet, G. (2011). Securing a clean energy future: The Australian Government's Climate Change Plan: Australia Department of Climate Change and Energy Efficiency.

Gross, W.F.M. (1898). Atmospheric Resistance to the Motion of Railway Trains. *The Engineer, UK*.

GWEC. (2012). Global Wind Report Annual Market Update. Retrieved 20th June 2012, from http://www.gwec.net/index.php?id=180

Hansen, M. (2013). *Aerodynamics of wind turbines*: Routledge.

Hau, E. (2005). *Wind Turbines Fundamentals Technologies Application Economics* (1st ed.). Germany: Springer.

Hughes, L. (2003). Climate change and Australia: trends, projections and impacts. *Austral Ecology, 28*(4), 423-443.

IEC. (2011). International Electrical Commision. Retrieved 11th November, 2011, from http://www.iec.ch/etech/2012/etech_1112/tech-3.htm

Jamieson, P. (2011). *Innovation in wind turbine design*: Wiley.

Johansen J., Sorenson, N. (2006). Aerodynamic Investigation of Winglets on Wind Turbine Blades using CFD. Denmark: RISO National Laboratory.

Kuo, B., & Sarigul-Klijn, N. (2012). Conceptual study of micro-tab device in airframe noise reduction:(II) 3D computation. *Aerospace Science and Technology, 17*(1), 32-39.

Kubota, T., & Ahmad, S. (2006). Wind environment evaluation of neighborhood areas in major towns of Malaysia. *Journal of Asian Architecture and Building Engineering, 5*(1), 199-206.

Lee, H., Park, S., Kim, H., Rhee, Shin H., & Kim, C. (2012). Computational methods for performance analysis of horizontal axis tidal stream turbines. *Applied Energy, 98*, 512-523.

Lee, S., & Lee, S. (2014). Numerical and experimental study of aerodynamic noise by a small wind turbine. *Renewable Energy, 65*, 108-112.

Liang, H., Sun, L., Zong, Z., Zhou, L., & Zou, L. (2013). Analytical modelling for a three-dimensional hydrofoil with winglets operating beneath a free surface. *Applied Mathematical Modelling, 37*(5), 2679-2701.

Lien, F.S., Yee, E., & Cheng, Y. (2004). Simulation of mean flow and turbulence over a 2D building array using high-resolution CFD and a distributed drag force approach. *Journal of Wind Engineering and Industrial Aerodynamics, 92*(2), 117-158.

Lim, H., Thomas, T., & Castro, I. (2009). Flow around a cube in a turbulent boundary layer: LES and experiment. *Journal of Wind Engineering and Industrial Aerodynamics, 97*(2), 96-109.

Liu, Z., & Hill, D. (2000). Issues surrounding multiple frames of reference models for turbo compressor applications.

Manwell, J., McGowa, J., Rogers, A. (2009). *Wind Energy Explained Theory Design and Application* (2nd ed.). UK: John Wiley & Sons.

Mattos S.de B., Macedo P. A., Filho da Silva H. D. (2003). *Considerations about Winglet Design*. Paper presented at the 21st Applied Aerodynamics Conference, Orlando Florida.

Maughmer, Mark D. (2003). Design of winglets for high-performance sailplanes. *Journal of Aircraft, 40*(6), 1099-1106.

Mishnaevsky Jr, L., Freere, P., Sinha, R., Acharya, P., Shrestha, R., & Manandhar, Pushkar. (2011). Small wind turbines with timber blades for developing countries: Materials choice, development, installation and experiences. *Renewable Energy, 36*(8), 2128-2138.

Rajendran, C., Madhu, G., Tide, P.S., Kanthavel, K. (2011). Aerodynamic Perforamance Analysis of Horizontal Axis Wind Turbines Using CFD Technique. *European Journal of Scientific Research 65*, 28-37.

Ricciardelli, F., & Polimeno, S. (2006). Some characteristics of the wind flow in the lower urban boundary layer. *Journal of wind engineering and industrial aerodynamics, 94*(11), 815-832.

Savage, MG, & Larose, GL. (2003). An experimental study of the aerodynamic influence of a pair of winglets on a flat plate model. *Journal of wind engineering and industrial aerodynamics, 91*(1), 113-126.

Shimizu, Y., van Bussel, G.J.W., Matsumura, S., & Bruining, A. (1992). New technology of power augmentation on horizontal axis wind turbines using Mie vanes. *Journal of Wind Engineering and Industrial Aerodynamics, 39*(1), 119-127.

Shun, S., & Ahmed, N.A. (2012). Wind Turbine Performance Improvements using Active Flow Control Techniques. *Procedia Engineering, 49*, 83-91.

Sun, Heng., & Huang, Suyi. (2001). Simulation of Wind Flow Around a Building with ak–ε Model. *Theoretical and Computational Fluid Dynamics, 14*(4), 283-292.

Tu, J., Yeoh, H. G., Liu, C. (2008). *Computational Fluid Dynamics: A Pratical Approach* (1st ed.). UK: Butterworth-Heinemann.

Tutar, M., & Oguz, G. (2002). Large eddy simulation of wind flow around parallel buildings with varying configurations. *Fluid Dynamics Research, 31*(5), 289-315.

UIUC. (2012). UIUC Applied Aerodynamics Group. Retrieved 5th January, 2012, from http://aerospace.illinois.edu/m-selig/ads/coord_database.html

Valentine, S. (2010). Braking wind in Australia: A critical evaluation of the renewable energy target. *Energy Policy, 38*(7), 3668-3675.

Van Bussel, G.J.W., Mertens, S., Polinder, H., & Sidler, H.F.A. (2004). *TURBY®: concept and realisation of a small VAWT for the built environment.* Paper presented at the Proceedings of the EAWE/EWEA Special Topic conference" The Science of making Torque from Wind", Delft, The Netherlands.

Vermeer, L. J., Sørensen, J. N., & Crespo, A. (2003). Wind turbine wake aerodynamics. *Progress in Aerospace Sciences, 39*(6-7), 467-510.

Versteeg, H.K., & Malalasekera, W. (1995). An Introduction to Computational Fluid Dynamics: The Finite Volume Approach: Longman Scientific, Technical.

Whitcomb, Richard T. (1976). *A design approach and selected wind-tunnel results at high subsonic speeds for wing-tip mounted winglets*: National Aeronautics and Space Administration (NASA).

Wood, D. (2011). *Small wind turbines: analysis, design, and application*: Springer.

WWEA. (2013). 2013 Small Wind World Report Update. Retrieved 15th February, 2013, from http://www.wwindea.org/webimages/SWWR_summary.pdf

Yen, D.T., van Dam, C.P., Smith, R.L., & Collins, S.D. (2001). *Active load control for wind turbine blades using MEM translational tabs.* Paper presented at the 2001 ASME Wind Energy Symposium.

Yergin, D. (1988). Energy Security in the 1990s. *Foreign Affairs, 67*(1), 110-132.

BIBLIOGRAPHY

Akwa, J. , Vielmo, H. , & Petry, A. (2012). A review on the performance of Savonius wind turbines. *Renewable and Sustainable Energy Reviews, 16*(5), 3054-3064.

Bavanish, B., & Thyagarajan, K. (2013). Optimization of power coefficient on a horizontal axis wind turbine using bem theory. *Renewable and Sustainable Energy Reviews, 26*, 169-182.

Butterfield, P., Scott, G., & Musial, W., (1992). Comparison of wind tunnel airfoil performance data with wind turbine blade data. *Journal of solar energy engineering, 114*(2), 119-124.

Choi, N., Hyun S., Hyun, J., & Chun, K. (2013). Numerical study on the horizontal axis turbines arrangement in a wind farm: Effect of separation distance on the turbine aerodynamic power output. *Journal of Wind Engineering and Industrial Aerodynamics, 117*, 11-17.

Du, Z., & Selig, M. (1998). A 3-D stall-delay model for horizontal axis wind turbine performance prediction. *AIAA Paper, 21*.

Du, Z., & Selig, M.S. (2000). The effect of rotation on the boundary layer of a wind turbine blade. *Renewable Energy, 20*(2), 167-181.

Fuglsang, P, & Madsen, HA. (1999). Optimization method for wind turbine rotors. *Journal of Wind Engineering and Industrial Aerodynamics, 80*(1), 191-206.

Hansen, A.C, & Butterfield, CP. (1993). Aerodynamics of horizontal-axis wind turbines. *Annual Review of Fluid Mechanics, 25*(1), 115-149.

Hu, D., Hua, O., & Du, Zhaohui. (2006). A study on stall-delay for horizontal axis wind turbine. *Renewable Energy, 31*(6), 821-836.

Joselin G.M., Iniyan, S., Sreevalsan, E., & Rajapandian, S. (2007). A review of wind energy technologies. *Renewable and sustainable energy Reviews, 11*(6), 1117-1145.

Jung, Nam., No, S., & Ryu, K. (2005). Aerodynamic performance prediction of a 30kW counter-rotating wind turbine system. *Renewable Energy, 30*(5), 631-644.

Kishinami, K., Taniguchi, H., Suzuki, J., Ibano, H., Kazunou, T., & Turuhami, M. (2005). Theoretical and experimental study on the aerodynamic characteristics of a horizontal axis wind turbine. *Energy, 30*(11), 2089-2100.

Lanzafame, R, & Messina, M. (2010). Power curve control in micro wind turbine design. *Energy, 35*(2), 556-561.

Mirecki, A., Roboam, X., & Richardeau, F. (2007). Architecture complexity and energy efficiency of small wind turbines. *Industrial Electronics, IEEE Transactions on, 54*(1), 660-670.

Sedaghat, A., & Mirhosseini, M. (2012). Aerodynamic design of a 300kW horizontal axis wind turbine for province of Semnan. *Energy Conversion and Management, 63*, 87-94.

Shen, Zhong., Mikkelsen, R., Sørensen, N., & Bak, C. (2005). Tip loss corrections for wind turbine computations. *Wind Energy, 8*(4), 457-475.

Simms, A., Schreck, S., Hand, M., & Fingersh, L.J. (2001). *NREL unsteady aerodynamics experiment in the NASA-Ames wind tunnel: a comparison of predictions to measurements*: National Renewable Energy Laboratory Colorado, USA.

Singh, R.K., & Ahmed, M.R. (2013). Blade design and performance testing of a small wind turbine rotor for low wind speed applications. *Renewable Energy, 50*, 812-819.

Spera, David A. (1994). Introduction to modern wind turbines. *Wind turbine technology: fundamental concepts of wind Turbine engineering. ASME Press, New York*, 47-72.

Sumner, J., Watters, C., & Masson, C. (2010). CFD in wind energy: the virtual, multiscale wind tunnel. *Energies, 3*(5), 989-1013.

Tadamasa, A., Zangeneh. M. (2011). Numerical prediction of wind turbine noise. *Renewable Energy, 36*(7).

Thumthae, C., & Chitsomboon, Tawit. (2009). Optimal angle of attack for untwisted blade wind turbine. *Renewable energy, 34*(5), 1279-1284.

Xu, G., & Sankar, L. (2000). Computational study of horizontal axis wind turbines. *Journal of solar energy engineering, 122*(1), 35-39.

Yusaf, T., Goh, S., & Borserio, J.A. (2011). Potential of renewable energy alternatives in Australia. *Renewable and sustainable energy reviews, 15*(5), 2214-2221.

LIST OF PUBLICATIONS

The following is a list of publications arisen from this work

Ali, A., Golde, S., Alam, F., Moria, H . (2011). A review of power generation from wind in Australia. *Proceedings of the 9th International Conference of Mechanical Engineering* (ICME2011).

Ali, A., Alam, F., Djamovski, V., Watkins, S. (2012). "Experimental and Computational Study of a Micro Vertical Axis Wind Turbine." *Procedia Engineering* 49: 254-262.

Ali, A., Chowdhury, H., Longanathan, B., Aldawi, F., Alam, Firoz. (2013) An aerodynamic study of a domestic scale horizontal axis wind turbine with varied tip configurations. *Proceedings of International Conference on Mechanical Engineering and Renewable Energy* (ICMERE2013).

APPENDIX A: Technical Drawings of Wind Turbine

A.1: **Full Scale Horizontal Axis Wind Turbine Assembly**

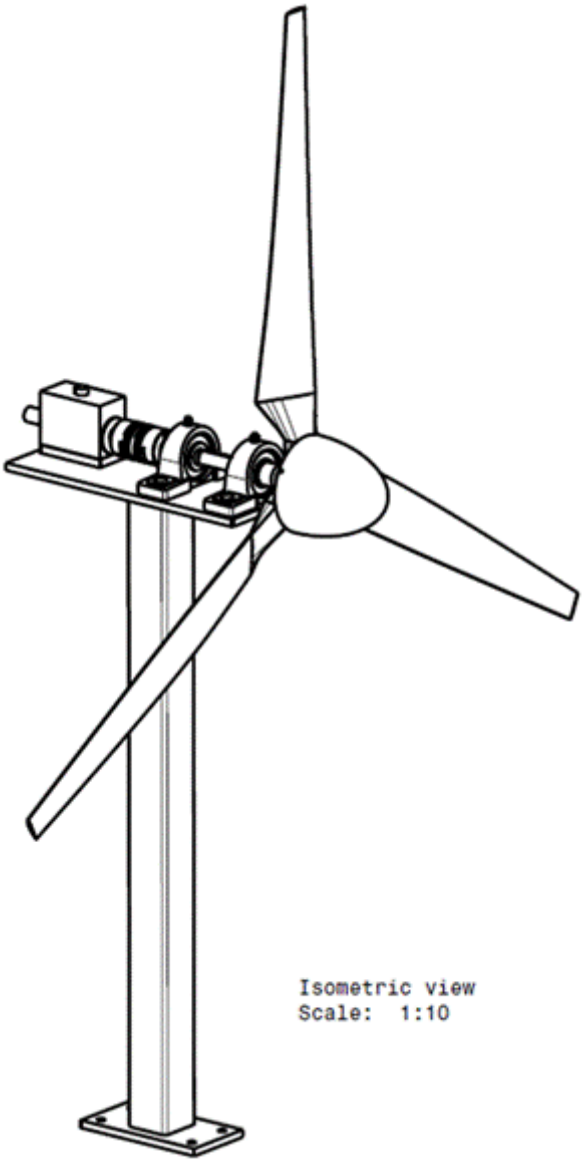

Figure A. 1: Full Scale Wind Turbine Isometric View

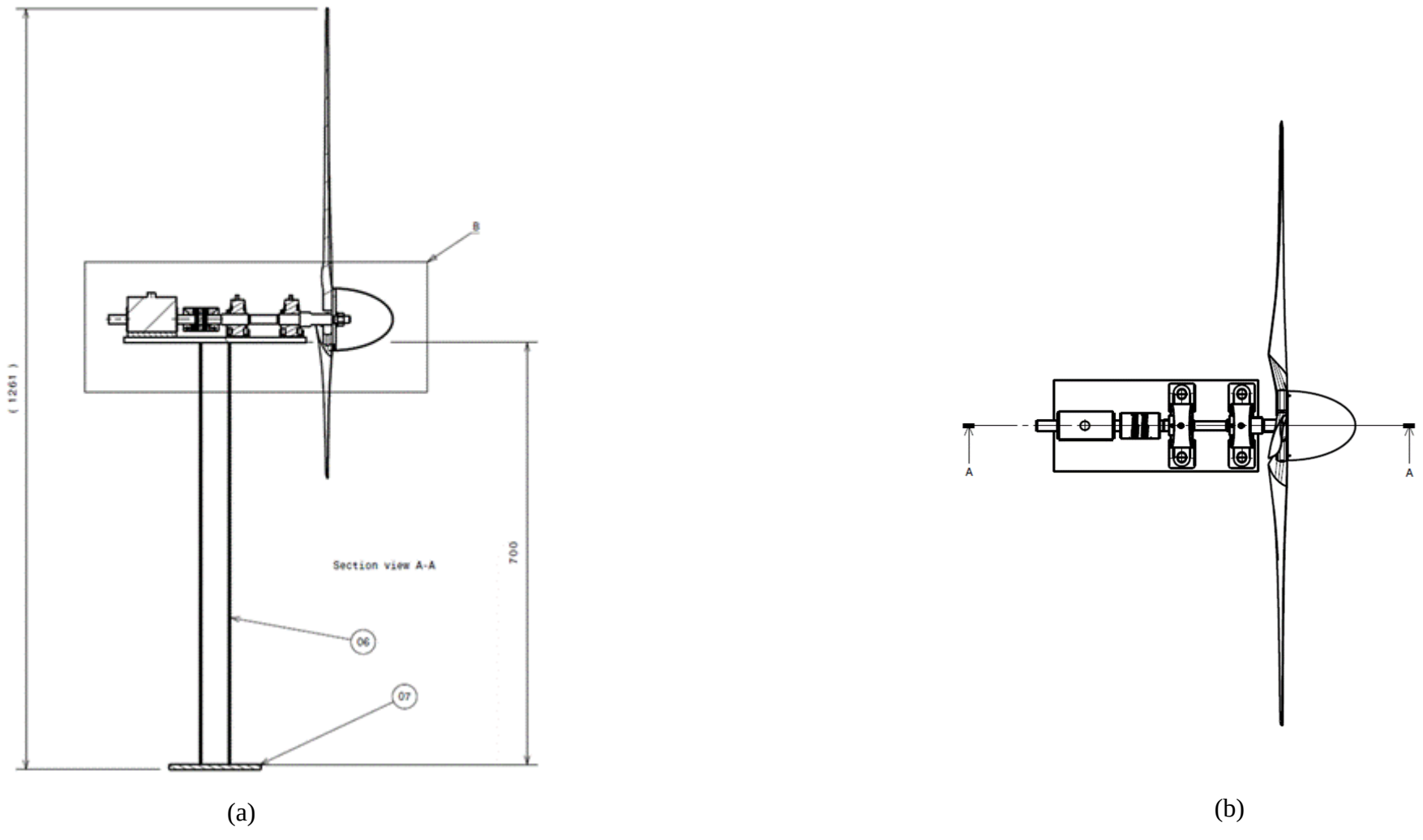

(a) (b)

Figure A. 2: Wind turbine assembly (a) Side view (b) Top view

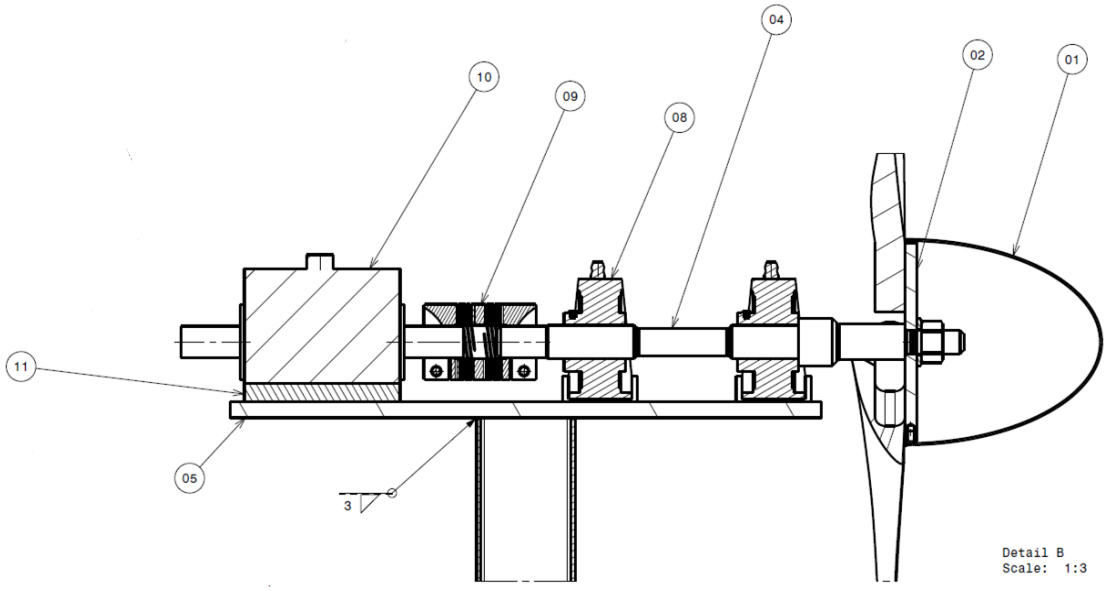

Figure A. 3: Side section view B-B

Table A. 1: Wind turbine components

Component	Description
01	Nose cone
02	Hub
03	Blade
04	Shaft
05	Top plate
06	Stand
07	Base plate
08	Bearing housing unit
09	Flexible coupling
10	HBM torque transducer
11	Wedge plate

A.2: **Nose Cone**

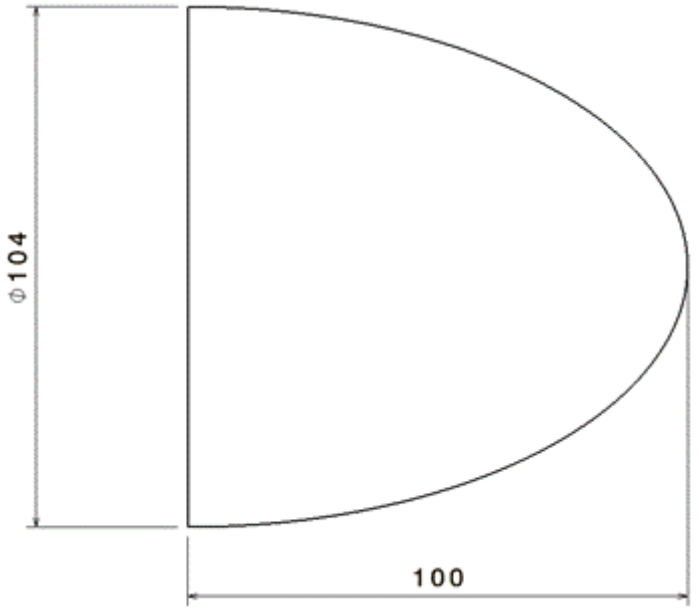

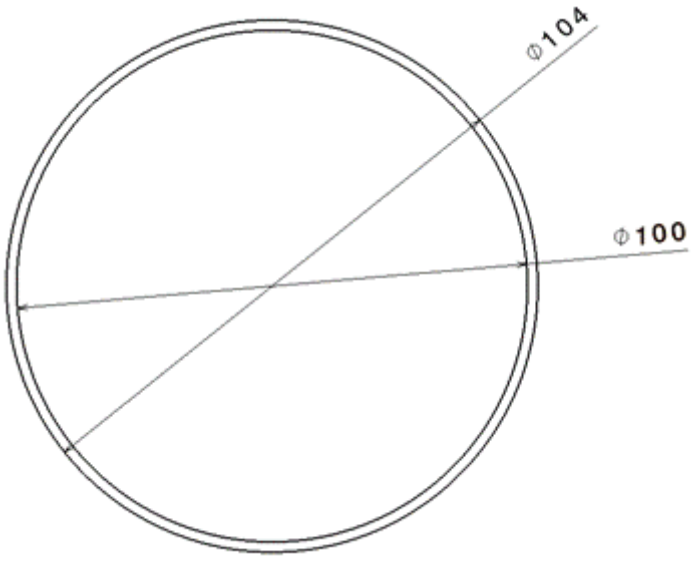

Figure A. 4: Geometry of nose cone

A.3: **Hub**

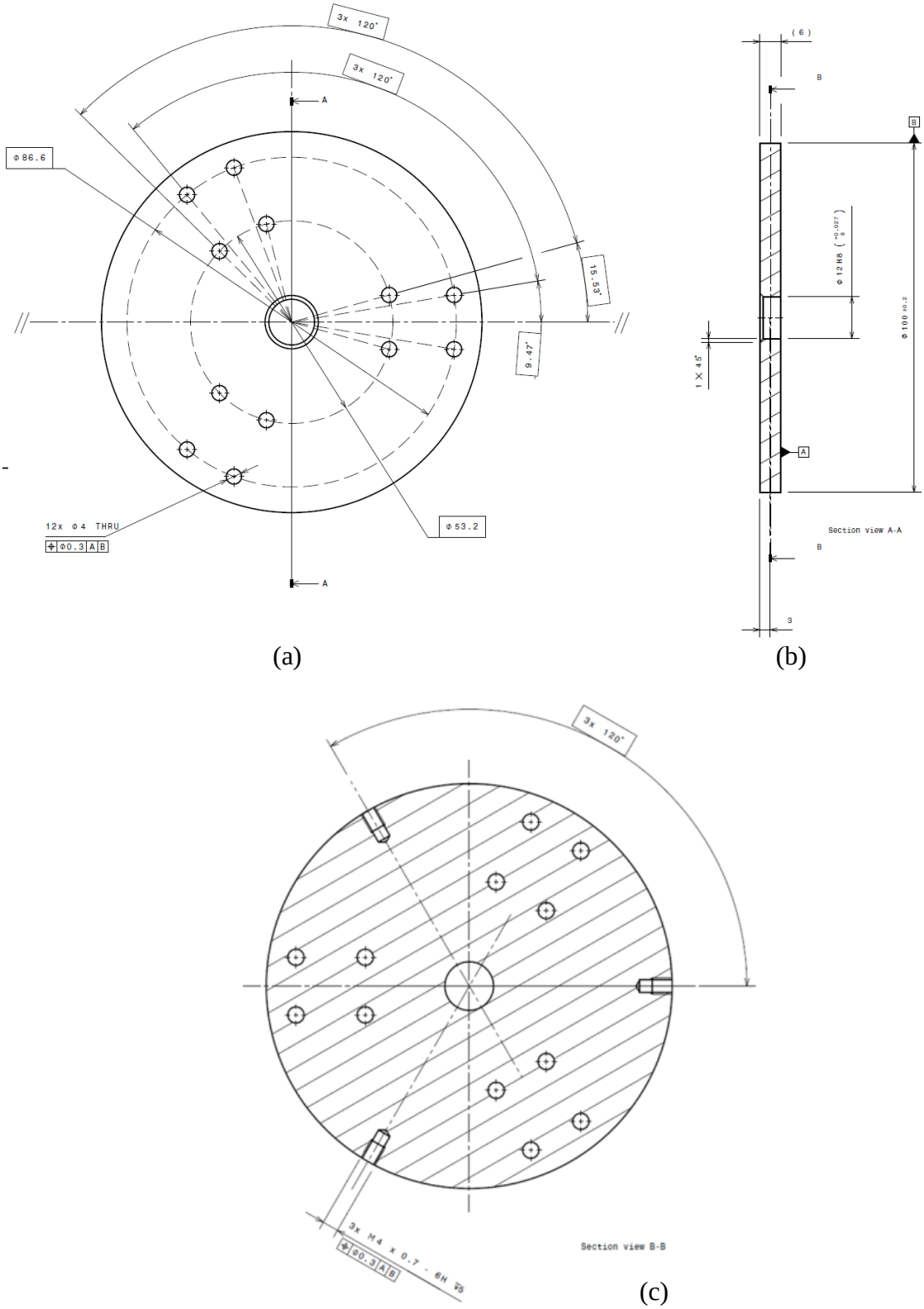

Figure A. 5: Wind turbine hub (a) front view (b) section view A-A(c) section view B-B

A.4: **Shaft**

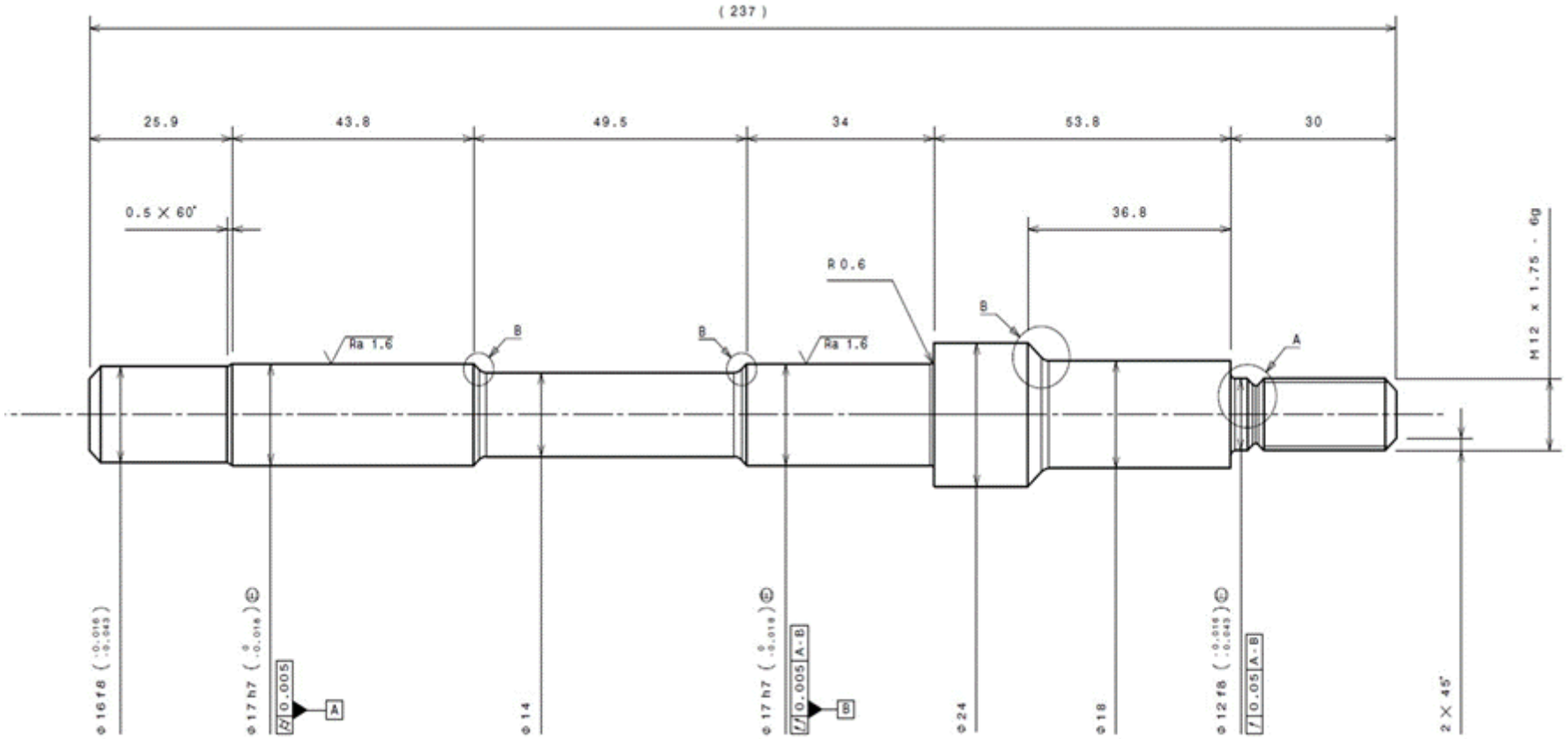
(237)
25.9
43.8
49.5
34
53.8
30
0.5 X 60°
36.8
R 0.6
Ra 1.6
Ra 1.6
B
B
B
A
M12 x 1.75 - 6g
Φ 16 f8 (-0.016 -0.043)
Φ 17 h7 (0 -0.018) Ⓔ
0.005 A
Φ 14
Φ 17 h7 (0 -0.018) Ⓔ
0.005 A-B
Φ 24
Φ 18
Φ 12 f8 (-0.016 -0.043) Ⓔ
0.05 A-B
2 X 45°

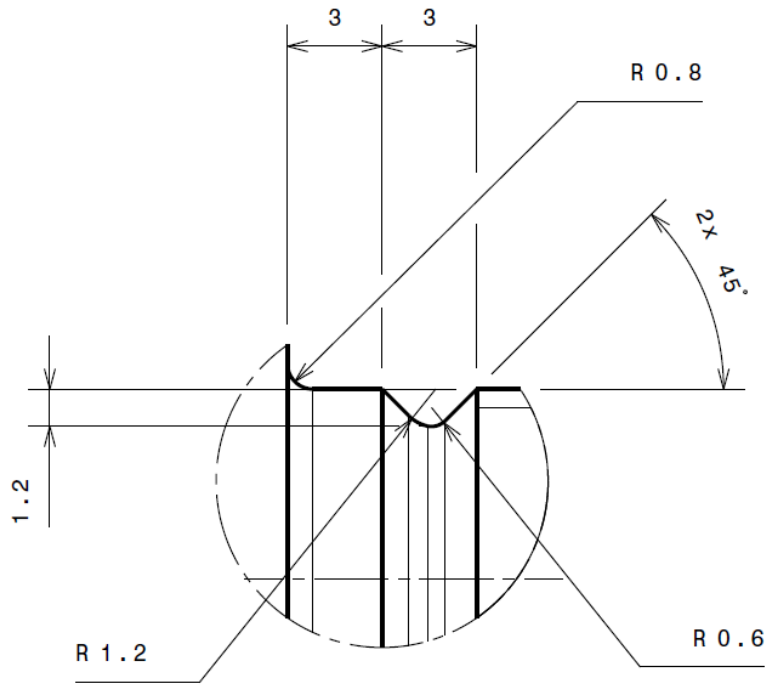

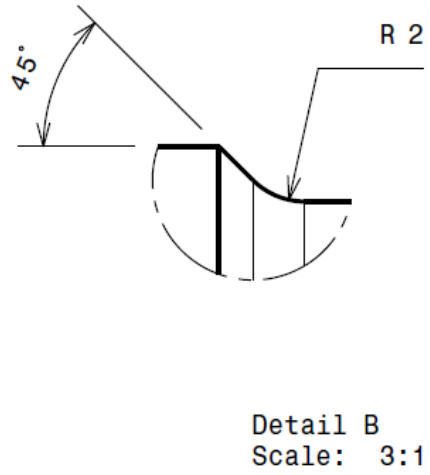

Figure A. 6: Geometry of main shaft of wind turbine

A.5: **Top Plate**

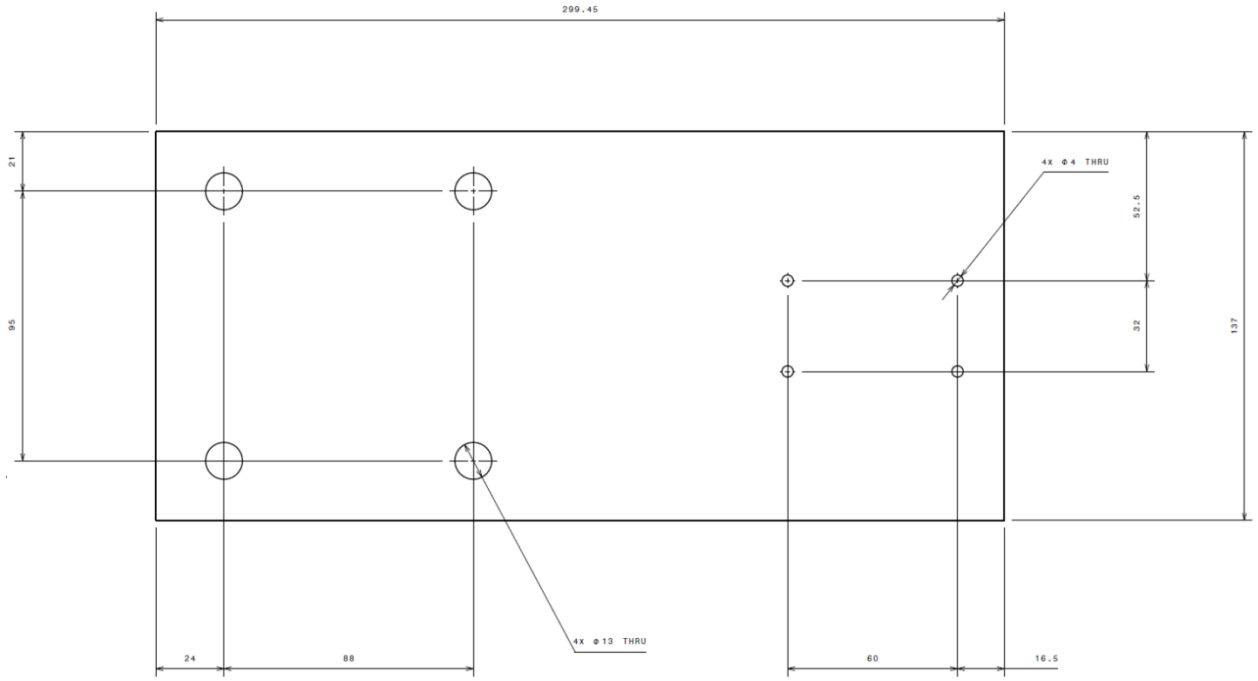

(a)

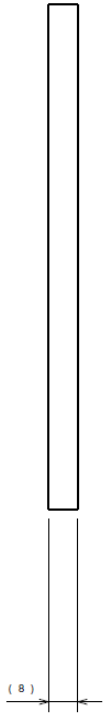

(b)

Figure A. 7: Geometry of top plate

A.6: **Bottom Plate**

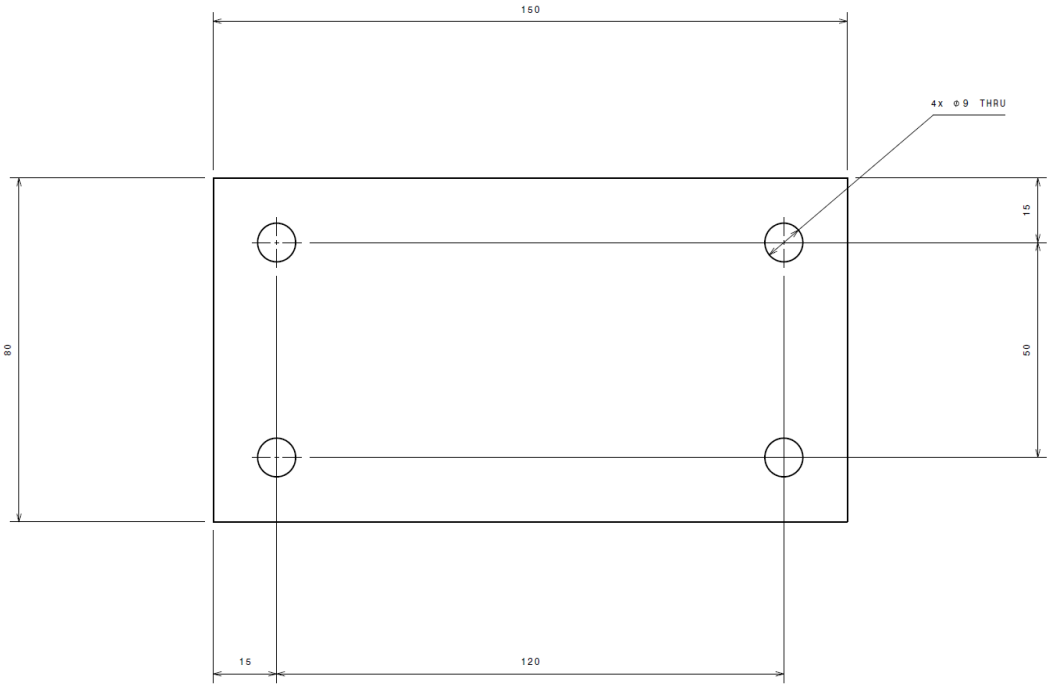

(a)

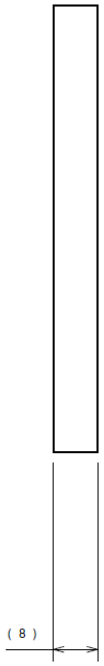

(b)

Figure A. 8: Bottom base Geometry

A.7: **Flexible Coupling**

A flexible beam coupling is used for the experiment of the wind turbine due to its robustness and light weight. Detailed specification of the coupling is given Table A.7.

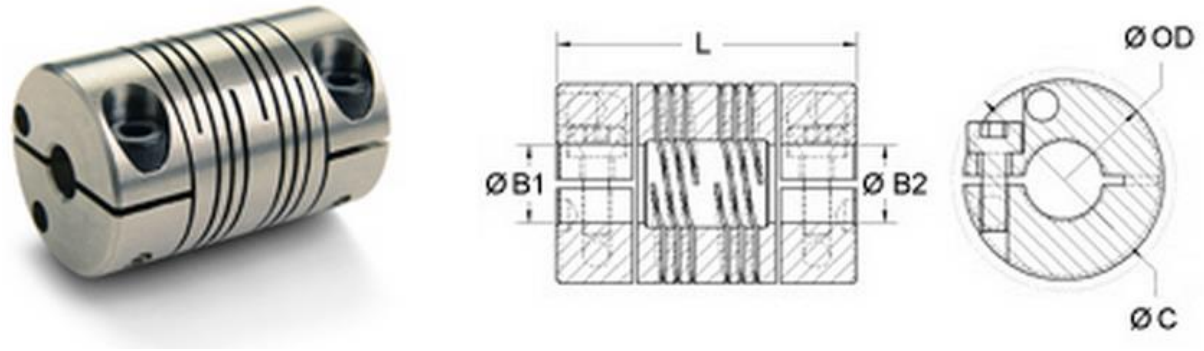

Figure A. 9: Aluminium flexible beam coupling

Table A. 2: Specification of flexible beam coupling

Product Number	FCMR38-16-16-A
Product Type	Beam Coupling
Style	Clamp
Material	7075 Aluminium
Finish	Bright
Dimensions	
Bore B1	16mm
Bore B2	16 mm
Outer Diameter OD	38.1 mm
Length L	57.2 mm
Shaft Penetration	26.47 mm
Clearance Diameter C MAX	41.71 mm
Fastening Hardware	
Cap Screw	M5
Screw Material	Alloy Steel with Nypatch
Screw Finish	Black Oxide
Seating Torque	9.5 Nm

Hex Wrench	4.0 mm
Torque Specifications	
Static Torque	10.73 Nm
Dynamic Torque Non-Reversing	5.37 Nm
Dynamic Torque Reversing	2.68 Nm
Misalignment	
Angular Misalignment	3°
Partial Misalignment	0.76 mm
Axial Motion	0.38 mm
Additional Information	
Torsional Stiffness	0.39 Deg/Nm
Moment of Inertia	30.032×10^{-6} kg-m^2
Maximum Speed	6000RPM
Bore Tolerance	+.025mm / -.000mm
Temperature Range	-40°F to 225°F
	-40°C to 107°C

A.8: **Self-Aligning Ball Bearing**

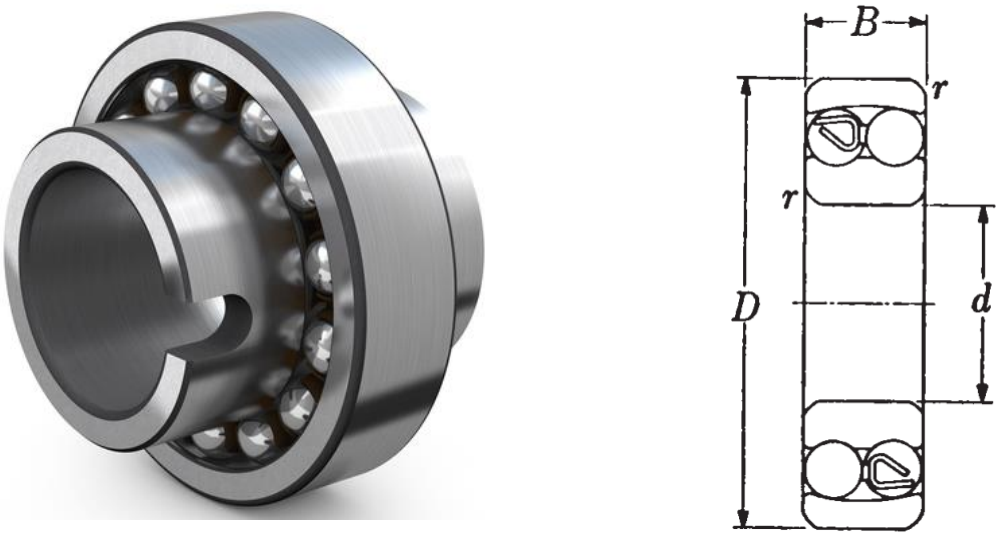

Figure A. 10: Self-aligning ball bearing

Table A. 3: Self-aligning ball bearing specification

Bore d	17
Outer Diameter O.D	47
Width B	14
Fillet Radius r (mm)	1.5
Load Ratings	3180N (Static) 12543N (Dynamic)
Weight	130 grams

APPENDIX B: Instrumentation

B.1: **Load Sensor Specification**

The JR3 sensor is a monolithic aluminium (optionally stainless steel or titanium) device Instrumented with metal foil strain gages which sense the loads imposed on the sensor. The strain gage signals are connected to the external amplifier and signal conditioning equipment through the sensor cable. In the external electronic system the strain gage signals are amplified and combined to produce signals representing the force and moment loads for all axes. Unpredictability

Sensors are produced in a wide variety of load ratings and bolt patterns. The physical size of the sensor varies, depending on factors such as force and moment ratings and required mounting dimensions.

The axes on standard JR3 sensors are oriented with the X and Y axes in the plane of the sensor body, and the Z axis perpendicular to the X and Y axes. The reference point for all loading data is the geometric centre of the sensor. When viewed from the Robot Side of the sensor the forces and moments are related by the Right Hand Rule.

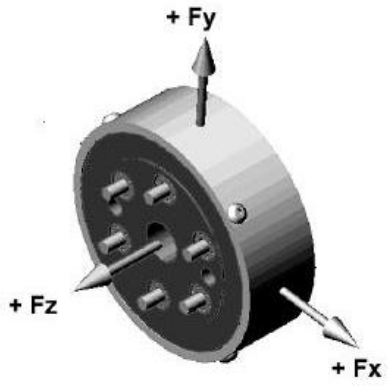

Figure B. 1: Sensor axis orientation

All JR3 sensors use captive button-head bolts to mount the sensor with recommended torque. Sensors transmit digital output data to the receiver electronics in a synchronous serial format.

All low level analogue signals and the Analogue to Digital (A/D) circuitry are within the sensor body, shielded from electromagnetic interference by the metallic sensor body. Data for all six axes is returned to the receiver at a rate of 8 kHz. The data stream also includes feedback monitoring the sensor power supply voltage and information about sensor characteristics and calibration. Transmission of sensor calibration data from the sensor allows sensors to be interchanged with no need for any adjustment of the receiver circuitry. Feedback of the sensor power voltage allows use of long lengths of small gage wire in the sensor cable. Sensor power and data signals can be passed through slip rings with no increase in noise or loss of accuracy. Standard digital output sensors utilise either a 6 pin RJ-11 or an 8 pin RJ-45 modular style jack depending on the sensor model.

The nominal load rating of JR3 sensors is the X or Y axis force rating. The Z axis rating is twice the X or Y axis rating. The torque rating for all axes is the X or Y axis force rating times the sensor diameter.

Typical features and options for our "M" sensors include:

- Internal electronics for enhanced noise immunity
- Digital output option for use with a JR3 DSP-based receiver card
- Analogue output option for use with pre-existing data acquisition systems
- Half-bridge strain gage configuration for cost-effectiveness
- Fewer internal loading flexures for cost-effectiveness
- ISO 9409 standard bolt patterns with captive screws for easy, no-adapter-plate-needed installation

Typical specifications:

- Accuracy of nominally 1% of Full Scale (FS)
- Repeatability better than absolute accuracy
- Linearity of 0,5% of FS from +FS to -FS
- and 0,1% of FS at loading below 1/4 FS
- Resolution of 1/4000 FS

JR3 sensors (M series) with load rating 200N, 400N and 1000N were used for the measurement of aerodynamic properties of different experimental arrangements.

APPENDIX C: Fortus 900 mc 3D Printing Machine

C.1: **Fortus 900 mc**

All three wind turbine blade design configuration were manufactured at RMIT Advanced Manufacturing Precinct using the Fortus 900 mc as shown in Figure C.1. As mentioned in this thesis, the blades were manufactured using an ABS Polycarbonate material.

Figure C. 1: Fortus 900 mc for 3D printing of the wind turbine blades

Table C. 1: Fortus 900 mc

Specification	**Description**
Model no	Fortus 900 mc
Build Envelope	+36 x 24 x 36 in (914 x 610 x 914 mm)
System Size/Weight	109.1 x 66.3 x 79.8 in (2772 x 1683 x 2027 mm) With crate: 7247 lbs. (3287 kg) Without crate: 6325 lbs. (2869 kg)
Material Options	ABSi PC-ISO ABS-M30 PC ABS-M30i NYLON 12 ABS-ESD7 ULTEM™ 9085 PC-ABS PPSF
Throughput Comparison	2.1 x
Achievable Accuracy	Parts are produced within an accuracy of: ± .0035 in (± .089 mm) or ± .0015 in/in (± .0015 mm/mm)

APPENDIX D: Variation of Aerodynamic Forces For Three Different Blade Tip Configurations

D.1: **Wind Turbine blade With no Winglet**

Figure C.1 illustrates the variation of the aerodynamic lift force on a straight blade with increasing wind speed for a range of yaw angles (0° to 90°). As shown in Figure C.1, maximum value in lift is obtained at yaw angle of 30° with an approximate value of 5 N.

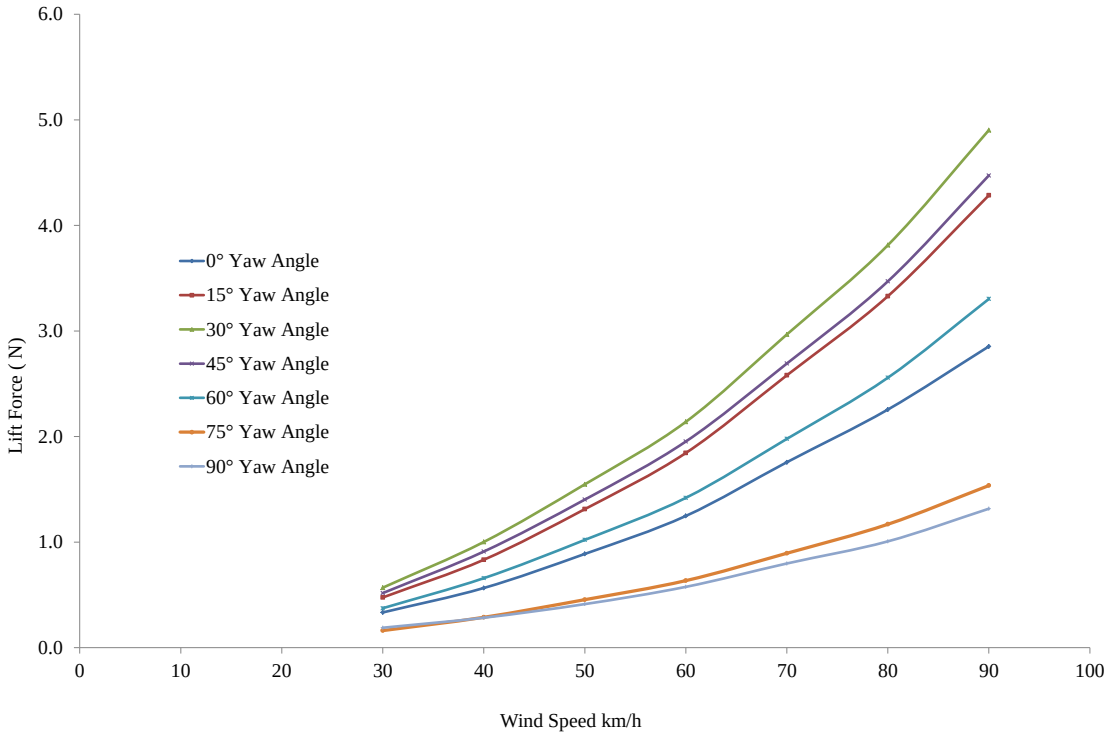

Figure D. 1: Lift force variation with increasing wind speed at different yaw angle for turbine blade (Straight blade)

D.2: **Wind Turbine blade With no Winglet**

The drag force exerted on the blade is also measured for a range of wind speeds and yaw angle. It is shown in Figure C.2 that the drag force increases with increasing wind speed as well as yaw angle. As expected maximum drag force value is obtained at 90° yaw angle as pressure drag is evidently dominant.

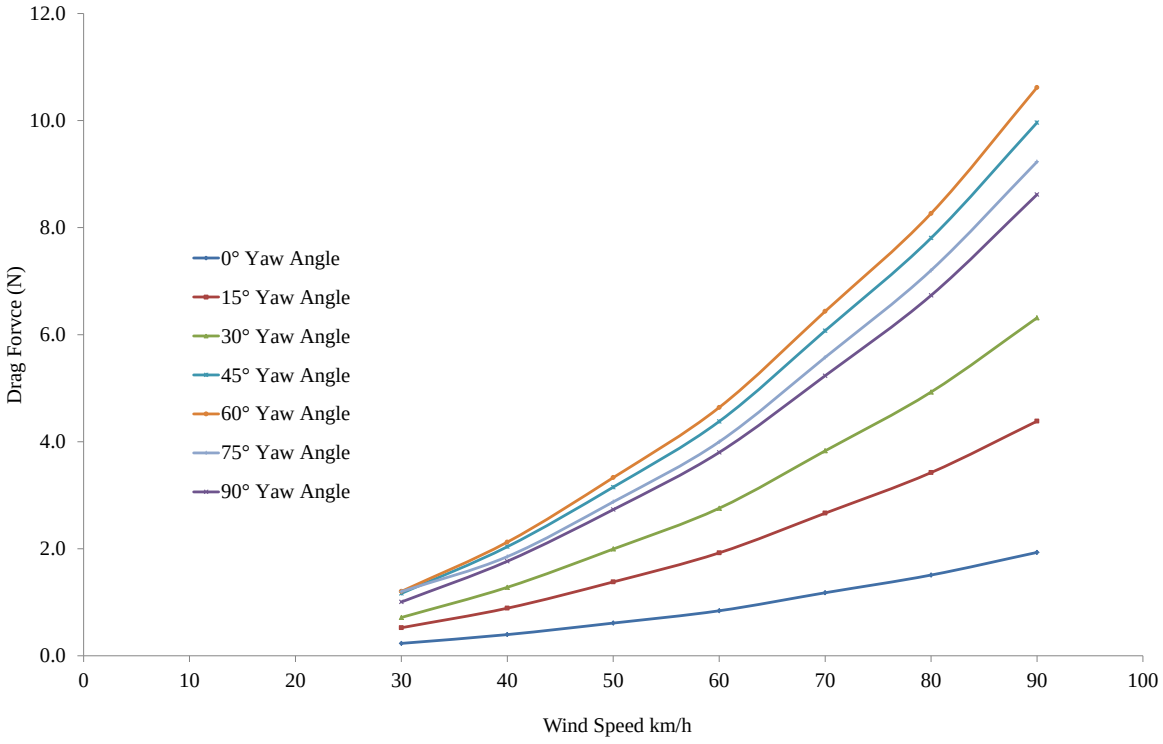

Figure D. 2: Drag force variation with increasing wind speed at different yaw angle for turbine blade (Straight blade)

D.3: **Wind Turbine Blade With a Forward Facing Winglet Attached**

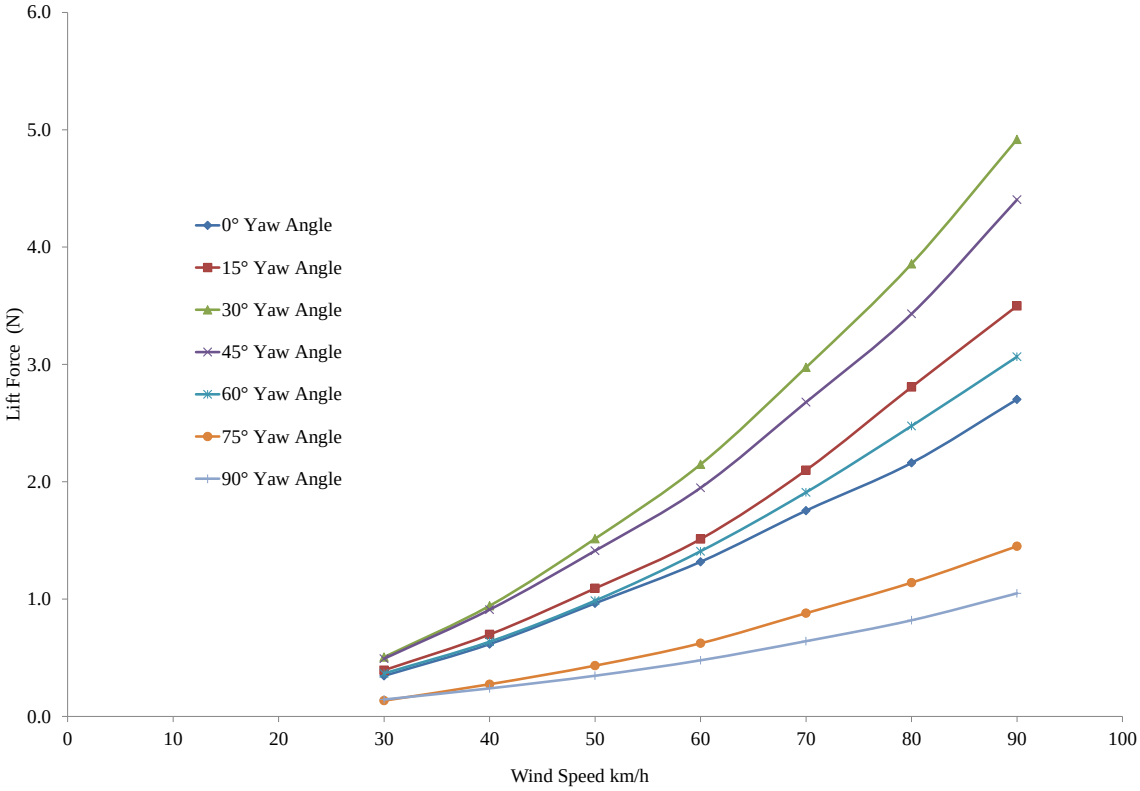

Figure D. 3: Lift force variation with increasing wind speed at different yaw angle for forward facing winglet blade

D.4: **Wind Turbine Blade With a Forward Facing Winglet Attached**

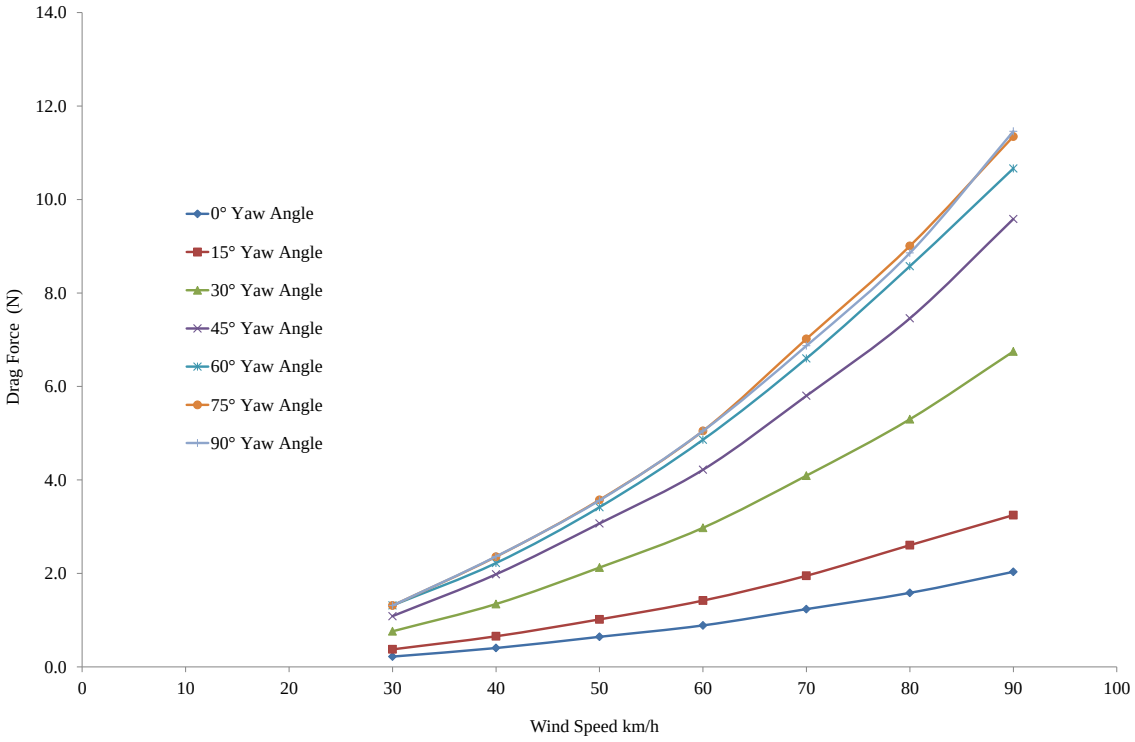

Figure D. 4: Drag force variation with increasing wind speed at different yaw angle for forward facing winglet blade

D.5: **Wind Turbine Blade With a Backward Facing Winglet Attached**

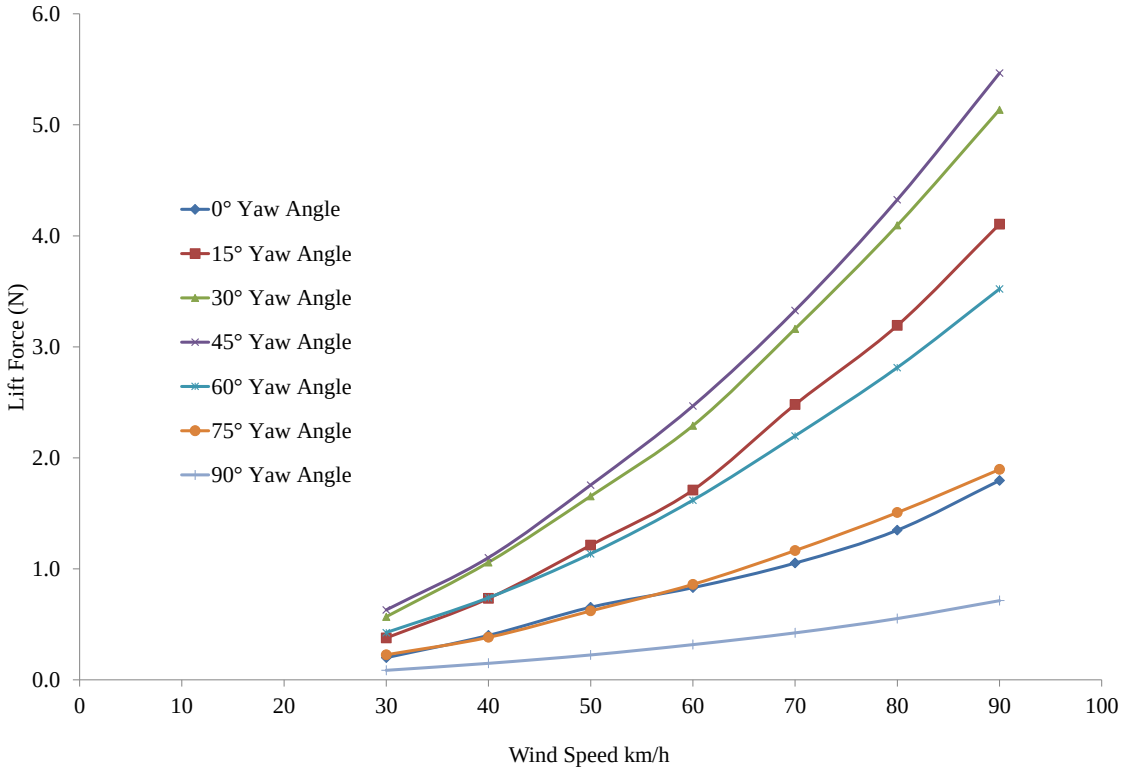

Figure D. 5: Lift force variation with increasing wind speed at different yaw angle for backward facing winglet blade

D.6: **Wind Turbine Blade With a Backward Facing Winglet Attached**

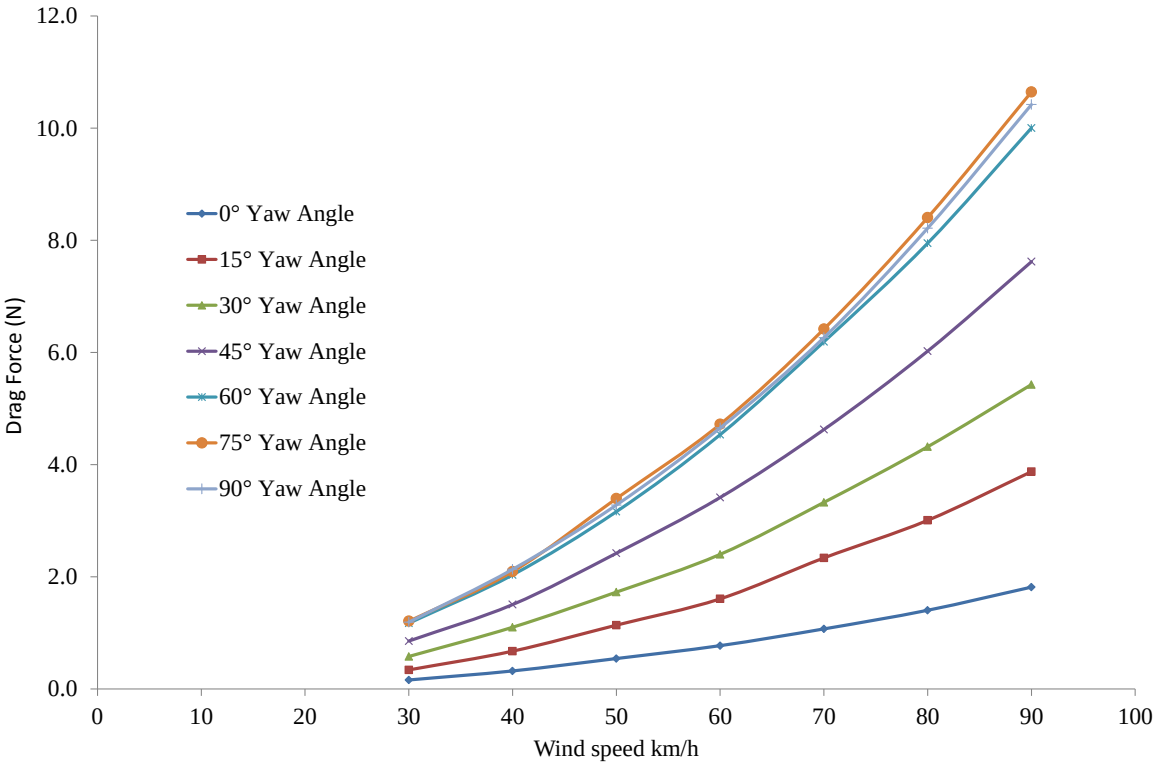

Figure D. 6: Drag force variation with increasing wind speed at different yaw angle for backward facing winglet blade

APPENDIX E: Aerofoil Data

E.1: **SG6051**

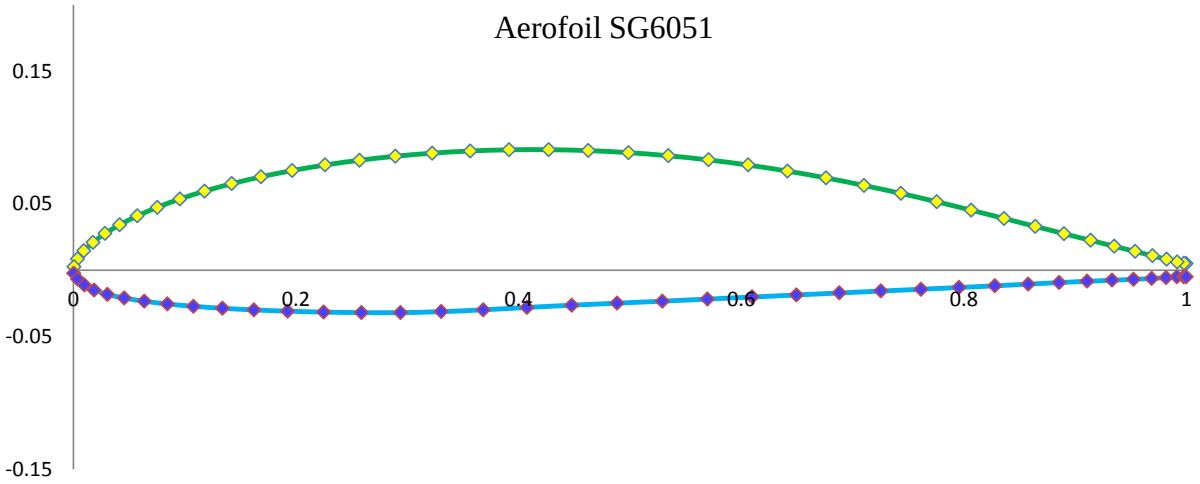

Figure E. 1: SG6051 Aerofoil

Table E. 1: SG6051 aerofoil coordinates

Upper Surface		Lower Surface	
X	Y	X	Y
1	0.005	0.00042	-0.0022
0.9979	0.00527	0.00365	-0.00654
0.99187	0.00631	0.00985	-0.01097
0.98234	0.00826	0.01874	-0.01489
0.96969	0.01097	0.03064	-0.01812
0.95403	0.01425	0.04567	-0.02084
0.93543	0.0181	0.06366	-0.02323
0.9141	0.02256	0.08447	-0.02531
0.89031	0.02759	0.10794	-0.02708
0.8643	0.03312	0.13392	-0.02857
0.83636	0.03906	0.16222	-0.02979

0.80674	0.0453
0.77574	0.05168
0.74358	0.05795
0.71038	0.06395
0.67633	0.06962
0.6416	0.07477
0.60629	0.07931
0.57064	0.0832
0.53475	0.08631
0.49871	0.08866
0.46275	0.09019
0.427	0.09088
0.3916	0.0908
0.35675	0.08992
0.32259	0.08828
0.28931	0.08595
0.25709	0.08295
0.22611	0.07934
0.19655	0.07516
0.16857	0.07045
0.14233	0.06527
0.11797	0.05967
0.0956	0.0537
0.07537	0.04745
0.05737	0.04097
0.04167	0.03436
0.02838	0.0277
0.01756	0.02109
0.00931	0.01469
0.00369	0.00848
0.00058	0.00263

0.19263	-0.03075
0.22493	-0.03144
0.25883	-0.03183
0.29407	-0.03182
0.33051	-0.03112
0.36831	-0.02972
0.40753	-0.02795
0.44777	-0.02626
0.48846	-0.02473
0.52924	-0.0232
0.56988	-0.02165
0.61011	-0.02008
0.64967	-0.01854
0.68829	-0.01704
0.72569	-0.0156
0.76161	-0.01423
0.79579	-0.01293
0.82796	-0.01165
0.858	-0.01039
0.88576	-0.00922
0.91097	-0.00824
0.93337	-0.00744
0.95273	-0.00678
0.96889	-0.00613
0.9819	-0.00546
0.99169	-0.00501
0.99787	-0.00493
1	-0.005

APPENDIX F: Wind Turbine Blade Design Calculation

F.1: **Optimum Blade Design (For optimum chord distribution)**

Table F. 1: Optimum blade design calculation

Elements	r/R	Sectional Radius (r) mm	Radius of Blade mm (R)	Chord mm	AoA α	c/R	Twist Angle	Angle of Relative Wind
1	0.16	79	500	179.71	5	0.36	25	35.23
2	0.27	132	500	108.50	5	0.22	18.09	23.09
3	0.37	184	500	77.71	5	0.16	11.98	16.98
4	0.48	237	500	60.53	5	0.12	8.38	13.38
5	0.58	289	500	49.58	5	0.099	6.02	11.02
6	0.69	342	500	41.98	5	0.084	4.36	9.36
7	0.79	394	500	36.40	5	0.072	3.14	8.13
8	0.90	447	500	32.13	5	0.064	2.19	7.19
9	1	500	500	28.75	5	0.057	1.45	6.44

F.2: **Adopted Blade Design (For linearised chord distribution)**

Table F. 2: Adopted blade design calculation

Elements	r/R	Sectional Radius (r) mm	Radius of Blade mm (R)	Chord mm	AoA α	c/R	Twist Angle	Angle of Relative Wind
1	0.16	79	500	70.39	5	0.36	25	35.23
2	0.27	132	500	65.19	5	0.22	18.09	23.09
3	0.37	184	500	59.98	5	0.16	11.98	16.98
4	0.48	237	500	54.78	5	0.12	8.38	13.38
5	0.58	289	500	49.57	5	0.099	6.02	11.02
6	0.69	342	500	44.36	5	0.084	4.36	9.36
7	0.79	394	500	39.16	5	0.072	3.14	8.13
8	0.90	447	500	33.95	5	0.064	2.19	7.19
9	1	500	500	28.75	5	0.057	1.45	6.44